Available online at www.sciencedirect.com
SCIENCE DIRECT®
Comput. Methods Appl. Mech. Engrg. 194 (2005) 2285–2335
Computer methods in applied mechanics and engineering
www.elsevier.com/locate/cma

A unified formulation of small-strain corotational finite elements: I. Theory

C.A. Felippa [a,*], B. Haugen [b]

[a] *Department of Aerospace Engineering Sciences and Center for Aerospace Structures, University of Colorado, Campus Box 429, Boulder, CO 80309-0429, United States*
[b] *FEDEM Technology Inc., 2933 5th St., Boulder, CO 80304, United States*

Received 20 January 2004; received in revised form 18 July 2004; accepted 20 July 2004

Abstract

This paper presents a unified theoretical framework for the corotational (CR) formulation of finite elements in geometrically nonlinear structural analysis. The key assumptions behind CR are: (i) strains from a corotated configuration are small while (ii) the magnitude of rotations from a base configuration is not restricted. Following a historical outline the basic steps of the element independent CR formulation are presented. The element internal force and consistent tangent stiffness matrix are derived by taking variations of the internal energy with respect to nodal freedoms. It is shown that this framework permits the derivation of a set of CR variants through selective simplifications. This set includes some previously used by other investigators. The different variants are compared with respect to a set of desirable qualities, including self-equilibrium in the deformed configuration, tangent stiffness consistency, invariance, symmetrizability, and element independence. We discuss the main benefits of the CR formulation as well as its modeling limitations.

Keywords: Geometrically nonlinear structural analysis; Corotational description; Shell finite elements

1. Introduction

Three Lagrangian kinematic descriptions are in present use for finite element analysis of geometrically nonlinear structures: (1) total Lagrangian (TL), (2) updated Lagrangian (UL), and (3) corotational

* Corresponding author. Tel.: +1 303 492 6547; fax: +1 303 492 4990.
E-mail addresses: carlos.felippa@colorado.edu (C.A. Felippa), bjorn.haugen@fedem.co (B. Haugen).
URL: http://www.titan.colorado.edu/Felippa.d/FelippaHome.d/Home.html.

0045-7825/$ - see front matter
doi:10.1016/j.cma.2004.07.035

(CR). The CR description is the most recent of the three and the least developed one. Unlike the others, its domain of application is limited by a priori kinematic assumptions:

Displacements and rotations may be arbitrarily large, but deformations must be small. (1)

Because of this restriction, CR has not penetrated the major general-purpose FEM codes that cater to nonlinear analysis. A historical sketch of its development is provided in Section 2.

As typical of Lagrangian kinematics, all descriptions: TL, UL and CR, follow the body (or element) as it moves. The *deformed* configuration is any one taken during the analysis process and need not be in equilibrium. It is also known as the *current*, *strained* or *spatial* configuration in the literature, and is denoted here by $\mathscr{C}^D$. The new ingredient in the CR description is the "splitting" or decomposition of the motion tracking into two components, as illustrated in Fig. 1.

1. The *base* configuration $\mathscr{C}^0$ serves as the origin of displacements. If this happens to be one actually taken by the body at the start of the analysis, it is also called *initial* or *undeformed*. The name *material* configuration is used primarily in the continuum mechanics literature.
2. The *corotated* configuration $\mathscr{C}^R$ varies from element to element (and also from node to node in some CR variants). For each individual element, its CR configuration is obtained through a *rigid body motion* of the element base configuration. The associated coordinate system is Cartesian and follows the element like a "shadow" or "ghost", prompting names such as *shadow* and *phantom* in the Scandinavian literature. Element deformations are measured with respect to the corotated configuration.

In static problems the base configuration usually remains fixed throughout the analysis. In dynamic analysis the base and corotated configurations are sometimes called the *inertial* and *dynamic* reference configurations, respectively. In this case the base configuration may move at uniform velocity (a Galilean inertial system) following the mean trajectory of an airplane or satellite.

From a mathematical standpoint the explicit presence of a corotated configuration as intermediary between base and current is unnecessary. The motion split may be exhibited in principle as a multiplicative decomposition of the displacement field. The device is nonetheless useful to teach not only the physical meaning but to visualize the strengths and limitations of the CR description.

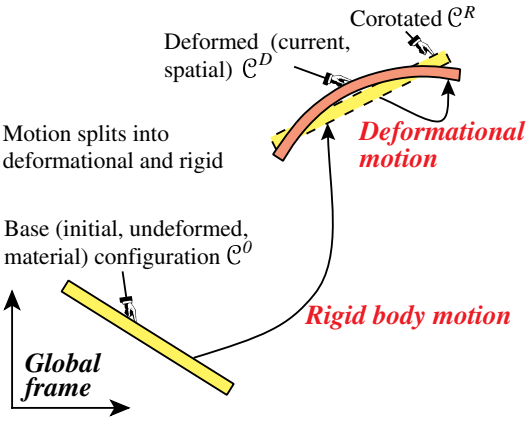

Fig. 1. The CR kinematic description. Deformation from corotated to deformed (current) configuration grossly exaggerated for visibility.

2. The emergence of CR

The CR formulation represents a confluence of developments in continuum mechanics, treatment of finite rotations, nonlinear finite element analysis and body-shadowing methods.

2.1. Continuum mechanics sources

In continuum mechanics the term "corotational" (often spelled "co-rotational") appears to be first mentioned in Truesdell and Toupin's influential exposition of field theories [81, Section 148]. It is used there to identify Jaumann's stress flux rate, introduced in 1903 by Zaremba. By 1955 this rate had been incorporated in hypoelasticity [82] along with other invariant flux measures. Analogous differential forms have been used to model endochronic plasticity [85]. Models labeled "co-rotational" have been used in rheology of non-Newtonian fluids; cf. [17,78]. These continuum models place no major restrictions on strain magnitude. Constraints of that form, however, have been essential to make the idea practical in nonlinear structural FEA, as discussed below.

The problem of handling three-dimensional finite rotations in continuum mechanics is important in all Lagrangian kinematic descriptions. The challenge has spawned numerous publications, for example [1,4,5,34,42–44,62,71,72]. For use of finite rotations in mathematical models, particularly shells, see [60,70,77]. There has been an Euromech Colloquium devoted entirely to that topic [61].

The term "corotational" in an FEM paper title was apparently first used by Belytschko and Glaum [8]. The survey paper by Belytschko [9] discusses the concept from the standpoint of continuum mechanics.

2.2. FEM sources

In the introduction of a key contribution, Nour-Omid and Rankin [54] attribute the original concept of corotational procedures in FEM to Wempner [86] and Belytschko and Hsieh [7].

The idea of a CR frame attached to individual elements was introduced by Horrigmoe and Bergan [10,39,40]. This activity continued briskly under Bergan at NTH-Trondheim with contributions by Kråkeland [46], Nygård [15,56,57], Mathisen [48,49], Levold [47] and Bjærum [18]. It was summarized in a 1989 review paper [56]. Throughout this work the CR configuration is labeled as either "shadow element" or "ghost-reference." As previously noted the device is not mathematically necessary but provides a convenient visualization tool to explain CR. The shadow element functions as intermediary that separates rigid and deformational motions, the latter being used to determine the element energy and internal force. However the variation of the forces in a rotating frame was not directly used in the formation of the tangent stiffness, leading to a loss of consistency. Crisfield [22–24] developed the concept of "consistent CR formulation" where the stiffness matrix appears as the true variation of the internal force. An approach blending the TL, UL and CR descriptions was investigated in the mid-1980s at Chalmers [50–52].

In 1986 Rankin and Brogan [63] at Lockheed introduced the concept of "element independent CR formulation" or EICR, which is further discussed below. The formulation relies heavily on the use of projection operators, without explicit use of "shadow" configurations. It was further refined by Rankin, Nour-Omid and coworkers [54,64–67], and became essential part of the nonlinear shell analysis program STAGS [68].

The thesis of Haugen on nonlinear thin shell analysis [37] resulted in the development of the formulation discussed in this paper. This framework is able to generate a set of hierarchical CR formulations. The work combines tools from the EICR (projectors and spins) with the shadow element concept and assumed strain element formulations. Spins (instead of rotations) are used as incremental nodal freedoms. This simplifies the EICR "front end" and facilitates attaining consistency.

Battini and Pacoste at KTH-Stockholm [2,3,58] have recently used the CR approach, focusing on stability applications. The work by Teigen [79] should be cited for the careful use of offset nodes linked to element nodes by eccentricity vectors in the CR modeling of prestressed reinforced-concrete members.

2.3. Shadows of the past

The CR approach has also roots on an old idea that preceeds FEM by over a century: the separation of rigid body and purely deformational motions in continuum mechanics. The topic arose in theories of small strains superposed on large rigid motions. Truesdell [80, Section 55] traces the subject back to Cauchy in 1827. In the late 1930s Biot advocated the use of incremental deformations on an initially stressed body by using a truncated polar decomposition. However, this work, collected in a 1965 monograph [16], was largely ignored as it was written in an episodic manner, using long-hand notation by then out of fashion. A rigurous outline of the subject is given in [83, Section 68] but without application examples.

Technological applications of this idea surged after WWII from a different quarter: the aerospace industry. The rigid-plus-deformational decomposition idea for an *entire structure* was originally used by aerospace designers in the 1950s and 1960s in the context of dynamics and control of orbiting spacecraft as well as aircraft structures. The primary motivation was to trace the mean motion.

The approach was systematized by Fraeijs de Veubeke [25], in a paper that essentially closed the subject as regards handling of a complete structure. The motivation was clearly stated in the Introduction of that article, which appeared shortly before the author's untimely death:

> The formulation of the motion of a flexible body as a continuum through inertial space is unsatisfactory from several viewpoints. One is usually not interested in the details of this motion but in its main characteristics such as the motion of the center of mass and, under the assumptions that the deformations remain small, the history of the average orientation of the body. The last information is of course essential to pilots, real and artificial, in order to implement guidance corrections. We therefore try to define a set of Cartesian mean axes accompanying the body, or dynamic reference frame, with

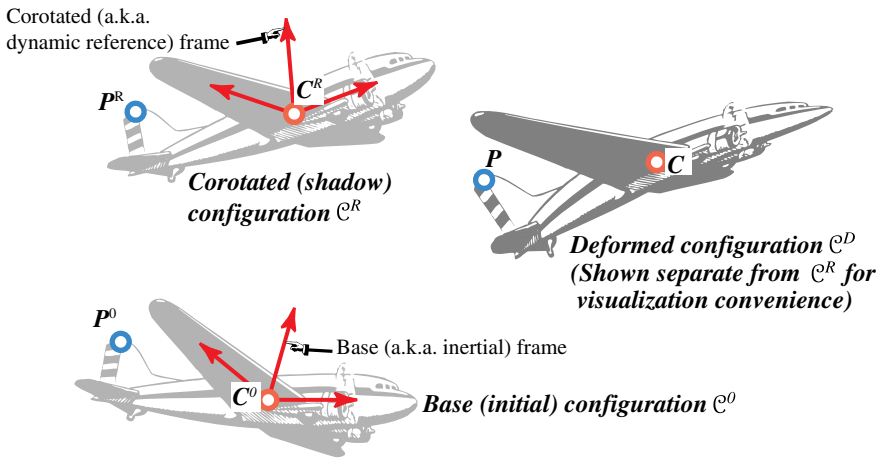

Fig. 2. The concept of separation of base (a.k.a. inertial) and CR (a.k.a. dynamic) configurations in aircraft dynamics. Deformed configuration (with deformations grossly exaggerated) shown separate from CR configuration for visibility. In reality points C and C_R coincide.

respect to which the relative displacements, velocities or accelerations of material points due to the deformations are minimum in some global sense. If the body does not deform, any set of axes fixed into the body is of course a natural dynamic reference frame.

Clearly the focus of this paper was on a whole structure, as illustrated in Fig. 2 for an airplane. This will be called the *shadowing problem*. A body moves to another position in space: find its mean rigid body motion and use this information to locate and orient a corotated Cartesian frame.

Posing the shadowing problem in three dimensions requires fairly advanced mathematics. Using two "best fit" criteria Fraeijs de Veubeke showed that the origin of the dynamic frame must remain at the center of mass of the displaced structure: C^R in Fig. 2. However, the orientation of this frame leads to an eigenvalue problem that may exhibit multiple solutions due to symmetries, leading to non uniqueness. (This is obvious by thinking of the polar and singular-value decompositions, which were not used in that article.) That this is not a rare occurrence is demonstrated by considering rockets, satellites or antennas, which often have axisymmetric shape.

Remark 1. Only $\mathscr{C}^D$ (shown in darker shade in Fig. 2) is an *actual* configuration taken by the pictured aircraft structure. Both reference configurations $\mathscr{C}^0$ and $\mathscr{C}^R$ are *virtual* in the sense that they are not generally occupied by the body at any instance. This is in contrast to the FEM version of this idea.

2.4. Linking FEM and CR

The practical extension of Fraeijs de Veubeke's idea to geometrically nonlinear structural analysis by FEM relies on two modifications:

1. *Multiple frames*. Instead of one CR frame for the whole structure, there is one per element. This is renamed the *CR element frame*.
2. *Geometric-based RBM separation*. The rigid body motion is separated directly from the total element motion using elementary geometric methods. For example in a 2-node bar or beam one axis is defined by the displaced nodes, while for a 3-node triangle two axes are defined by the plane passing through the three corners. See Fig. 3.

The first modification is essential to success. It helps to fulfill assumption (1): the element deformational displacements and rotations remain *small* with respect to the CR frame. If this assumption is violated for a coarse discretization, break it into more elements. Small deformations are the key to *element reuse* in the EICR discussed below. If intrinsically large strains occur, however, the breakdown prescription fails. In that case CR offers no advantages over TL or UL.

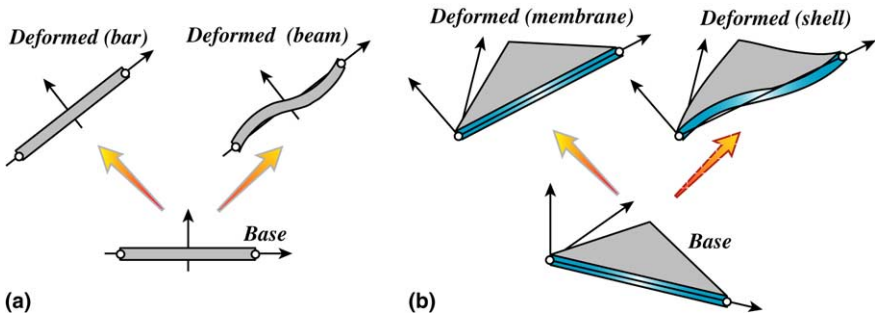

Fig. 3. Geometric tracking of CR frame: (a) bar or beam element in 2D and (b) membrane or shell element in 3D.

The second modification is inessential. Its purpose is to speed up the implementation of geometrically simple elements. The CR frame determination may be refined later, using more advanced tools such as polar decomposition and best-fit criteria, if warranted.

Remark 2. CR is occassionally confused with the *convected-coordinate* description of motion, which is used in branches of fluid mechanics and rheology. Both may be subsumed within the class of *moving coordinate* kinematic descriptions. The CR description, however, *maintains orthogonality* of the moving frame(s) thus achieving an exact decomposition of rigid-body and deformational motions. This property enhances computational efficiency, since transformation inverses become transposes. On the other hand, convected coordinates form a curvilinear system that "fits" the change of metric as the body deforms. The difference tends to disappear as the discretization becomes progressively finer, but the fact remains that the convected metric must encompass deformations. Such deformations are more important in solid than in fluid mechanics (because classical fluid models "forget" displacements). The idea finds more use in UL descriptions, in which the individual element metric is updated as the motion progresses.

2.5. Element independent CR

As previously noted, one of the sources of the present work is the element-independent corotational (EICR) description developed by Rankin and coworkers [54,63–67]. Here is a summary description taken from the Introduction to [54]:

> In the co-rotation approach, the deformational part of the displacement is extracted by purging the rigid body components before any element computation is performed. This pre-processing of the displacements may be performed outside the standard element routines and thus is independent of element type (except for slight distinctions between beams, triangular and quadrilateral elements).

Why is the EICR worth study? The question fits in a wider topic: why CR? That is, what can CR do that TL or UL cannot? The topic is elaborated in the Conclusions section, but we advance a practical reason: *reuse of small-strain elements*, including possibly *materially nonlinear* elements.

The qualifier *element independent* does not imply that the CR equations are independent of the FEM discretization. Rather it emphasizes that the key operations of adding and removing rigid body motions can be visualized as a *front end filter* that lies between the assembler/solver and the element library, as

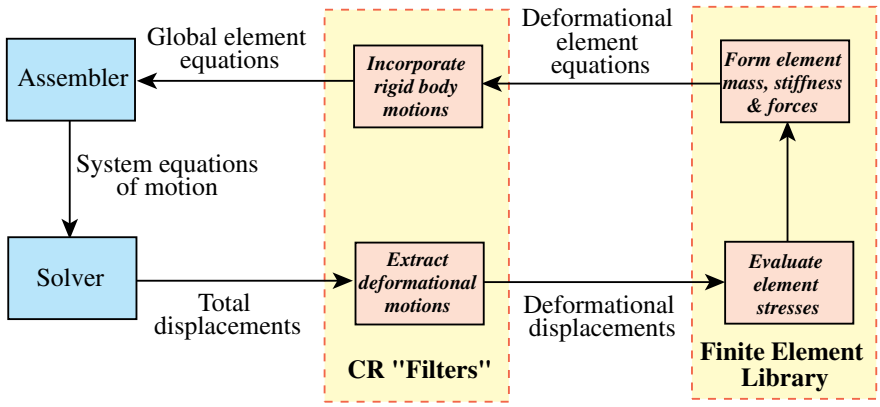

Fig. 4. The EICR as a modular interface to a linear FEM library. The flowchart is mainly conceptual. For computational efficiency the interface logic may be embedded with each element through inlining techniques.

sketched in Fig. 4. The filter is purely geometric. For example, suppose that a program has four different triangular shell elements with the same node and degree-of-freedom configuration. Then the front end operations are identical for all four. Adding a fifth small-strain element of this type incurs relatively little extra work to "make it geometrically nonlinear."

This modular organization is of interest because it implies that the element library of an existing FEM program being converted to the CR description need not be drastically modified, *as long as the analysis is confined to small deformations*. Since that library is typically the most voluminous and expensive part of a production FEM code, *element reuse* is a key advantage because it protects a significant investment. For a large-scale commercial code, the investment may be thousands of man-years.

Of course modularity and computational efficiency can be conflicting attributes. Thus in practice the front end logic may be embedded with each element through techniques such as code inlining. If so the flowchart of Fig. 4 should be interpreted as conceptual.

3. Corotational kinematics

This section outlines CR kinematics of finite elements, collecting the most important relations. Mathematical derivations pertaining to finite rotations are consigned to Appendix A. The presentation assumes static analysis, with deviations for dynamics briefly noted where appropriate.

3.1. Configurations

To describe Lagrangian kinematics it is convenient to introduce a rich nomenclature for configurations. For the reader's convenience those used in geometrically nonlinear static analysis using the TL, UL or CR descriptions are collected in Table 1. Three: base, corotated and deformed, have already been introduced. Two more: iterated and target, are connected to the incremental-iterative solution process covered in Part II [38]. The generic configuration is used as placeholder for any kinematically admissible one. The perturbed configuration is used in variational derivations of FEM equations.

Two remain: reference and globally-aligned. The *reference configuration* is that to which element computations are referred. This depends on the description chosen. For Total Lagrangian (TL) the reference is the base configuration. For Updated Lagrangian (UL) it is the converged or accepted solution of the previous increment. For corotational (CR) the reference splits into CR and base configurations.

The *globally-aligned configuration* is a special corotated configuration: a rigid motion of the base that makes the body or element align with the global axes introduced below. This is used as a "connector" device to teach the CR description, and does not imply the body ever occupies that configuration.

The separation of rigid and deformational components of motion is done at the element level. As noted previously, techniques for doing this have varied according to the taste and background of the investigators that developed those formulations. The approach covered here uses shadowing and projectors.

3.2. Coordinate systems

A typical finite element, undergoing 2D motion to help visualization, is shown in Fig. 5. This diagram as well as that of Fig. 6 introduces kinematic quantities. For the most part the notation follows that used by Haugen [37], with subscripting changes.

Configurations taken by the element during the response analysis are linked by a Cartesian *global frame*, to which all computations are ultimately referred. There are actually two such frames: the *material global frame* with axes $\{X_i\}$ and position vector $\mathbf{X}$, and the *spatial global frame* with axes $\{x_i\}$ and position vector $\mathbf{x}$. The material frame tracks the base configuration whereas the spatial frame tracks the CR and deformed

Table 1
Configurations in nonlinear static analysis by incremental-iterative methods

Name	Alias	Explanation	Equilibrium required?	Identification
Generic	Admissible	A kinematically admissible configuration	No	$\mathscr{C}$
Perturbed		Kinematically admissible variation of a generic configuration	No	$\mathscr{C}+\delta\mathscr{C}$
Deformed	Current Spatial	Actual configuration taken during the analysis process Contains others as special cases	No	$\mathscr{C}^D$
Base[a]	Initial Undeformed Material	The configuration defined as the origin of displacements	Yes	$\mathscr{C}^0$
Reference		Configuration to which computations are referred	TL,UL: Yes. CR: $\mathscr{C}^R$ no, $\mathscr{C}^0$ yes	TL: $\mathscr{C}^0$, UL: $\mathscr{C}^{n-1}$, CR: $\mathscr{C}^R$ and $\mathscr{C}^0$
Iterated[b]		Configuration taken at the kth iteration of the nth increment step	No	$\mathscr{C}^n_k$
Target[b]		Equilibrium configuration accepted	Yes	$\mathscr{C}^n$ at the nth increment step
Corotated[c]	Shadow Ghost	Body or element-attached configuration obtained from $\mathscr{C}^0$ through a rigid body motion (CR description only)	No	$\mathscr{C}^R$
Globally-aligned	Connector	Corotated configuration forced to align With the global axes. Used as "connector" in explaining the CR description	No	$\mathscr{C}^G$

[a] $\mathscr{C}^0$ is often the same as the *natural state* in which body (or element) is undeformed and stress-free.
[b] Used only in Part II [38] in the description of solution procedures.
[c] In dynamic analysis $\mathscr{C}^0$ and $\mathscr{C}^R$ are called the inertial and dynamic-reference configurations, respectively, when they apply to the entire structure.

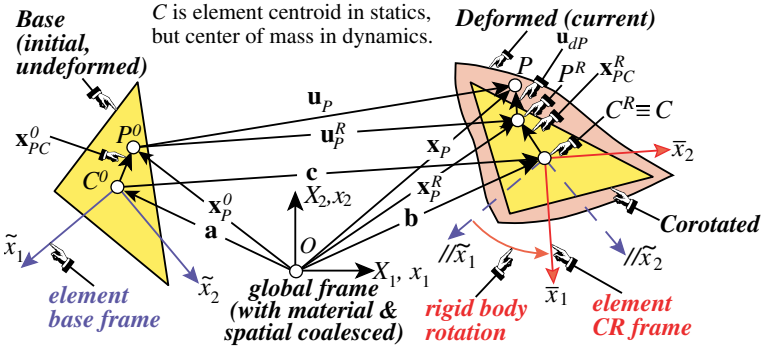

Fig. 5. CR element kinematics, focusing on the motion of generic point P. Two-dimensional kinematics pictured for visualization convenience.

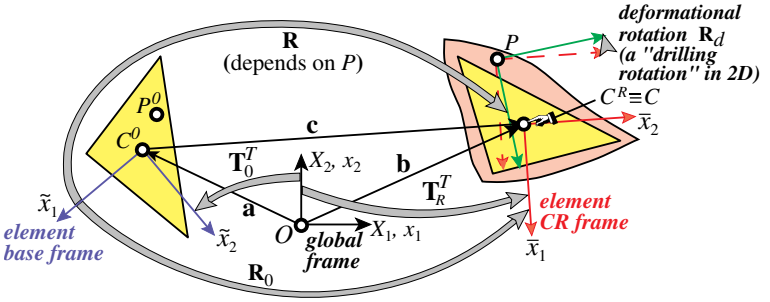

Fig. 6. CR element kinematics, focusing on rotational transformation between frames.

(current) configurations. The distinction agrees with the usual conventions of dual-tensor continuum mechanics [81, Section 13]. Here both frames are taken to be *identical*, since for small strains nothing is gained by separating them (as is the case, for example, in the TL description). Thus only one set of global axes, with dual labels, is drawn in Figs. 5 and 6.

Lower case coordinate symbols such as $\mathbf{x}$ are used throughout most of the paper. Occasionally it is convenient for clarity to use upper case coordinates for the base configuration, as in Appendix C.

The global frame is the same for all elements. By contrast, each element e is assigned two local Cartesian frames, one fixed and one moving:

$\{\tilde{x}_i\}$. The element *base frame* (blue in Fig. 5). It is oriented by three unit base vectors $\mathbf{i}_i^0$, which are rows of a 3×3 orthogonal rotation matrix (rotator) $\mathbf{T}_0$, or equivalently columns of $\mathbf{T}_0^{\mathrm{T}}$.

$\{\bar{x}_i\}$. The element *corotated or CR frame* (red in Fig. 5). It is oriented by three unit base vectors $\mathbf{i}_i^R$, which are rows of a 3×3 orthogonal rotation matrix (rotator) $\mathbf{T}_R$, or equivalently columns of $\mathbf{T}_R^{\mathrm{T}}$.

Note that the element index e has been suppressed to reduced clutter. That convention will be followed throughout unless identification with elements is important. In that case e is placed as superscript.

The base frame $\{\tilde{x}_i\}$ is chosen according to usual FEM practices. For example, in a 2-node spatial beam element, $\tilde{x}_1$ is defined by the two end nodes whereas $\tilde{x}_2$ and $\tilde{x}_3$ lie along principal inertia directions. An important convention, however, is that the origin is always placed at the element centroid C^0. For each deformed (current) element configuration, a fitting of the base element defines its CR configuration, also known as the element "shadow". Centroids C^R and $C\equiv C^D$ coincide. The CR frame $\{\bar{x}_i\}$ originates at C^R. Its orientation results from matching a rigid motion of the base frame, as discussed later. When the

current element configuration reduces to the base at the start of the analysis, the base and CR frames coalesce: $\{\tilde{x}_i \equiv \bar{x}_i\}$. At that moment there are only two different frames: global and local, which agrees with linear FEM analysis.

Notational conventions: use of G, 0, R and D as superscripts or subscripts indicate pertinence to the globally-aligned, base, corotated and deformed configurations, respectively. Symbols with a overtilde or overbar are measured to the base frame $\{\tilde{x}_i\}$ or the CR frame $\{\bar{x}_i\}$, respectively. Vectors without a superposed symbol are referred to global coordinates $\{x_i \equiv x_i\}$. Examples: $\mathbf{x}^R$ denote global coordinates of a point in $\mathscr{C}^R$ whereas $\tilde{\mathbf{x}}^G$ denote base coordinates of a point in $\mathscr{C}^G$. Symbols $\mathbf{a}$, $\mathbf{b}$ and $\mathbf{c} = \mathbf{b} - \mathbf{a}$ are abbreviations for the centroidal translations depicted in Fig. 5, and more clearly in Fig. 7(b). A generic, coordinate-free vector is denoted by a superposed arrow, for example $\vec{\mathbf{u}}$, but such entities rarely appear in this work.

The rotators $\mathbf{T}_0$ and $\mathbf{T}_R$ are the well known local-to-global displacement transformations of FEM analysis. Given a global displacement $\mathbf{u}$, $\tilde{\mathbf{u}} = \mathbf{T}_0\mathbf{u}$ and $\bar{\mathbf{u}} = \mathbf{T}_R\mathbf{u}$.

3.3. Coordinate transformations

Figs. 5 and 6, although purposedly restricted to 2D, are still too busy. Fig. 7, which pictures the 2D motion of a bar in three frames, displays essentials better. The (fictitious) globally-aligned configuration $\mathscr{C}^G$ is explicitly shown. This helps to follow the ensuing sequence of geometric relations.

Begin with a generic point $\mathbf{x}^G$ in $\mathscr{C}^G$. This point is mapped to global coordinates $\mathbf{x}^0$ and $\mathbf{x}^R$ in the base and corotated configurations $\mathscr{C}^0$ and $\mathscr{C}^R$, respectively, through

$$\mathbf{x}^0 = \mathbf{T}_0^{\mathrm{T}}\mathbf{x}^G + \mathbf{a}, \quad \mathbf{x}^R = \mathbf{T}_R^{\mathrm{T}}\mathbf{x}^G + \mathbf{b}, \tag{2}$$

in which rotators $\mathbf{T}_0$ and $\mathbf{T}_R$ were introduced in the previous subsection. To facilitate code checking, for the 2D motion pictured in Fig. 7(b) the global rotators are

$$\mathbf{T}_0 = \begin{bmatrix} c_0 & s_0 & 0 \\ -s_0 & c_0 & 0 \\ 0 & 0 & 1 \end{bmatrix}, \quad \mathbf{T}_R = \begin{bmatrix} c_R & s_R & 0 \\ -s_R & c_R & 0 \\ 0 & 0 & 1 \end{bmatrix}, \quad c_0 = \cos\varphi_0, \quad s_0 = \sin\varphi_0, \quad \text{etc.} \tag{3}$$

When (2) are transformed to the base and corotated frames, the position vector $\mathbf{x}^G$ must repeat: $\tilde{\mathbf{x}}^0 = \mathbf{x}^G$ and $\bar{\mathbf{x}}^R = \mathbf{x}^G$, because the motion pictured in Fig. 7(a) is rigid. This condition requires

$$\tilde{\mathbf{x}}^0 = \mathbf{T}_0(\mathbf{x}^0 - \mathbf{a}), \quad \bar{\mathbf{x}}^R = \mathbf{T}_R(\mathbf{x}^R - \mathbf{b}). \tag{4}$$

These may be checked by inserting $\mathbf{x}^0$ and $\mathbf{x}^R$ from (2) and noting that $\mathbf{x}^G$ repeats.

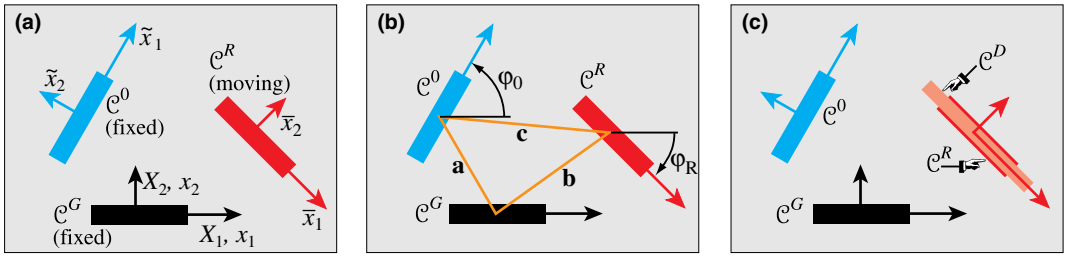

Fig. 7. Further distillation to essentials of Fig. 5. A bar moving in 2D is shown: (a) Rigid motion from globally-aligned to base and corotated configurations; (b) key geometric quantities that define rigid motions in 2D; (c) as in (a) but followed by a stretch from corotated to deformed. The globally-aligned configuration is fictitious: only a convenient link up device.

3.4. Rigid displacements

The rigid displacement is a vector joining corresponding points in $\mathscr{C}^0$ and $\mathscr{C}^R$. This may be referred to the global, base or corotated frames. For convenience call the $\mathscr{C}^0 \to \mathscr{C}^R$ rotator $\mathbf{R}_0 = \mathbf{T}_R^{\mathrm{T}}\mathbf{T}_0$. Also introduce $\tilde{\mathbf{c}} = \mathbf{T}_0^{\mathrm{T}}\mathbf{c}$ and $\bar{\mathbf{c}} = \mathbf{T}_R^{\mathrm{T}}\mathbf{c}$. Some useful expressions are

$$\begin{aligned}
\mathbf{u}_{\mathrm{r}} &= \mathbf{x}^R - \mathbf{x}^0 = (\mathbf{T}_R^{\mathrm{T}} - \mathbf{T}_0^{\mathrm{T}})\mathbf{x}^G + \mathbf{c} = (\mathbf{R}_0 - \mathbf{I})\mathbf{T}_0^{\mathrm{T}}\mathbf{x}^G + \mathbf{c} = (\mathbf{R}_0 - \mathbf{I})\mathbf{T}_0^{\mathrm{T}}\tilde{\mathbf{x}}^0 + \mathbf{c} \\
&= (\mathbf{R}_0 - \mathbf{I})\mathbf{T}_0^{\mathrm{T}}\bar{\mathbf{x}}^R + \mathbf{c} = (\mathbf{R}_0 - \mathbf{I})(\mathbf{x}^0 - \mathbf{a}) + \mathbf{c} = (\mathbf{I} - \mathbf{R}_0^{\mathrm{T}})(\mathbf{x}^R - \mathbf{b}) + \mathbf{c}, \\
\tilde{\mathbf{u}}_{\mathrm{r}} &= \mathbf{T}_0\mathbf{u}_{\mathrm{r}} = \mathbf{T}_0(\mathbf{R}_0 - \mathbf{I})\mathbf{T}_0^{\mathrm{T}}\tilde{\mathbf{x}}^0 + \tilde{\mathbf{c}} = (\widetilde{\mathbf{R}}_0 - \mathbf{I})\tilde{\mathbf{x}}^0 + \tilde{\mathbf{c}}, \\
\bar{\mathbf{u}}_{\mathrm{r}} &= \mathbf{T}_R\mathbf{u}_{\mathrm{r}} = \mathbf{T}_R(\mathbf{I} - \mathbf{R}_0^{\mathrm{T}})\mathbf{T}_R^{\mathrm{T}}\bar{\mathbf{x}}^R + \bar{\mathbf{c}} = (\mathbf{I} - \overline{\mathbf{R}}_0^{\mathrm{T}})\bar{\mathbf{x}}^R + \bar{\mathbf{c}}.
\end{aligned} \tag{5}$$

Here $\mathbf{I}$ is the 3×3 identity matrix, whereas $\widetilde{\mathbf{R}}_0 = \mathbf{T}_0\mathbf{R}_0\mathbf{T}_0^{\mathrm{T}}$ and $\overline{\mathbf{R}}_0 = \mathbf{T}_R\mathbf{R}_0\mathbf{T}_R^{\mathrm{T}}$ denote the $\mathscr{C}^0 \to \mathscr{C}^R$ rotator referred to the base and corotated frames, respectively.

3.5. Rotator formulas

Traversing the links pictured in Fig. 8 shows that any rotator can be expressed in terms of the other two

$$\mathbf{T}_0 = \mathbf{T}_R\mathbf{R}_0, \mathbf{T}_R = \mathbf{T}_0\mathbf{R}_0^{\mathrm{T}},\ \mathbf{R}_0 = \mathbf{T}_R^{\mathrm{T}}\mathbf{T}_0,\ \mathbf{R}_0^{\mathrm{T}} = \mathbf{T}_0^{\mathrm{T}}\mathbf{T}_R. \tag{6}$$

In the CR frame: $\overline{\mathbf{R}}_0 = \mathbf{T}_R\mathbf{R}_0\mathbf{T}_R^{\mathrm{T}}$, whence

$$\overline{\mathbf{R}}_0 = \mathbf{T}_0\mathbf{T}_R^{\mathrm{T}}, \quad \overline{\mathbf{R}}_0^{\mathrm{T}} = \mathbf{T}_R\mathbf{T}_0^{\mathrm{T}}. \tag{7}$$

Notice that $\mathbf{T}_0$ is fixed since $\mathscr{C}^G$ and $\mathscr{C}^0$ are fixed throughout the analysis, whereas $\mathbf{T}_R$ and $\mathbf{R}_0$ change. The variations of these rotators are subjected to the following constraints:

$$\begin{aligned}
&\delta\mathbf{T}_0 = \delta\mathbf{T}_0^{\mathrm{T}} = \mathbf{0}, \quad \delta\mathbf{T}_R = \mathbf{T}_0\delta\mathbf{R}_0^{\mathrm{T}}, \quad \delta\mathbf{T}_R^{\mathrm{T}} = \delta\mathbf{R}_0\mathbf{T}_0^{\mathrm{T}}, \quad \delta\mathbf{R}_0 = \delta\mathbf{T}_R^{\mathrm{T}}\mathbf{T}_0, \\
&\delta\mathbf{R}_0^{\mathrm{T}} = \mathbf{T}_0^{\mathrm{T}}\delta\mathbf{T}_R, \quad \mathbf{T}_R^{\mathrm{T}}\delta\mathbf{T}_R + \delta\mathbf{T}_R^{\mathrm{T}}\mathbf{T}_R = \mathbf{0}, \quad \mathbf{R}_0^{\mathrm{T}}\delta\mathbf{R}_0 + \delta\mathbf{R}_0^{\mathrm{T}}\mathbf{R}_0 = \mathbf{0}.
\end{aligned} \tag{8}$$

The last two become the orthogonality conditions $\mathbf{T}_R^{\mathrm{T}}\mathbf{T}_R = \mathbf{I}$ and $\mathbf{R}_0^{\mathrm{T}}\mathbf{R}_0 = \mathbf{I}$, respectively, and provide $\delta\mathbf{R}_0 = -\mathbf{R}_0\delta\mathbf{R}_0^{\mathrm{T}}\mathbf{R}_0$, $\delta\mathbf{R}_0^{\mathrm{T}} = -\mathbf{R}_0^{\mathrm{T}}\delta\mathbf{R}_0\mathbf{R}_0^{\mathrm{T}}$, etc.

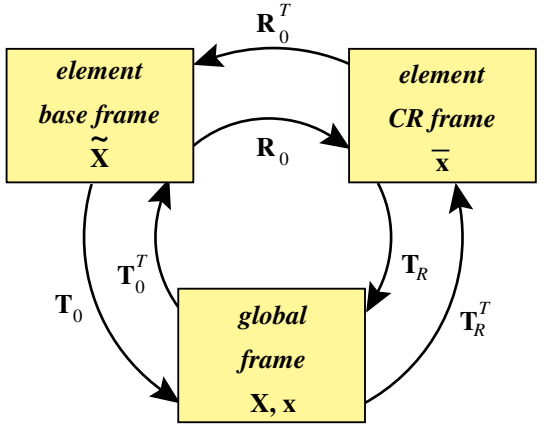

Fig. 8. Rotator frame links.

We denote by $\boldsymbol{\omega}$ and $\bar{\boldsymbol{\omega}}$ the axial vectors of $\mathbf{R}_0$ and $\overline{\mathbf{R}}_0$, respectively, using the exponential map form of the rotator described in Section A.10. The variations $\delta\boldsymbol{\omega}$ and $\delta\bar{\boldsymbol{\omega}}$ are used to form the skew-symmetric spin matrices $\mathrm{Spin}(\delta\boldsymbol{\omega}) = \delta\mathbf{R}_0\,\mathbf{R}_0^{\mathrm{T}} = -\mathrm{Spin}(\delta\boldsymbol{\omega})^{\mathrm{T}}$ and $\mathrm{Spin}(\delta\bar{\boldsymbol{\omega}}) = \delta\overline{\mathbf{R}}_0\overline{\mathbf{R}}_0^{\mathrm{T}} = -\mathrm{Spin}(\delta\bar{\boldsymbol{\omega}})^{\mathrm{T}}$. These matrices are connected by congruential transformations:

$$\mathrm{Spin}(\delta\boldsymbol{\omega}) = \mathbf{T}_0^{\mathrm{T}}\mathrm{Spin}(\delta\bar{\boldsymbol{\omega}})\mathbf{T}_0, \quad \mathrm{Spin}(\delta\bar{\boldsymbol{\omega}}) = \mathbf{T}_0\mathrm{Spin}(\delta\boldsymbol{\omega})\mathbf{T}_0^{\mathrm{T}}. \tag{9}$$

Using these relations the following catalog of rotator variation formulas can be assembled:

$$\begin{aligned}
\delta\mathbf{T}_R &= \mathbf{T}_0\delta\mathbf{R}_0^{\mathrm{T}} = -\mathbf{T}_R\delta\mathbf{R}_0\mathbf{R}_0^{\mathrm{T}} = -\mathbf{T}_R\mathrm{Spin}(\delta\boldsymbol{\omega}) = -\mathbf{R}_0^{\mathrm{T}}\mathrm{Spin}(\delta\bar{\boldsymbol{\omega}})\mathbf{T}_0,\\
\delta\mathbf{T}_R^{\mathrm{T}} &= \delta\mathbf{R}_0\mathbf{T}_0^{\mathrm{T}} = -\mathbf{R}_0\delta\mathbf{R}_0^{\mathrm{T}}\mathbf{T}_R^{\mathrm{T}} = \mathrm{Spin}(\delta\boldsymbol{\omega})\mathbf{T}_R^{\mathrm{T}} = \mathbf{T}_0^{\mathrm{T}}\mathrm{Spin}(\delta\bar{\boldsymbol{\omega}})\mathbf{R}_0.\\
\delta\mathbf{R}_0 &= \delta\mathbf{T}_R^{\mathrm{T}}\mathbf{T}_0 = -\mathbf{R}_0\delta\mathbf{R}_0^{\mathrm{T}}\mathbf{R}_0 = \mathrm{Spin}(\delta\boldsymbol{\omega})\mathbf{R}_0 = \mathbf{T}_0^{\mathrm{T}}\mathrm{Spin}(\delta\bar{\boldsymbol{\omega}})\overline{\mathbf{R}}_0\mathbf{T}_0,\\
\delta\mathbf{R}_0^{\mathrm{T}} &= \mathbf{T}_0^{\mathrm{T}}\delta\mathbf{T}_R = -\mathbf{R}_0^{\mathrm{T}}\delta\mathbf{R}_0\mathbf{R}_0^{\mathrm{T}} = -\mathbf{R}_0^{\mathrm{T}}\mathrm{Spin}(\delta\boldsymbol{\omega}) = -\mathbf{T}_0^{\mathrm{T}}\overline{\mathbf{R}}_0^{\mathrm{T}}\mathrm{Spin}(\delta\bar{\boldsymbol{\omega}})\mathbf{T}_0,\\
\delta\overline{\mathbf{R}}_0 &= \mathbf{T}_0\delta\mathbf{R}_0\mathbf{T}_0^{\mathrm{T}} = -\mathbf{T}_0\mathbf{R}_0\delta\mathbf{R}_0^{\mathrm{T}}\mathbf{T}_R^{\mathrm{T}} = \mathbf{T}_0\mathrm{Spin}(\delta\boldsymbol{\omega})\mathbf{T}_R^{\mathrm{T}} = \mathrm{Spin}(\delta\bar{\boldsymbol{\omega}})\overline{\mathbf{R}}_0,\\
\delta\overline{\mathbf{R}}_0^{\mathrm{T}} &= \mathbf{T}_0\delta\mathbf{R}_0^{\mathrm{T}}\mathbf{T}_0^{\mathrm{T}} = -\mathbf{T}_R\delta\mathbf{R}_0\mathbf{R}_0^{\mathrm{T}}\mathbf{T}_0^{\mathrm{T}} = -\mathbf{T}_R\mathrm{Spin}(\delta\boldsymbol{\omega})\mathbf{T}_0^{\mathrm{T}} = -\overline{\mathbf{R}}_0^{\mathrm{T}}\mathrm{Spin}(\delta\bar{\boldsymbol{\omega}}).
\end{aligned} \tag{10}$$

3.6. Degrees of freedom

For simplicity it will be assumed that an N^e-node CR element has *six degrees of freedom* (DOF) *per node*: three translations and three rotations. This assumption covers the shell and beam elements evaluated in Part II [38]. The geometry of the element is defined by the N^e coordinates $\mathbf{x}_a^0$, $a = 1, \ldots, N^e$ in the base (initial) configuration, where a is a node index.

The notation used for DOFs at the structure and element level is collected in Table 2. If the structure has N nodes, the set $\{\mathbf{u}_a, \mathbf{R}_a\}$ for $a = 1, \ldots, N$ collectively defines the structure node displacement vector $\mathbf{v}$. Note, however, that $\mathbf{v}$ is not a vector in the usual sense because the rotators $\mathbf{R}_a$ do not transform as vectors when finite rotations are considered. The interpretation as an array of numbers that defines the deformed configuration of the structure is more appropriate.

The element total node displacements $\mathbf{v}^e$ are taken from $\mathbf{v}$ in the usual manner. Given $\mathbf{v}^e$, the key CR operation is to extract the deformational components of the translations and rotations for each node. That sequence of operations is collected in Table 3. Note that the computation of the centroid is done by simply

Table 2
Degree of Freedom and Conjugate Force Notation

Notation	Frame	Level	Description
$\hat{\mathbf{v}} = [\,\hat{\mathbf{v}}_1 \quad \cdots \quad \hat{\mathbf{v}}_N\,]^{\mathrm{T}}$ with $\hat{\mathbf{v}}_a = \begin{bmatrix}\mathbf{u}_a\\ \mathbf{R}_a\end{bmatrix}$	Global	Structure	Total displacements and rotations at structure nodes Translations: $\mathbf{u}_a$, rotations: $\mathbf{R}_a$, for $a = 1, \ldots, N$
$\delta\mathbf{v} = [\,\delta\mathbf{v}_1 \quad \cdots \quad \delta\mathbf{v}_N\,]^{\mathrm{T}}$ with $\delta\mathbf{v}_a = \begin{bmatrix}\delta\mathbf{u}_a\\ \delta\boldsymbol{\omega}_a\end{bmatrix}$	Global	Structure	Incremental displacements and spins at structure nodes used in incremental-iterative solution procedure Translations: $\delta\mathbf{u}_a$, spins: $\delta\boldsymbol{\omega}_a$; conjugate forces: $\mathbf{n}_a$ and $\mathbf{m}_a$, respectively, for $a = 1, \ldots, N$
$\delta\bar{\mathbf{v}}^e = [\,\delta\bar{\mathbf{v}}_1^e \quad \cdots \quad \delta\bar{\mathbf{v}}_{N^e}^e\,]^{\mathrm{T}}$ with $\delta\bar{\mathbf{v}}_a^e = \begin{bmatrix}\delta\bar{\mathbf{u}}_a^e\\ \delta\bar{\boldsymbol{\omega}}_a^e\end{bmatrix}$	Local CR	Element	Localization of above to element e in CR frame Translations: $\delta\bar{\mathbf{u}}_a^e$, spins: $\delta\bar{\boldsymbol{\omega}}_a^e$; conjugate forces: $\bar{\mathbf{n}}_a^e$ and $\bar{\mathbf{m}}_a^e$, respectively, for $a = 1, \ldots, N^e$
$\bar{\mathbf{v}}_{\mathrm{d}}^e = [\,\bar{\mathbf{v}}_{\mathrm{d}1}^e \quad \cdots \quad \bar{\mathbf{v}}_{\mathrm{d}N^e}^e\,]^{\mathrm{T}}$ with $\bar{\mathbf{v}}_{\mathrm{d}a}^e = \begin{bmatrix}\bar{\mathbf{u}}_{\mathrm{d}a}^e\\ \bar{\boldsymbol{\theta}}_{\mathrm{d}a}^e\end{bmatrix}$	Local CR	Element	Deformational displacements and rotations at element nodes Translations: $\bar{\mathbf{u}}_{\mathrm{d}a}^e$, rotations: $\bar{\boldsymbol{\theta}}_{\mathrm{d}a}^e$; conjugate forces: $\bar{\mathbf{n}}_a$ and $\bar{\mathbf{m}}_a$, respectively, for $a = 1, \ldots, N^e$

N = number of nodes in structure; N^e = number of nodes in element e; a, b: node indices.

Table 3
Forming the deformational displacement vector

Step	Operation for each element e and node $a = 1, \ldots, a$
1.	From the initial global nodal coordinates $\mathbf{x}_a^e$ compute centroid position $\mathbf{a}^e = \mathbf{x}_{C0}^e = (1/N^e)\sum_{a=1}^{N^e}\mathbf{x}_a^e$. Form rotator $\mathbf{T}_0^e$ as per element type convention Compute node coordinates in the element base frame: $\tilde{\mathbf{x}}_a^e = \mathbf{T}_0^e(\mathbf{x}_a^e - \mathbf{a}^e)$
2.	Compute node coordinates in deformed (current) configuration: $\mathbf{x}_a^e = \mathbf{x}_a^e + \mathbf{u}_a^e$ and the centroid position vector $\mathbf{b}^e = \mathbf{x}_C^e = (1/N^e)\sum_{a=1}^{N^e}\mathbf{x}_a^e$. Establish the deformed local CR system $\mathbf{T}^e$ by a best-fit procedure, and $\mathbf{R}_0^e = \mathbf{T}^e(\mathbf{T}_0^e)^{\mathrm{T}}$. Form local-CR node coordinates of CR configuration: $\bar{\mathbf{x}}_{Ra}^e = \mathbf{T}^e(\mathbf{x}_a^e - \mathbf{b}^e)$
3.	Compute the deformational translations $\bar{\mathbf{u}}_{\mathrm{d}a} = \bar{\mathbf{x}}_a^e - \bar{\mathbf{x}}_{Ra}^e$. $\mathbf{R}_{\mathrm{d}} = \mathbf{T}_n\mathbf{R}_a\mathbf{T}_0^{\mathrm{T}}$ Compute the deformational rotator $\overline{\mathbf{R}}_{\mathrm{d}a}^e = \mathbf{T}^e\mathbf{R}_a^e(\mathbf{T}_0^e)^{\mathrm{T}}$. Extract the deformational angles $\bar{\theta}_{\mathrm{d}a}^e$ from the axial vector of $\overline{\mathbf{R}}_{\mathrm{d}a}^e$

averaging the coordinates of the element nodes. For 2-node beams and 3-node triangles this is appropriate. For 4-node quadrilaterals this average does not generally coincides with the centroid, but this has made little difference in actual computations.

3.7. EICR matrices

Before studying element deformations, it is convenient to introduce several auxiliary matrices: $\mathbf{P} = \mathbf{P}_u - \mathbf{P}_\omega$, $\mathbf{S}$, $\mathbf{G}$, $\mathbf{H}$ and $\mathbf{L}$, which appear in expressions of the EICR front-end. As noted, elements treated here possess N^e nodes and six degrees of freedom (DOF) per node. The notation and arrangement used for DOFs at different levels is defined in Table 2. Subscripts a and b denote node indices that run from 1 to N^e. All EICR matrices are built node-by-node from node-level blocks. Fig. 9(a) illustrates the concept of perturbed configuration $\mathscr{C}^D + \delta\mathscr{C}$, whereas Fig. 9(b) is used for examples. The CR and deformed configuration are "frozen"; the latter being varied in the sense of variational calculus.

The *translational projector matrix* $\mathbf{P}_u$ or simply *T-projector* is dimensioned $6N^e \times 6N^e$. It is built from 3×3 numerical submatrices $\mathbf{U}_{ab} = (\delta_{ab} - 1/N^e)\mathbf{I}$, in which $\mathbf{I}$ is the 3×3 identity matrix and δ_{ab} the Kronecker delta. Collecting blocks for all N^e nodes and completing with 3×3 zero and identity blocks

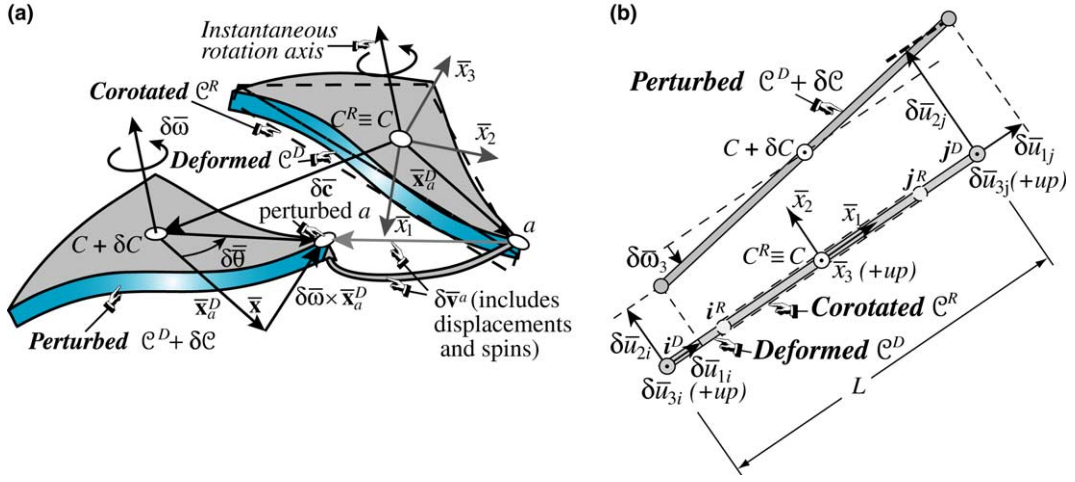

Fig. 9. Concept of perturbed configuration to illustrate derivation of EICR matrices: (a) facet triangular shell element moving in 3D space; (b) 2-node bar element also in 3D but depicted in the $\{\bar{x}_1, \bar{x}_2\}$ plane of its CR frame. Deformations grossly exaggerated for visualization convenience; strains and local rotations are in fact infinitesimal.

as placeholders for the spins and rotations gives a $6N^e \times 6N^e$ matrix $\mathbf{P}_u$. Its configuration is illustrated below for $N^e = 2$ (e.g., bar, beam, spar and shaft elements) and $N^e = 3$ (e.g., triangular shell elements)

$$N_e = 2: \ \mathbf{P}_u = \begin{bmatrix} \frac{1}{2}\mathbf{I} & \mathbf{0} & -\frac{1}{2}\mathbf{I} & \mathbf{0} \\ \mathbf{0} & \mathbf{I} & \mathbf{0} & \mathbf{0} \\ -\frac{1}{2}\mathbf{I} & \mathbf{0} & \frac{1}{2}\mathbf{I} & \mathbf{0} \\ \mathbf{0} & \mathbf{0} & \mathbf{0} & \mathbf{I} \end{bmatrix}, \quad N_e = 3: \ \mathbf{P}_u = \begin{bmatrix} \frac{2}{3}\mathbf{I} & \mathbf{0} & -\frac{1}{3}\mathbf{I} & \mathbf{0} & -\frac{1}{3}\mathbf{I} & \mathbf{0} \\ \mathbf{0} & \mathbf{I} & \mathbf{0} & \mathbf{0} & \mathbf{0} & \mathbf{0} \\ -\frac{1}{3}\mathbf{I} & \mathbf{0} & \frac{2}{3}\mathbf{I} & \mathbf{0} & -\frac{1}{3}\mathbf{I} & \mathbf{0} \\ \mathbf{0} & \mathbf{0} & \mathbf{0} & \mathbf{I} & \mathbf{0} & \mathbf{0} \\ -\frac{1}{3}\mathbf{I} & \mathbf{0} & -\frac{1}{3}\mathbf{I} & \mathbf{0} & \frac{2}{3}\mathbf{I} & \mathbf{0} \\ \mathbf{0} & \mathbf{0} & \mathbf{0} & \mathbf{0} & \mathbf{0} & \mathbf{I} \end{bmatrix}. \tag{11}$$

For any $N^e \geqslant 1$ it is easy to verify that $\mathbf{P}_u^2 = \mathbf{P}_u$, with $6N^e - 3$ unit eigenvalues and 3 zero eigenvalues. Thus $\mathbf{P}_u$ is an orthogonal projector [41, Section 1.3]. Physically, it extracts the deformational part from the total translational displacements.

Matrix $\mathbf{S}$ is called the *spin-lever* or *moment-arm* or matrix. It is dimensioned $3N^e \times 3$ and has the configuration (written in transposed form to save space):

$$\mathbf{S} = \begin{bmatrix} -\mathbf{S}_1^{\mathrm{T}} & \mathbf{I} & -\mathbf{S}_2^{\mathrm{T}} & \mathbf{I} & \cdots & -\mathbf{S}_{N^e}^{\mathrm{T}} & \mathbf{I} \end{bmatrix}^{\mathrm{T}} \tag{12}$$

in which $\mathbf{I}$ is the 3×3 identity matrix and $\mathbf{S}_a$ are *node spin-lever* 3×3 submatrices. Let $\mathbf{x}_a = \begin{bmatrix} x_{1a} & x_{2a} & x_{3a} \end{bmatrix}^{\mathrm{T}}$ generically denote the 3-vector of coordinates of node *a referred to the element centroid*. Then $\mathbf{S}_a = \mathrm{Spin}(\mathbf{x}_a)$. The coordinates, however, may be those of three different configurations: $\mathscr{C}^0$, $\mathscr{C}^R$ and $\mathscr{C}^D$, referred to two frame types: global or local. Accordingly superscripts and overbars (or tildes) are used to identify one of six combinations. For example

$$\mathbf{S}_a^0 = \begin{bmatrix} 0 & -x_{3a}^0 - a_3 & x_{2a}^0 - a_2 \\ x_{3a}^0 - a_3 & 0 & -x_{1a}^0 - a_1 \\ -x_{2a}^0 - a_2 & x_{1a}^0 - a_1 & 0 \end{bmatrix}, \quad \overline{\mathbf{S}}_a^R = \begin{bmatrix} 0 & -\bar{x}_{3a}^R & \bar{x}_{2a}^R \\ \bar{x}_{3a}^R & 0 & -\bar{x}_{1a}^R \\ -\bar{x}_{2a}^R & \bar{x}_{1a}^R & 0 \end{bmatrix},$$
$$\overline{\mathbf{S}}_a^D = \begin{bmatrix} 0 & -\bar{x}_{3a}^D & \bar{x}_{2a}^D \\ \bar{x}_{3a}^D & 0 & -\bar{x}_{1a}^D \\ -\bar{x}_{2a}^D & \bar{x}_{1a}^D & 0 \end{bmatrix} \tag{13}$$

are node spin-lever matrices for base-in-global-frame, CR-in-local-frame and deformed-in-local-frame, respectively. The element matrix (12) inherits the notation; in this case $\mathbf{S}^0$, $\overline{\mathbf{S}}^R$ and $\overline{\mathbf{S}}^D$, respectively. For instance, $\mathbf{S}$ matrices for the 2-node space $i - j$ bar element pictured in Fig. 9(b) are 12×3. If the length of the bar in $\mathscr{C}^D$ is L, the deformed bar spin-lever matrix referred to the local CR frame is

$$\overline{\mathbf{S}}^D = \frac{1}{2}L \begin{bmatrix} 0 & 0 & 0 & 0 & 0 & 0 & 0 & 0 & 0 & 0 & 0 & 0 \\ 0 & 0 & 1 & 0 & 0 & 0 & 0 & 0 & -1 & 0 & 0 & 0 \\ 0 & -1 & 0 & 0 & 0 & 0 & 0 & 1 & 0 & 0 & 0 & 0 \end{bmatrix}^{\mathrm{T}}. \tag{14}$$

The first column is identically zero since the torque about the bar axis $\bar{x}_1$ vanishes in straight bar models.

Matrix $\mathbf{G}$, introduced by Haugen [37], is dimensioned $3 \times 6N^e$, and will be called the *spin-fitter* matrix. It links variations in the element spin (instantaneous rotations) at the *centroid of the deformed configuration* in response to variations in the nodal DOFs. See Fig. 9(a). $\mathbf{G}$ comes in two flavors, global and local

$$\delta\boldsymbol{\omega} \stackrel{\mathrm{def}}{=} \mathbf{G}\delta\mathbf{v}^e = \sum_a \mathbf{G}_a \delta\mathbf{v}_a^e, \quad \delta\bar{\boldsymbol{\omega}} \stackrel{\mathrm{def}}{=} \overline{\mathbf{G}}\delta\bar{\mathbf{v}}^e = \sum_a \overline{\mathbf{G}}_a \delta\bar{\mathbf{v}}_a^e, \quad \text{with} \quad \sum_a \equiv \sum_{a=1}^{N^e}. \tag{15}$$

Here the spin axial vector variation $\delta\boldsymbol{\omega}^e$ denotes the instantaneous rotation at the centroid, measured in the global frame, when the deformed configuration is varied by the $6N^e$ components of $\delta\mathbf{v}^e$. When referred to the local CR frame, these become $\delta\bar{\boldsymbol{\omega}}^e$ and $\delta\bar{\mathbf{v}}^e$, respectively. For construction, both $\mathbf{G}$ and $\overline{\mathbf{G}}$ may be split into node-by-node contributions using the 3×6 submatrices $\mathbf{G}_a$ and $\overline{\mathbf{G}}_a$ shown above. As an example, $\mathbf{G}$ matrices for the space bar element shown in Fig. 9(b) is 3×12. The spin-lever matrix in $\mathscr{C}^D$ referred to the local CR frame is

$$\overline{\mathbf{G}}^D = \frac{1}{L}\begin{bmatrix} 0 & 0 & 0 & 0 & 0 & 0 & 0 & 0 & 0 & 0 & 0 & 0 \\ 0 & 0 & 1 & 0 & 0 & 0 & 0 & 0 & -1 & 0 & 0 & 0 \\ 0 & -1 & 0 & 0 & 0 & 0 & 0 & 1 & 0 & 0 & 0 & 0 \end{bmatrix}. \tag{16}$$

The first row is conventionally set to zero as the spin about the bar axis $\bar{x}_1$ is not defined by the nodal freedoms. This "torsion spin" is defined, however, in 3D beam models by the end torsional rotations.

Unlike $\mathbf{S}$, the entries of $\mathbf{G}$ depend not only on the element geometry, but on a developer's decision: how the CR configuration $\mathscr{C}^R$ is fitted to $\mathscr{C}^D$. For the triangular shell element this matrix is given in Appendix B. For quadrilateral shells and space beam elements it is given in Part II [38].

Matrices $\overline{\mathbf{S}}^D$ and $\overline{\mathbf{G}}^D$ satisfy the biorthogonality property

$$\mathbf{GS} = \mathbf{D}, \tag{17}$$

where $\mathbf{D}$ is a 3×3 diagonal matrix of zeros and ones. A diagonal entry of $\mathbf{D}$ is zero if a spin component is undefined by the element freedoms. For instance in the case of the space bar, the product $\overline{\mathbf{G}}^D\overline{\mathbf{S}}^D$ of (14) and (16) is diag(0, 1, 1). Aside from these special elements (e.g., bar, spars, shaft elements), $\mathbf{D} = \mathbf{I}$. This property results from the fact that the three columns of $\mathbf{S}$ are simply the displacement vectors associated with the rigid body rotations $\delta\bar{\omega}_i = 1$. When premultiplied by $\mathbf{G}$ one merely recovers the amplitudes of those three modes.

The *rotational projector* or simply *R-projector* is generically defined as $\mathbf{P}_\omega = \mathbf{SG}$. Unlike the T-projector $\mathbf{P}_u$ such as those in (11), the R-projector depends on configuration and frame of reference. Those are identified in the usual manner; e.g., $\overline{\mathbf{P}}^R_\omega = \overline{\mathbf{S}}^R_\omega\overline{\mathbf{G}}^R_\omega$. This $6N^e\times 6N^e$ matrix is an orthogonal projector of rank equal to that of $\mathbf{D} = \mathbf{GS}$. If $\mathbf{GS} = \mathbf{I}$, $\mathbf{P}_\omega$ has rank 3. The complete *projector matrix* of the element is defined as

$$\mathbf{P} = \mathbf{P}_u - \mathbf{P}_\omega. \tag{18}$$

This is shown to be a projector, that is $\mathbf{P}^2 = \mathbf{P}$, in Section 4.2.

Two additional $6N^e\times 6N^e$ matrices, denoted by $\mathbf{H}$ and $\mathbf{L}$, appear in the EICR. $\mathbf{H}$ is a block diagonal matrix built of $2N^e$ 3×3 blocks

$$\mathbf{H} = \mathrm{diag}[\,\mathbf{I}\quad \mathbf{H}_1\quad \mathbf{I}\quad \mathbf{H}_2\quad \cdots \mathbf{I}\quad \mathbf{H}_{N^e}\,],\quad \mathbf{H}_a = \mathbf{H}(\boldsymbol{\theta}_a),\quad \mathbf{H}(\boldsymbol{\theta}) = \partial\boldsymbol{\theta}/\partial\boldsymbol{\omega}. \tag{19}$$

Here $\mathbf{H}_a$ denotes the Jacobian derivative of the rotational axial vector with respect to the spin axial vector evaluated at node a. An explicit expression of $\mathbf{H}(\boldsymbol{\theta})$ is given in (101) of Appendix A. The local version in the CR frame is

$$\bar{\mathbf{H}} = \mathrm{diag}\big[\,\mathbf{I}\quad \overline{\mathbf{H}}_{\mathrm{d}1}\quad \mathbf{I}\quad \overline{\mathbf{H}}_{\mathrm{d}2}\quad \cdots\quad \mathbf{I}\quad \overline{\mathbf{H}}_{\mathrm{d}N^e}\,\big],\quad \overline{\mathbf{H}}_{\mathrm{d}a} = \overline{\mathbf{H}}(\bar{\boldsymbol{\theta}}_{\mathrm{d}a}),\quad \overline{\mathbf{H}}(\bar{\boldsymbol{\theta}}_{\mathrm{d}}) = \partial\bar{\boldsymbol{\theta}}_{\mathrm{d}}/\partial\bar{\boldsymbol{\omega}}_{\mathrm{d}}. \tag{20}$$

$\mathbf{L}$ is a block diagonal matrix built of $2N^e$ 3×3 blocks

$$\mathbf{L} = \mathrm{diag}[\,\mathbf{0}\quad \mathbf{L}_1\quad \mathbf{0}\quad \mathbf{L}_2\quad \cdots\quad \mathbf{0}\quad \mathbf{L}_{N^e}\,],\quad \mathbf{L}_a = \mathbf{L}(\boldsymbol{\theta}_a, \mathbf{m}_a), \tag{21}$$

where $\mathbf{m}_a$ is the three-vector of moments (conjugate to $\delta\boldsymbol{\omega}_a$) at node a. The expression of $\mathbf{L}(\boldsymbol{\theta}, \mathbf{m})$ is provided in (102) of Appendix A. The local form $\overline{\mathbf{L}}$ has the same block organization with $\mathbf{L}_a$ replaced by $\overline{\mathbf{L}}_a = \mathbf{L}(\bar{\boldsymbol{\theta}}_{\mathrm{d}a}, \bar{\mathbf{m}}_a)$.

3.8. Deformational translations

Consider a generic point P^0 of the base element of Fig. 5, with global position vector $\mathbf{x}_P^0$. P^0 rigidly moves to P^R in $\mathscr{C}^R$ with position vector $\mathbf{x}_P^R = \mathbf{x}_P^0 + \mathbf{u}_P^R = \mathbf{x}_P^0 + \mathbf{c} + \mathbf{x}_{PC}^R$. Next the element deforms to occupy $\mathscr{C}^D$. P^R displaces to P, with global position vector $\mathbf{x}_P = \mathbf{x}_P^0 + \mathbf{u}_P = \mathbf{x}_P^0 + \mathbf{c} + \mathbf{x}_{PC}^R + \mathbf{u}_{\mathrm{d}P}$.

The global vector from C^0 to P^0 is $\mathbf{x}_P^0 - \mathbf{a}$, which in the base frame becomes $\tilde{\mathbf{x}}_P^0 = \mathbf{T}_0(\mathbf{x}_P^0 - \mathbf{a})$. The global vector from $C^R \equiv C$ to P_R is $\mathbf{x}_P^R - \mathbf{b}$, which in the element CR frame becomes $\bar{\mathbf{x}}_P^R = \mathbf{T}_R(\mathbf{x}_{PC}^R - \mathbf{b})$. But $\tilde{\mathbf{x}}_P^0 = \bar{\mathbf{x}}_P^R$ since the $\mathscr{C}^0 \to \mathscr{C}^R$ motion is rigid. The global vector from P_R to P is $\mathbf{u}_{\mathrm{d}P} = \mathbf{x}_P - \mathbf{x}_P^R$, which represents a deformational displacement. In the CR frame this becomes $\bar{\mathbf{u}}_{\mathrm{d}P} = \mathbf{T}_R(\mathbf{x}_P - \mathbf{x}_P^R)$.

The total displacement vector is the sum of rigid and deformational parts: $\mathbf{u}_P = \mathbf{u}_{\mathrm{r}P} + \mathbf{u}_{\mathrm{d}P}$. The rigid displacement is given by expressions collected in (5), of which $\mathbf{u}_{\mathrm{r}P} = (\mathbf{R}_0 - \mathbf{I})(\mathbf{x}_P^0 - \mathbf{a}) + \mathbf{c}$ is the most useful. The deformational part is extracted as $\mathbf{u}_{\mathrm{d}P} = \mathbf{u}_P - \mathbf{u}_{\mathrm{r}P} = \mathbf{u}_P - \mathbf{c} + (\mathbf{I} - \mathbf{R}_0)(\mathbf{x}_P^0 - \mathbf{a})$. Dropping P to reduce clutter this becomes

$$\mathbf{u}_{\mathrm{d}} = \mathbf{u} - \mathbf{c} + (\mathbf{I} - \mathbf{R}_0)(\mathbf{x}^0 - \mathbf{a}). \tag{22}$$

The element centroid position is calculated by averaging its node coordinates. Consequently

$$\mathbf{c} = (1/N^e)\sum_b \mathbf{u}_b, \quad \mathbf{u}_a - \mathbf{c} = \sum_b \mathbf{U}_{ab}\mathbf{u}_b \quad \text{with} \quad \sum_b \equiv \sum_{b=1}^{N^e} \tag{23}$$

in which $\mathbf{U}_{ab} = (\delta_{ab} - 1/N^e)\mathbf{I}$ is a building block of the T-projector introduced in the foregoing section. Evaluate (22) at node a, insert (23), take variations using (10) to handle $\delta\mathbf{R}_0$, use (2) to map $\mathbf{R}_0(\mathbf{x}^0 - \mathbf{a}) = \mathbf{x}^R - \mathbf{b}$, and employ the cross-product skew-symmetric property (56) to extract $\delta\boldsymbol{\omega}$

$$\begin{aligned}
\delta\mathbf{u}_{\mathrm{d}a} &= \delta(\mathbf{u}_a - \mathbf{c}) - \delta\mathbf{R}_0(\mathbf{x}_a^0 - \mathbf{a}) = \sum_b \mathbf{U}_{ab}\delta\mathbf{u}_b - \mathrm{Spin}(\delta\boldsymbol{\omega})\mathbf{R}_0(\mathbf{x}_a^0 - \mathbf{a}) \\
&= \sum_b \mathbf{U}_{ab}\delta\mathbf{u}_b - \mathrm{Spin}(\delta\boldsymbol{\omega})(\mathbf{x}_a^R - \mathbf{b}) = \sum_b \mathbf{U}_{ab}\delta\mathbf{u}_b + \mathrm{Spin}(\mathbf{x}_a^R - \mathbf{b})\delta\boldsymbol{\omega} \\
&= \sum_b \mathbf{U}_{ab}\delta\mathbf{u}_b + \sum_b \mathbf{S}_a^R\mathbf{G}_b\delta\mathbf{v}_b.
\end{aligned} \tag{24}$$

Here matrices $\mathbf{S}$ and $\mathbf{G}$ have been introduced in (12)–(15). The deformational displacement in the element CR frame is $\bar{\mathbf{u}}_{\mathrm{d}} = \mathbf{T}_R\mathbf{u}_{\mathrm{d}}$. From the last of (5) we get $\bar{\mathbf{u}}_{\mathrm{d}} = \bar{\mathbf{u}} - \bar{\mathbf{c}} - (\mathbf{I} - \overline{\mathbf{R}}_0^{\mathrm{T}})\bar{\mathbf{x}}^R$, where $\overline{\mathbf{R}}_0 = \mathbf{T}_R\mathbf{R}_0\mathbf{T}_R^{\mathrm{T}}$. Proceeding as above one gets

$$\delta\bar{\mathbf{u}}_{\mathrm{d}a} = \sum_b \mathbf{U}_{ab}\delta\bar{\mathbf{u}}_b + \sum_b \overline{\mathbf{S}}_a^D\overline{\mathbf{G}}_b\delta\bar{\mathbf{v}}_b. \tag{25}$$

The node lever matrix $\mathbf{S}_a^R$ of (24) changes in (25) to $\overline{\mathbf{S}}_a^D$, which uses the node coordinates of the *deformed* element configuration.

3.9. Deformational rotations

Denote by $\mathbf{R}_P$ the rotator associated with the motion of the material particle originally at P^0; see Fig. 6. Proceeding as in the translational analysis this is decomposed into the rigid rotation $\mathbf{R}_0$ and a deformational rotation: $\mathbf{R}_P = \mathbf{R}_{\mathrm{d}P}\mathbf{R}_0$. The sequence matters because $\mathbf{R}_{\mathrm{d}P}\mathbf{R}_0 \neq \mathbf{R}_0\mathbf{R}_{\mathrm{d}P}$. The order $\mathbf{R}_{\mathrm{d}P}\mathbf{R}_0$: rigid rotation followed by deformation, is consistent with those used by Rankin, Bergan and coworkers; e.g. [54,56]. (From the standpoint of continuum mechanics based on the polar decomposition theorem [81, Section 37] the left stretch measure is used.) Thus $\mathbf{R}_{\mathrm{d}P} = \mathbf{R}_P\mathbf{R}_0^{\mathrm{T}}$, which can be mapped to the local CR system as $\overline{\mathbf{R}}_{\mathrm{d}} = \mathbf{T}_R\mathbf{R}_{\mathrm{d}}\mathbf{T}_R^{\mathrm{T}}$. Dropping the label P for brevity we get

$$\mathbf{R}_{\rm d} = \mathbf{R}\mathbf{R}_0^{\rm T} = \mathbf{R}\mathbf{T}_0^{\rm T}\mathbf{T}_R, \quad \overline{\mathbf{R}}_{\rm d} = \mathbf{T}_R\mathbf{R}_{\rm d}\mathbf{T}_R^{\rm T} = \mathbf{T}_R\mathbf{R}\mathbf{T}_0^{\rm T}. \tag{26}$$

The deformational rotation (26) is taken to be small but finite. Thus a procedure to extract a rotation axial vector $\theta_{\rm d}$ from a given rotator is needed. Formally this is $\bar{\boldsymbol{\theta}}_{\rm d} = \text{axial}[\text{Log}_e(\overline{\mathbf{R}}_{\rm d})]$, but this can be prone to numerical instabilities. A robust procedure is presented in Section A.11. The axial vector is evaluated at the nodes and identified with the rotational DOF.

Evaluating (26) at a node a, taking variations and going through an analysis similar to that carried out in the foregoing section yields

$$\begin{aligned}
\delta\boldsymbol{\theta}_{{\rm d}a} &= \frac{\partial\boldsymbol{\theta}_{{\rm d}a}}{\partial\boldsymbol{\omega}_{{\rm d}a}}\sum_b \frac{\partial\boldsymbol{\omega}_{{\rm d}a}}{\partial\boldsymbol{\omega}_b}\delta\boldsymbol{\omega}_b = \mathbf{H}_a\sum_b(\delta_{ab}[\mathbf{0}\quad\mathbf{I}] - \mathbf{G}_b)\delta\mathbf{v}_b,\\
\delta\bar{\boldsymbol{\theta}}_{{\rm d}a} &= \frac{\partial\bar{\boldsymbol{\theta}}_{{\rm d}a}}{\partial\bar{\boldsymbol{\omega}}_{{\rm d}a}}\sum_b \frac{\partial\bar{\boldsymbol{\omega}}_{{\rm d}a}}{\partial\bar{\boldsymbol{\omega}}_b}\delta\bar{\boldsymbol{\omega}}_b = \overline{\mathbf{H}}_a\sum_b\left(\delta_{ab}[\mathbf{0}\quad\mathbf{I}] - \overline{\mathbf{G}}_b\right)\delta\bar{\mathbf{v}}_b,
\end{aligned} \tag{27}$$

where $\mathbf{G}_b$ is defined in (15) and $\mathbf{H}_a$ in (19).

4. Internal forces

The element internal force vector $\bar{\mathbf{p}}^e$ and tangent stiffness matrix $\overline{\mathbf{K}}^e$ are computed in the CR configuration based on small deformational displacements and rotations. Variations of the element DOF, collected in $\mathbf{v}_{\rm d}^e$ as indicated in Table 2, must be linked to variations in the global frame to flesh out the EICR interface of Fig. 4. This section develops the necessary relations.

4.1. Force transformations

Consider an individual element e with N^e nodes with six DOF (three translations and three rotations) at each. Assume the element to be linearly elastic, undergoing only small deformations. Its internal energy is assumed to be a function of the deformational displacements: $U^e = U^e(\bar{\mathbf{v}}_{\rm d}^e)$ with array $\bar{\mathbf{v}}_{\rm d}^e$ organized as shown in Table 2. U^e is a frame independent scalar. The element internal force vector $\bar{\mathbf{p}}^e$ in the CR frame is given by $\bar{\mathbf{p}}^e = \partial U^e/\partial\bar{\mathbf{v}}_{\rm d}^e$. For each node $a = 1,\ldots,N^e$

$$\bar{\mathbf{p}}_a^e = \frac{\partial U^e}{\partial\bar{\mathbf{v}}_{{\rm d}a}^e} \quad \text{or} \quad \begin{bmatrix}\bar{\mathbf{p}}_{ua}^e\\ \bar{\mathbf{p}}_{\theta a}^e\end{bmatrix} = \begin{bmatrix}\dfrac{\partial U^e}{\partial\bar{\mathbf{u}}_{{\rm d}a}}\\ \dfrac{\partial U^e}{\partial\bar{\boldsymbol{\theta}}_{{\rm d}a}}\end{bmatrix}, \tag{28}$$

where the second form separates the translational and rotational (moment) forces. To refer these to the global frame we need to relate local-to-global kinematic variations:

$$\begin{bmatrix}\delta\bar{\mathbf{u}}_{{\rm d}a}^e\\ \delta\bar{\boldsymbol{\theta}}_{{\rm d}a}^e\end{bmatrix} = \sum_{b=1}^{N^e}\mathbf{J}_{ab}\begin{bmatrix}\delta\mathbf{u}_a^e\\ \delta\boldsymbol{\omega}_a^e\end{bmatrix}, \quad \mathbf{J}_{ab} = \begin{bmatrix}\dfrac{\partial\bar{\mathbf{u}}_{{\rm d}b}^e}{\partial\mathbf{u}_a^e} & \dfrac{\partial\bar{\mathbf{u}}_{{\rm d}b}^e}{\partial\boldsymbol{\omega}_a^e}\\ \dfrac{\partial\bar{\boldsymbol{\theta}}_{{\rm d}b}^e}{\partial\mathbf{u}_a^e} & \dfrac{\partial\bar{\boldsymbol{\theta}}_{{\rm d}b}^e}{\partial\boldsymbol{\omega}_a^e}\end{bmatrix}. \tag{29}$$

From virtual work invariance, $(\bar{\mathbf{p}}_u^e)^{\rm T}\delta\bar{\mathbf{u}}_d^e + (\bar{\mathbf{p}}_\theta^e)^{\rm T}\delta\bar{\boldsymbol{\theta}}_{\rm d}^e = (\mathbf{p}_u^e)^{\rm T}\delta\mathbf{u}^e + (\mathbf{p}_\theta^e)^{\rm T}\delta\boldsymbol{\omega}^e$, whence

$$\begin{bmatrix}\mathbf{p}_{ua}^e\\ \mathbf{p}_{\theta a}^e\end{bmatrix} = \sum_{b=1}^{N^e}\mathbf{J}_{ab}^{\rm T}\begin{bmatrix}\bar{\mathbf{p}}_{ua}^e\\ \bar{\mathbf{p}}_{\theta a}^e\end{bmatrix}, \quad a = 1,\ldots,N^e. \tag{30}$$

It is convenient to split the Jacobian in (29) as $\mathbf{J}_{ab} = \overline{\mathbf{H}}_b \overline{\mathbf{P}}_{ab} \mathbf{T}_a$ and $\mathbf{J}_{ab}^{\mathrm{T}} = \mathbf{T}_a^{\mathrm{T}} \overline{\mathbf{P}}_{ab}^{\mathrm{T}} \overline{\mathbf{H}}_b^{\mathrm{T}}$. These matrices are provided from three transformation stages, flowcharted in Fig. 10:

$$
\begin{bmatrix} \delta\bar{\mathbf{u}}^e_{\mathrm{d}b} \\ \delta\bar{\boldsymbol{\theta}}^e_{\mathrm{d}b} \end{bmatrix} = \begin{bmatrix} \mathbf{I} & \mathbf{0} \\ \mathbf{0} & \overline{\mathbf{H}}_{\mathrm{d}b} \end{bmatrix} \begin{bmatrix} \delta\bar{\mathbf{u}}^e_b \\ \delta\bar{\boldsymbol{\omega}}^e_b \end{bmatrix}, \text{ with } \overline{\mathbf{H}}_{\mathrm{d}b} = \begin{bmatrix} \dfrac{\partial\bar{\boldsymbol{\theta}}^e_{\mathrm{d}b}}{\partial\bar{\boldsymbol{\omega}}^e_{\mathrm{d}b}} \end{bmatrix},
$$

$$
\begin{bmatrix} \delta\bar{\mathbf{u}}^e_b \\ \delta\bar{\boldsymbol{\omega}}^e_b \end{bmatrix} = \overline{\mathbf{P}}_{ab} \begin{bmatrix} \delta\bar{\mathbf{u}}^e_a \\ \delta\bar{\boldsymbol{\omega}}^e_a \end{bmatrix} \quad \text{with } \overline{\mathbf{P}}_{ab} = \begin{bmatrix} \dfrac{\partial\bar{\mathbf{u}}^e_{\mathrm{d}b}}{\partial\bar{\mathbf{u}}^e_a} & \dfrac{\partial\bar{\mathbf{u}}^e_{\mathrm{d}b}}{\partial\bar{\boldsymbol{\omega}}^e_a} \\ \dfrac{\partial\bar{\boldsymbol{\omega}}^e_{\mathrm{d}b}}{\partial\bar{\mathbf{u}}^e_a} & \dfrac{\partial\bar{\boldsymbol{\omega}}^e_{\mathrm{d}b}}{\partial\bar{\boldsymbol{\omega}}^e_a} \end{bmatrix}, \tag{31}
$$

$$
\begin{bmatrix} \delta\bar{\mathbf{u}}^e_a \\ \delta\bar{\boldsymbol{\omega}}^e_a \end{bmatrix} = \mathbf{T}_a \begin{bmatrix} \delta\mathbf{u}^e_a \\ \delta\boldsymbol{\omega}^e_a \end{bmatrix} = \begin{bmatrix} \mathbf{T}_R & \mathbf{0} \\ \mathbf{0} & \mathbf{T}_R \end{bmatrix} \begin{bmatrix} \delta\mathbf{u}^e_a \\ \delta\boldsymbol{\omega}^e_a \end{bmatrix},
$$

The 3×3 matrix $\mathbf{L}$ is the Jacobian derivative already encountered in (21). An explicit expression in terms of $\boldsymbol{\theta}$ is given in (101) of Appendix A. To express compactly the transformations for the entire element it is convenient to assemble the $6N^e \times 6N^e$ matrices

$$
\overline{\mathbf{P}} = \begin{bmatrix} \overline{\mathbf{P}}_{11} & \overline{\mathbf{P}}_{12} & \cdots & \overline{\mathbf{P}}_{1N^e} \\ \overline{\mathbf{P}}_{21} & \overline{\mathbf{P}}_{22} & \cdots & \overline{\mathbf{P}}_{2N^e} \\ \cdots & \cdots & \cdots & \cdots \\ \overline{\mathbf{P}}_{N^e1} & \overline{\mathbf{P}}_{N^e2} & \cdots & \overline{\mathbf{P}}_{N^eN^e} \end{bmatrix}, \tag{32}
$$

$$
\mathbf{T} = \mathrm{diag}[\,\mathbf{T}_R \quad \mathbf{T}_R \quad \cdots \quad \mathbf{T}_R\,]
$$

and $\overline{\mathbf{H}}$ is defined in (20). Then the element transformations can be written

$$
\delta\mathbf{v}^e_{\mathrm{d}} = \overline{\mathbf{H}}\overline{\mathbf{P}}\mathbf{T}\delta\mathbf{v}^e, \quad \mathbf{p}^e = \mathbf{T}^{\mathrm{T}}\overline{\mathbf{P}}^{\mathrm{T}}\overline{\mathbf{H}}^{\mathrm{T}}\bar{\mathbf{p}}^e. \tag{33}
$$

The 6×6 matrix $\overline{\mathbf{P}}_{ab}$ in (31) extracts the deformational part of the displacement at node b in terms of the total displacement at node a, both referred to the CR frame. At the element level, $\delta\bar{\mathbf{v}}^e_{\mathrm{d}} = \overline{\mathbf{P}}\delta\bar{\mathbf{v}}^e$ extracts the deformational part by "projecting out" the rigid body modes. For this reason $\overline{\mathbf{P}}$ is called a *projector*. As noted in Section 3.5, $\overline{\mathbf{P}}$ may be decomposed into a translational projector or T-projector $\overline{\mathbf{P}}_u$ and a rotational projector or R-projector $\overline{\mathbf{P}}_\omega$, so that $\overline{\mathbf{P}} = \overline{\mathbf{P}}_u - \overline{\mathbf{P}}_\omega$. The projector has a rank deficiency of 6. The T-projector is a purely numeric matrix exemplified by (11). The R-projector can be expressed as $\overline{\mathbf{P}}_\omega = \overline{\mathbf{S}}\overline{\mathbf{G}}$, where $\overline{\mathbf{S}}$ is defined in (12) and $\overline{\mathbf{G}}$ in (15). Additional properties are studied below.

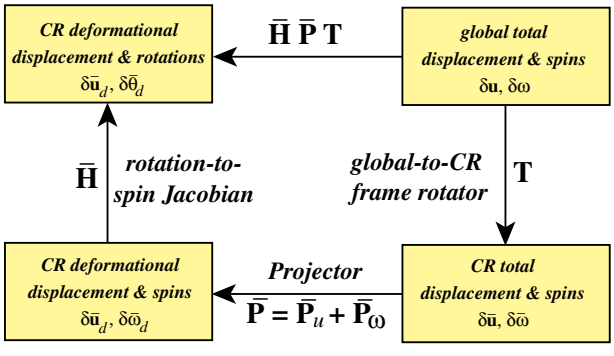

Fig. 10. Staged transformation sequence from deformed to global DOFs.

Remark 3. Rankin and coworkers [54,63–67] use an internal force transformation in which the incremental nodal rotations are used instead of the spins. This results in an extra matrix, $\overline{\mathbf{H}}^{-1}$ appearing in the sequence (33). The projector derived in those papers differs from the one constructed here in two ways: (1) only the R-projector is considered, and (2) the origin of the CR frame is not placed at the element centroid but at an element node defined by local node numbering. Omitting the T-projection is inconsequential if the element is "clean" with respect to translational rigid body motions [30, Section 5].

4.2. Projector properties

In this section the bar over $\mathbf{P}$, etc. is omitted for brevity, since the properties described below are frame independent. In Section 3.5 it was stated without proof that (18) verifies the orthogonal projector property $\mathbf{P}^2 = \mathbf{P}$. Since $\mathbf{P}^2 = (\mathbf{P}_u - \mathbf{P}_\omega)^2 = \mathbf{P}_u^2 - 2\mathbf{P}_u\mathbf{P}_\omega + \mathbf{P}_\omega^2$, satisfaction requires $\mathbf{P}_u^2 = \mathbf{P}_u$, $\mathbf{P}_\omega^2 = \mathbf{P}_\omega$, and $\mathbf{P}_u\mathbf{P}_\omega = \mathbf{0}$. Verification of $\mathbf{P}_u^2 = \mathbf{P}_u$ is trivial. Recalling that $\mathbf{P}_\omega = \mathbf{SG}$ we get

$$\mathbf{P}_\omega^2 = \mathbf{S}(\mathbf{GS})\mathbf{G} = \mathbf{S}\mathbf{I}\mathbf{G} = \mathbf{S}\mathbf{G} = \mathbf{P}_\omega. \tag{34}$$

This assumes $\mathbf{D} = \mathbf{I}$ in (17); verification for non-identity $\mathbf{D}$ is immediate upon removal of zero rows and columns. The orthogonality property $\mathbf{P}_u\mathbf{P}_\omega = \mathbf{P}_u\,\mathbf{SG} = \mathbf{0}$ follows by observing that $\mathrm{Spin}(\mathbf{x}_C) = \mathbf{0}$, where $\mathbf{x}_C$ are the coordinates of the element centroid in any frame with origin at C.

In the derivation of the consistent tangent stiffness, the variation of $\mathbf{P}^{\mathrm{T}}$ contracted with a force vector $\mathbf{f}$, where $\mathbf{f}$ is not varied, is required. The variation of the projector can be expressed as

$$\delta\mathbf{P} = \delta\mathbf{P}_u - \delta\mathbf{P}_\omega = -\delta\mathbf{P}_\omega = -\delta\mathbf{S}\,\mathbf{G} - \mathbf{S}\,\delta\mathbf{G}. \tag{35}$$

For the tangent stiffness one needs $\delta\mathbf{P}^{\mathrm{T}}\mathbf{f}$. This vector can be decomposed into a balanced (self-equilibrated) force $\mathbf{f}_b = \mathbf{P}\mathbf{f}$ and an unbalanced (out of equilibrium) force $\mathbf{f}_u = (\mathbf{I} - \mathbf{P})\mathbf{f}$. Then

$$\begin{aligned}\delta\mathbf{P}^{\mathrm{T}}\mathbf{f} &= -(\mathbf{G}^{\mathrm{T}}\delta\mathbf{S}^{\mathrm{T}} + \delta\mathbf{G}^{\mathrm{T}}\mathbf{S}^{\mathrm{T}})(\mathbf{f}_b + \mathbf{f}_u) = -\mathbf{G}^{\mathrm{T}}\delta\mathbf{S}^{\mathrm{T}}\mathbf{P}^{\mathrm{T}}\mathbf{f} - (\mathbf{G}^{\mathrm{T}}\delta\mathbf{S}^{\mathrm{T}} + \delta\mathbf{G}^{\mathrm{T}}\mathbf{S}^{\mathrm{T}})\mathbf{f}_u \\ &= -\mathbf{G}^{\mathrm{T}}\delta\mathbf{S}^{\mathrm{T}}\mathbf{P}^{\mathrm{T}}\mathbf{f} + \delta\mathbf{P}^{\mathrm{T}}\mathbf{f}_u,\end{aligned} \tag{36}$$

where $\mathbf{S}^{\mathrm{T}}\mathbf{f}_b = \mathbf{0}$ was used. This comes from the fact that the columns of $\mathbf{S}$ are the three rotational rigid body motions, which do not produce work on an self-equilibrated force vector.

The term $\delta\mathbf{P}^{\mathrm{T}}\mathbf{f}_u$ will be small if element configurations $\mathscr{C}^R$ and $\mathscr{C}^D$ are close because in this case $\mathbf{f}_u$ will approach zero. If $\mathbf{G}$ has the factorizable form shown below, however, we can show that $\delta\mathbf{P}^{\mathrm{T}}\mathbf{f}_u = \mathbf{0}$ identically, regardless of how close $\mathscr{C}^R$ and $\mathscr{C}^D$ are, as long as $\mathbf{f}$ is in translational equilibrium. Assume that $\mathbf{G}$ can be factored as

$$\mathbf{G} = \boldsymbol{\Xi}\boldsymbol{\Gamma} \quad \text{with } \delta\mathbf{G} = \delta\boldsymbol{\Xi}\boldsymbol{\Gamma}, \tag{37}$$

where $\boldsymbol{\Xi}$ is a coordinate dependent invertible 3×3 matrix, and $\boldsymbol{\Gamma}$is a constant $3\times 6N^e$ matrix. Since $\mathbf{G}S = \mathbf{I}$ as per (17), $\boldsymbol{\Xi}^{-1} = \boldsymbol{\Gamma}\mathbf{S}$, and $\delta\mathbf{G}\mathbf{S} + \mathbf{G}\delta\mathbf{S} = \delta\boldsymbol{\Xi}\boldsymbol{\Gamma}\mathbf{S} + \mathbf{G}\delta\mathbf{S} = 0$, whence $\delta\boldsymbol{\Xi} = -\,\mathbf{G}\delta\mathbf{S}\boldsymbol{\Xi}$. Then

$$\begin{aligned}\delta\mathbf{P}^{\mathrm{T}}\mathbf{f}_u &= -(\mathbf{G}^{\mathrm{T}}\delta\mathbf{S}^{\mathrm{T}} + \boldsymbol{\Gamma}^{\mathrm{T}}\delta\boldsymbol{\Xi}^{\mathrm{T}}\mathbf{S}^{\mathrm{T}})\mathbf{f}_u = -(\mathbf{G}^{\mathrm{T}}\delta\mathbf{S}^{\mathrm{T}} - \boldsymbol{\Gamma}^{\mathrm{T}}\boldsymbol{\Xi}^{\mathrm{T}}\delta\mathbf{S}^{\mathrm{T}}, \mathbf{G}^{\mathrm{T}}\mathbf{S}^{\mathrm{T}})\mathbf{f}_u \\ &= -(\mathbf{G}^{\mathrm{T}}\delta\mathbf{S}^{\mathrm{T}} - \mathbf{G}^{\mathrm{T}}\delta\mathbf{S}^{\mathrm{T}}\mathbf{P}_\omega^{\mathrm{T}})\mathbf{f}_u = -(\mathbf{G}^{\mathrm{T}}\delta\mathbf{S}^{\mathrm{T}}(\mathbf{I} - \mathbf{P}_\omega^{\mathrm{T}}))\mathbf{f}_u \\ &= -\mathbf{G}^{\mathrm{T}}\delta\mathbf{S}^{\mathrm{T}}(\mathbf{I} - \mathbf{P}_\omega^{\mathrm{T}})\mathbf{f}_u = -\mathbf{G}^{\mathrm{T}}\delta\mathbf{S}^{\mathrm{T}}(\mathbf{I} - \mathbf{P}_\omega^{\mathrm{T}})(\mathbf{I} - \mathbf{P}^{\mathrm{T}})\mathbf{f} = \mathbf{0},\end{aligned} \tag{38}$$

if $\mathbf{f}$ is in translational equilibrium: $\mathbf{f} = \mathbf{P}_\omega^{\mathrm{T}}\mathbf{f}$. This is always satisfied for any element that represents rigid body translations correctly [30, Section 5].

5. Tangent stiffness

We consider here only the stiffness derived from the internal energy. The load stiffness due to nonconservative forces, such as aerodynamic pressures, has to be treated separately.

5.1. Definition

The consistent tangent stiffness matrix $\mathbf{K}^e$ of element e is defined as the variation of the internal forces with respect to element global freedoms:

$$\delta\mathbf{p}^e \stackrel{\text{def}}{=} \mathbf{K}^e\,\delta\mathbf{v}^e, \quad \text{whence } \mathbf{K}^e = \frac{\partial\mathbf{p}^e}{\partial\mathbf{v}^e}. \tag{39}$$

Taking the variation of $\mathbf{p}^e$ in (33) gives rise to four terms

$$\begin{aligned}\delta\mathbf{p}^e &= \delta\mathbf{T}^{\mathrm{T}}\overline{\mathbf{P}}^{\mathrm{T}}\overline{\mathbf{H}}^{\mathrm{T}}\bar{\mathbf{p}}^e + \mathbf{T}^{\mathrm{T}}\delta\overline{\mathbf{P}}^{\mathrm{T}}\overline{\mathbf{H}}^{\mathrm{T}}\bar{\mathbf{p}}^e + \mathbf{T}^{\mathrm{T}}\overline{\mathbf{P}}^{\mathrm{T}}\delta\mathbf{H}^{\mathrm{T}}\bar{\mathbf{p}}^e + \mathbf{T}^{\mathrm{T}}\overline{\mathbf{P}}^{\mathrm{T}}\overline{\mathbf{H}}^{\mathrm{T}}\delta\bar{\mathbf{p}}^e\\ &= (\mathbf{K}^e_{\mathrm{GR}} + \mathbf{K}^e_{\mathrm{GP}} + \mathbf{K}^e_{\mathrm{GM}} + \mathbf{K}^e_{\mathrm{M}})\,\delta\mathbf{v}^e.\end{aligned} \tag{40}$$

The four terms identified in (40) receive the following names. $\mathbf{K}_M$ is the *material stiffness*, $\mathbf{K}_{\mathrm{GM}}$ the *moment-correction geometric stiffness*, $\mathbf{K}_{\mathrm{GP}}$ the *equilibrium projection geometric stiffness*, and $\mathbf{K}_{\mathrm{GR}}$ the *rotational geometric stiffness*. If nodal eccentricities treated by rigid links are considered, one more term appears, called the *eccentricity geometric stiffness*. This term is studied in [37].

5.2. Material stiffness

The material stiffness is generated by the variation of the element internal forces $\mathbf{p}^e$

$$\mathbf{K}^e_{\mathrm{M}}\,\delta\mathbf{v}^e = \mathbf{T}^{\mathrm{T}}_R\overline{\mathbf{P}}^{\mathrm{T}}\overline{\mathbf{H}}^{\mathrm{T}}\,\delta\bar{\mathbf{p}}^e. \tag{41}$$

The linear stiffness matrix in terms of the deformational freedoms in $\bar{\mathbf{v}}^e_{\mathrm{d}}$ is defined as the Hessian of the internal energy

$$\overline{\mathbf{K}}^e = \frac{\partial^2\bar{U}^e}{\partial\bar{\mathbf{v}}^e_{\mathrm{d}}\partial\bar{\mathbf{v}}^e_{\mathrm{d}}} = \frac{\partial\bar{\mathbf{p}}^e}{\partial\bar{\mathbf{v}}^e_{\mathrm{d}}}. \tag{42}$$

Using the transformation of $\delta\bar{\mathbf{v}}^e$ in (33) gives

$$\mathbf{K}^e_{\mathrm{M}} = \mathbf{T}^{\mathrm{T}}\overline{\mathbf{P}}^{\mathrm{T}}\overline{\mathbf{H}}^{\mathrm{T}}\overline{\mathbf{K}}^e\overline{\mathbf{H}}\overline{\mathbf{P}}\mathbf{T}. \tag{43}$$

Thus the material stiffness is given by a congruential transformation of the local stiffness $\overline{\mathbf{K}}^e$ to the global frame. This is formally the same as in linear analysis but here the transformation terms depend on the state. The expression (43) is valid only if $\overline{\mathbf{K}}^e$ is independent of the deformational $\bar{\mathbf{v}}^e_{\mathrm{d}}$ freedoms.

5.3. Geometric stiffness

To express compactly the geometric stiffness components it is convenient to introduce the arrays

$$\bar{\mathbf{p}}^e_P = \overline{\mathbf{P}}^{\mathrm{T}}\overline{\mathbf{H}}^{\mathrm{T}}\bar{\mathbf{p}}^e = \begin{bmatrix}\bar{\mathbf{n}}^e_1\\ \bar{\mathbf{m}}^e_1\\ \vdots\\ \bar{\mathbf{n}}^e_{N^e}\\ \bar{\mathbf{m}}^e_{N^e}\end{bmatrix}, \quad \overline{\mathbf{F}}_n = \begin{bmatrix}\mathrm{Spin}(\bar{\mathbf{n}}^e_1)\\ \mathbf{0}\\ \vdots\\ \mathrm{Spin}(\bar{\mathbf{n}}^e_{N^e})\\ \mathbf{0}\end{bmatrix}, \quad \overline{\mathbf{F}}_{mn} = \begin{bmatrix}\mathrm{Spin}(\bar{\mathbf{n}}^e_1)\\ \mathrm{Spin}(\bar{\mathbf{m}}^e_1)\\ \vdots\\ \mathrm{Spin}(\bar{\mathbf{n}}^e_{N^e})\\ \mathrm{Spin}(\bar{\mathbf{m}}^e_{N^e})\end{bmatrix}. \tag{44}$$

These are filled with the *projection node forces* $\bar{\mathbf{p}}_P^e$. Only the final form of the geometric stiffness components is given below, omitting the detailed derivations of [37]. The rotational geometric stiffness is generated by the variation of $\mathbf{T}$: $\mathbf{K}_{\mathrm{GR}}^e \delta\mathbf{v}^e = \delta\mathbf{T}^{\mathrm{T}} \overline{\mathbf{P}}^{\mathrm{T}} \overline{\mathbf{H}}^{\mathrm{T}} \bar{\mathbf{p}}^e$ and can be expressed as

$$\mathbf{K}_{\mathrm{GR}} = -\mathbf{T}^{\mathrm{T}} \overline{\mathbf{F}}_{nm} \overline{\mathbf{G}} \mathbf{T}, \tag{45}$$

$\mathbf{K}_{\mathrm{GR}}^e$ is the gradient of the internal force vector with respect to the rigid rotation of the element. This interpretation is physically intuitive because a rigid rotation of a stressed element necessarily reorients the stress vectors by that amount. Consequently the internal element forces must rigidly rotate to preserve equilibrium.

The moment-correction geometric stiffness is generated by the variation of the Jacobian $\mathbf{H}$: $\mathbf{K}_{\mathrm{RG}}^e \delta\mathbf{v}^e = \mathbf{T}_R^{\mathrm{T}} \overline{\mathbf{P}}^{\mathrm{T}} \delta\overline{\mathbf{H}}^{\mathrm{T}} \bar{\mathbf{p}}^e$. It is given by

$$\mathbf{K}_{\mathrm{GM}}^e = \mathbf{T}^{\mathrm{T}} \overline{\mathbf{P}}^{\mathrm{T}} \overline{\mathbf{L}} \overline{\mathbf{P}} \mathbf{T}, \tag{46}$$

where $\mathbf{L}$ is defined in Section 3.5.

The equilibrium projection geometric stiffness arises from the variation of the projector $\overline{\mathbf{P}}$ with respect to the deformed element geometry: $\mathbf{K}_{\mathrm{GP}}^e \delta\mathbf{v}^e = \mathbf{T}_R^{\mathrm{T}} \delta\mathbf{P}^{\mathrm{T}} \mathbf{H}^{\mathrm{T}} \bar{\mathbf{p}}^e$. As in Section 4.2, decompose $\bar{\mathbf{p}}^e$ into a balanced (self-equilibrated) force $\bar{\mathbf{p}}_b^e = \overline{\mathbf{P}}^{\mathrm{T}} \bar{\mathbf{p}}^e$ and an unbalanced force $\bar{\mathbf{p}}_u^e = \bar{\mathbf{p}}^e - \bar{\mathbf{p}}_b^e$. If $\delta\overline{\mathbf{P}}^{\mathrm{T}} \bar{\mathbf{p}}_u^e$ is either identically zero or may be neglected as discussed in Section 4.2, $\mathbf{K}_{\mathrm{GP}}^e$ is given by

$$\mathbf{K}_{\mathrm{GP}} = -\mathbf{T}^{\mathrm{T}} \overline{\mathbf{G}}^{\mathrm{T}} \overline{\mathbf{F}}_n \overline{\mathbf{P}} \mathbf{T}, \tag{47}$$

in which the balanced force $\bar{\mathbf{p}}_b^e$ is used in (44) to get $\overline{\mathbf{F}}_n$.

If $\mathbf{T}^{\mathrm{T}} \delta\overline{\mathbf{P}}^{\mathrm{T}} \bar{\mathbf{p}}_u^e$ cannot be neglected, as may happen in highly warped shell elements in a coarse mesh, the following correction term may be added to $\mathbf{K}_{\mathrm{GP}}^e$:

$$\Delta\mathbf{K}_{\mathrm{GP}} = -\mathbf{T}^{\mathrm{T}} \left(\overline{\mathbf{G}}^{\mathrm{T}} \overline{\mathbf{F}}_{nu} \overline{\mathbf{P}} + \frac{\partial \mathbf{G}}{\partial \mathbf{v}} \overline{\mathbf{S}} \bar{\mathbf{p}}_u^e \right) \mathbf{T}, \tag{48}$$

where $\mathbf{F}_{nu}$ is $\mathbf{F}_n$ of (44) when $\bar{\mathbf{p}}_u^e$ is inserted instead of $\bar{\mathbf{p}}^e$. In the computations reported in Part II [38] this term was not included.

$\mathbf{K}_{\mathrm{GP}}^e$ expresses the variation of the projection of the internal force vector $\bar{\mathbf{p}}_e$ as the element geometry changes. This can be interpreted mathematically as follows: In the vector space of element force vectors the subspace of self-equilibrium force vectors changes as the element geometry changes. The projected force vector thus has a gradient with respect to the changing self-equilibrium subspace, even though the element force $\bar{\mathbf{f}}^e$ does not change.

The complete form of the element tangent stiffness, excluding correction terms (48) for highly warped elements, is

$$\mathbf{K}^e = \mathbf{T}^{\mathrm{T}} (\overline{\mathbf{P}}^{\mathrm{T}} \overline{\mathbf{H}}^{\mathrm{T}} \overline{\mathbf{K}}^e \overline{\mathbf{H}} \overline{\mathbf{P}} + \overline{\mathbf{P}}^{\mathrm{T}} \overline{\mathbf{L}} \overline{\mathbf{P}} - \overline{\mathbf{F}}_{nm} \overline{\mathbf{G}} - \overline{\mathbf{G}}^{\mathrm{T}} \overline{\mathbf{F}}_n^{\mathrm{T}} \overline{\mathbf{P}}) \mathbf{T} = \mathbf{T}^{\mathrm{T}} \overline{\mathbf{K}}_R^e \mathbf{T}, \tag{49}$$

in which $\overline{\mathbf{K}}_R^e$, which is the *local tangent stiffness matrix* (the tangent stiffness matrix in the local CR frame of the element) is given by the parenthesized expression.

5.4. Consistency verification

The local tangent stiffness matrix $\overline{\mathbf{K}}_R^e$ given in (49) has some properties that may be exploited to verify the computer implementation [37,54]:

$$\begin{aligned} &\overline{\mathbf{K}}_R^e \overline{\mathbf{S}} = -\overline{\mathbf{F}}_{nm}, \quad \overline{\mathbf{S}}^{\mathrm{T}} \overline{\mathbf{K}}_R^e = -\mathbf{f}_n^{\mathrm{T}}, \quad \overline{\mathbf{K}}_{\mathrm{M}} \overline{\mathbf{S}} = \mathbf{0}, \quad \overline{\mathbf{K}}_{\mathrm{GR}} \overline{\mathbf{S}} = -\overline{\mathbf{F}}_{nm}, \\ &\overline{\mathbf{K}}_{\mathrm{GP}} \overline{\mathbf{S}} = \mathbf{0}, \quad \overline{\mathbf{S}}^{\mathrm{T}} \overline{\mathbf{K}}_{\mathrm{M}} = \mathbf{0}, \quad \overline{\mathbf{S}}^{\mathrm{T}} (\overline{\mathbf{K}}_{\mathrm{GR}} + \overline{\mathbf{K}}_{\mathrm{GP}}) = -\overline{\mathbf{F}}_n^{\mathrm{T}}. \end{aligned} \tag{50}$$

In addition, rigid-body-mode tests on the linear stiffness matrix $\overline{\mathbf{K}}^e$ using linearized projectors are discussed in [30]. The set (50) tests the programming of the nonlinear projector $\overline{\mathbf{P}}$ since it checks the null space of $\mathbf{P}$. It also indicates whether the projector matrix is used correctly in the stiffness formulation. However, satisfaction does not fully guarantee consistency between the internal force and the tangent stiffness because $\overline{\mathbf{H}}$ and $\overline{\mathbf{L}}$ are left unchecked. Full verification of consistency can be numerically done through finite difference techniques.

6. Three consistent CR formulations

From the foregoing unified forms of the internal force and tangent stiffness, three CR consistent formulations can be obtained by making simplifying assumptions at the internal force level. These satisfy self-equilibrium and symmetry to varying degree. The following subsections describe the three versions in order of increasing complexity. For all formulations one can take into account DOFs at eccentric nodes as described in [37].

6.1. Consistent CR formulation (C)

This variant is that developed by Bergan and coworkers in the 1980s at Trondheim and summarized in the review article [56]. The internal force (33) is simplified by taking $\overline{\mathbf{H}} = \mathbf{I}$ and $\overline{\mathbf{P}} = \mathbf{I}$, while retaining $\delta\bar{\mathbf{v}}^e_{\rm d} = \overline{\mathbf{H}}\,\overline{\mathbf{P}}\,\delta\bar{\mathbf{v}}^e$ for recovery of deformational DOFs. Since $\delta\overline{\mathbf{P}} = \delta\overline{\mathbf{H}} = \mathbf{0}$, the expression for the tangent stiffness of (40) simplifies to the material and rotational geometric stiffness terms:

$$\mathbf{p}^e = \mathbf{T}^{\rm T}\overline{\mathbf{K}}^e\bar{\mathbf{v}}^e_{\rm d}, \quad \mathbf{K}^e = \mathbf{T}^{\rm T}(\overline{\mathbf{K}}^e\overline{\mathbf{H}}\overline{\mathbf{P}} - \overline{\mathbf{F}}_{nm}\overline{\mathbf{G}})\mathbf{T}. \tag{51}$$

Here $\overline{\mathbf{F}}_{nm}$ is computed according to (44) with $\bar{\mathbf{p}}^e = \overline{\mathbf{K}}^e\bar{\mathbf{v}}_{\rm d}$. The internal force is in equilibrium with respect to the CR configuration $\mathscr{C}^R$. For a shell structure, the material stiffness approaches symmetry as the element mesh is refined if the membrane strains are small. As the mesh is refined, the deformational rotation axial vectors $\bar{\boldsymbol{\theta}}_{{\rm d}a}$ become smaller and approach vector properties that in turn make $\mathbf{H}(\boldsymbol{\theta}_{{\rm d}a})$ get close to the identity matrix. With small membrane strains $\overline{\mathbf{K}}^e$ is indifferent with respect to post-multiplication with $\overline{\mathbf{P}}$ because the $\mathscr{C}^R$ and $\mathscr{C}$ configurations will be close and $\overline{\mathbf{K}}^e\mathbf{P} \to \overline{\mathbf{K}}^e$. The consistent geometric stiffness is always unsymmetric, even at equilibrium. Because of this fact one cannot expect quadratic convergence for this formulation if a symmetric solver is used.

This formulation may be unsatisfactory for warped quadrilateral shell elements since the $\mathscr{C}^R$ and $\mathscr{C}^D$ reference configurations may be far apart. Only in the limit of a highly refined element mesh will the $\mathscr{C}^R$ and $\mathscr{C}^D$ references in general be close, and satisfactory equilibrium ensured.

6.2. Consistent equilibrated CR formulation (CE)

The internal force (33) is simplified by taking $\overline{\mathbf{H}} = \mathbf{I}$ so $\delta\mathbf{H} = \mathbf{0}$, but the projector $\overline{\mathbf{P}}$ is retained. This gives

$$\mathbf{p}^e = \mathbf{T}^{\rm T}\overline{\mathbf{P}}^{\rm T}\overline{\mathbf{K}}^e\bar{\mathbf{v}}^e_{\rm d}, \quad \mathbf{K}^e = \mathbf{T}^{\rm T}(\overline{\mathbf{P}}^{\rm T}\overline{\mathbf{K}}^e\overline{\mathbf{H}}\overline{\mathbf{P}} - \overline{\mathbf{F}}_{\mathbf{mn}}\overline{\mathbf{G}} - \overline{\mathbf{G}}^{\rm T}\overline{\mathbf{F}}_{\mathbf{n}}^{\rm T}\overline{\mathbf{P}})\mathbf{T}. \tag{52}$$

where $\overline{\mathbf{F}}_{nm}$ and $\overline{\mathbf{F}}_n$ are computed according to (44) with $\bar{\mathbf{p}}^e = \overline{\mathbf{P}}^{\rm T}\overline{\mathbf{K}}^e\bar{\mathbf{v}}^e_{\rm d}$.

Due to the presence of $\overline{\mathbf{P}}$ on both sides, the material stiffness of the CE formulation approaches symmetry as the mesh is refined regardless of strain magnitude. The geometric stiffness at the element level is non-symmetric, but the assembled global geometric stiffness will become symmetric as global equilibrium is approached, provided that there are no applied nodal moments and that displacement boundary conditions are conserving. A symmetrized global tangent stiffness maintains quadratic convergence for refined element meshes with this formulation.

6.3. Consistent symmetrizable equilibrated CR formulation (CSE)

All terms in (33) are retained, giving

$$\mathbf{p}^e = \mathbf{T}^{\mathrm{T}}\overline{\mathbf{P}}^{\mathrm{T}}\overline{\mathbf{H}}^{\mathrm{T}}\overline{\mathbf{K}}^e\bar{\mathbf{v}}^e_{\mathrm{d}}, \quad \mathbf{K}^e = \mathbf{T}^{\mathrm{T}}(\overline{\mathbf{P}}^{\mathrm{T}}\overline{\mathbf{H}}^{\mathrm{T}}\overline{\mathbf{K}}^e\overline{\mathbf{H}}\overline{\mathbf{P}} + \overline{\mathbf{P}}^{\mathrm{T}}\overline{\mathbf{L}}\overline{\mathbf{P}} - \overline{\mathbf{F}}_{nm}\overline{\mathbf{G}} - \overline{\mathbf{G}}^{\mathrm{T}}\overline{\mathbf{F}}_n^{\mathrm{T}}\overline{\mathbf{P}})\mathbf{T}. \tag{53}$$

where $\overline{\mathbf{F}}_{nm}$ and $\overline{\mathbf{F}}_n$ are computed according to (44) with $\bar{\mathbf{f}} = \overline{\mathbf{P}}^{\mathrm{T}}\overline{\mathbf{H}}\overline{\mathbf{K}}^e\bar{\mathbf{v}}^e_{\mathrm{d}}$. The assembled global geometric stiffness for this formulation becomes symmetric as global equilibrium is approached, as in the CE case, as long as there are no applied nodal moments and the loads as well as boundary conditions are conserving. Since the material stiffness is always symmetric, quadratic convergence with a symmetrized tangent stiffness can be expected without the refined-mesh-limit assumption of the CE formulation.

Remark 4. The relative importance of including the **H** matrix, which is neglected by most authors, and the physical significance of this Jacobian term are discussed in Part II [38].

6.4. Formulation requirements

It is convenient to set forward a set of requirements for geometrically nonlinear analysis with respect to which different CR formulations can be evaluated. They are listed below in order of decreasing importance.

Equilibrium. By this requirement is meant: to what extent the finite element internal force vector **p** is in self-equilibrium with respect to the deformed configuration $\mathscr{C}^D$? This is a fundamental requirement for tracing the correct equilibrium path in an incremental-iterative solution procedure.

Consistency. A formulation is called consistent if the tangent stiffness is the gradient of the internal forces with respect to the global DOF. This requirement determines the convergence rate of an incremental-iterative solution procedure. An inconsistent tangent stiffness may give poor convergence, but does not alter the equilibrium path since this is entirely prescribed by the foregoing equilibrium requirement. However, lack of consistency may affect the location of bifurcation (buckling) points and the branch switching mechanism for post-buckling analysis. In other words, an inconsistent tangent stiffness matrix may detect (''see'') a bifurcation where equilibrium is not satisfied from the residual equation. Subsequent traversal by branch-switching will then be difficult because the corrector iterations need to jump to the secondary path as seen by the residual equation.

Invariance. This requirement refers to whether the solution is insensitive to internal choices that may depend on node numbering. For example, does a local element-node reordering give an altered equilibrium path or change the convergence characteristics for the analysis for an otherwise identical mesh? The main contributor to lack of invariance is the way the deformational displacement vector is extracted from the total displacements, should the extraction be affected by the choice of the local CR frame. If lack of invariance is observed, it may be usually traced to the matrix **G**, which links the variation of the rigid body rotation to that of the nodal DOF.

Symmetrizability. This means that a symmetrized **K** can be used without loss of quadratic convergence rate in a true Newton solver even when the consistent tangent stiffness away from equilibrium is not symmetric. In the examples studied in Part II [38] this requirement was met when the material stiffness of the formulation was rendered symmetric.

Element independence. This is used in the sense of the EICR discussed in Section 2.5. It means that the matrix and vector operations that account for geometrically nonlinear effects are the same for all elements that possess the same node and DOF configuration.

Attributes of the C, CE and CSE formulations in light of the foregoing requirements are summarized in Table 4.

Table 4
Attributes of corotated formulations C, CE and CSE

Formulation	Self-equil. (1)	Consistent (2)	Invariant (3)	Symmetriz. (4)	Elem.Indep. (5)
C		√	√		√
CE	√	√	√		√
CSE	√	√	√	√	√

(1) Checked if element is in self-equilibrium in deformed configuration $\mathscr{C}^D$
(2) Checked if tangent stiffness is the **v** gradient of the element internal force
(3) Checked if the formulation is insensitive to choice of node numbering
(4) Checked if formulation maintains quadratic convergence of a true Newton solver with a symmetrized tangent stiffness matrix
(5) Checked if the matrix and vector operations that account for geometrically nonlinear effects are the same for all elements with the same node and DOF configuration

6.5. Limitations of the EICR formulation

The present CR framework, whether used in the C, CE or CSE formulation variants, is element independent in the EICR sense discussed in Section 2.5 since it does not contain gradients of intrinsically element dependent quantities such as the strain–displacement relationship. This treatment is appropriate for elements where the restriction to small strains automatically implies that the CR and deformed element configurations are close. This holds automatically for low order models such as two-node straight bars and beams, and three-node facet shell elements.

The main reason for limiting element independence to low-order elements is the softening effect of the nonlinear projector **P**. The use of **P** to restore the correct rigid body motions, and hence equilibrium with respect to the deformed element geometry, effectively reduces the eigenvalues of the material stiffness relative to the CR material stiffness $\overline{\mathbf{K}}^e$ before projection. This softening effect becomes significant if the $\mathscr{C}^R$ and $\mathscr{C}^D$ geometries are far apart.

Such softening effects are noticeable in four-node initially-warped shell elements. Assume that the element is initially endowed with "positive" warping, and consider only the effect of **P**. The element material stiffness of this initial positive warping is then $\mathbf{K}_+ = \mathbf{P}_+^{\mathrm{T}}\overline{\mathbf{K}}^e\mathbf{P}_+ = \mathbf{K}^e$. Apply displacements that switch this warping to the opposite of the initial one; that is, a "negative" warping. The new element material stiffness then becomes $\mathbf{K}_- = \mathbf{P}_-^{\mathrm{T}}\overline{\mathbf{K}}^e\mathbf{P}_- \neq \mathbf{K}_+$. One will intuitively want the two element configurations to have the same rigidity in the sense of the dominant nonzero eigenvalues of the tangent stiffness matrix. But it can be shown that the eigenvalues of the projected material stiffness matrix $\mathbf{K}_-$ can be significantly lower than those of the initial stiffness matrix $\mathbf{K}_+$. If the element stiffness $\mathbf{K}^e$ is referred to the flat element projection, one can restore symmetry of $\mathbf{K}_+$ and $\mathbf{K}_-$ with respect to dominant nonzero eigenvalues, but it is not possible to remove the softening effect.

This argument also carries over to higher order bar, arch and shell elements that are curved in the initial reference configuration. It follows that the EICR is *primarily useful for low-order elements of simple geometry*.

7. Conclusions

This paper presents a unified formulation for geometrically nonlinear analysis using the CR kinematic description, assuming small deformations. Although linear elastic material behavior has been assumed for brevity, extension to materially nonlinear behavior such as elastoplasticity and fracture within the confines of small deformations, is feasible as further discussed below. All terms in the internal force and tangent stiffness expressions are accounted for. It is shown how dropping selected terms in the former produces simpler CR versions used by previous investigators.

These versions have been tested on thin shell and flexible-mechanism structures, as reported in Part II [38]. Shells are modeled by triangle and quadrilateral elements. The linear stiffness of these elements is obtained with the ANDES (Assumed Natural DEviatoric Strains) formulation of high performance elements [27–32,53]. Test problems include benchmarks in buckling, nonlinear bifurcation and collapse.

Does the unified formulation close the book on CR? Hardly. Several topics either deserve further development or have been barely addressed:

(A) Relaxing the small-strain assumption to allow moderate deformations.
(B) Robust handling of extremely large rotations involving multiple revolutions.
(C) Integrating CR elements with rigid links and joint elements for flexible multibody dynamics.
(D) Using substructuring concepts for CR modeling of structural members with continuum elements.
(E) Achieving a unified form for CR dynamics, including nonconservative effects and multiphysics.

Topic (A) means the use of CR for problems where strains may locally reach moderate levels, say 1–10%, as in elastoplasticity and fracture, using appropriate strain and stress measures in the local frame. The challenge is that change of metric of the CR configuration should be accounted for, even if it means dropping the EICR property. Can CR compete against the more established TL and UL descriptions? It seems unreasonable to expect that CR can be of use in overall large strain problems such as metal forming, in which UL reigns supreme. But it may be competitive in *localized failure* problems, where most of the structure remain elastic although undergoing finite rotations.

Some data points are available: previous large-deformation work presented in [46,47,50,51,57]. More recently Skallerud et al. reported [75] that a submerged-pipeline failure shell code using the ANDES CR quadrilateral of [37] plus elastoplasticity [74] and fracture mechanics [21] was able to beat a well known commercial TL-based code by a factor of 600 in CPU time. This speedup is of obvious interest for stream lining design cycles and deployment planning.

Topic (B) is important in applications where a floating (free-free) structure undergoes several revolutions, as in combat airplane maneuvers, payload separation or orbital structure deployment. The technical difficulty is that expressions presented in the Appendix cannot handle finite rotations beyond $\pm 2\pi$, and thus require occasional resetting of the base configuration. While this can be handled via restarts for structures such as full airplanes, it can be more difficult when the *relative* rotation between components exceeds $\pm 2\pi$, as in separation, fragmentation or deployment problems.

Topics (C) and (D) have been addressed in the FEDEM program developed by SINTEF at Trondheim, Norway. This program combines the CR shell and beam elements of [37], grouped into substructures, with kinematic objects typical of rigid-body dynamics: eccentric links and joints. Basic tools used in FEDEM for combining joint models with flexible continuum elements are described in a recent book [73].

Finally, topic (E) is fertile ground for research. The handling of model components such as mass, damping and nonconservative effects in fluid-structure interaction and aeroelasticity is an active ongoing research topic. For example a recent paper [26] describes flight maneuver simulations of a complete F-16 fighter using CR elements to model the aircraft. As in statics, a key motivation for CR in dynamics is reuse of linear FEM force–stiffness libraries. Can that reuse extend to mass and damping libraries? And how do standard time integration methods perform when confronted with unsymmetric matrices? These topics have barely been addressed.

Acknowledgement

Preparation of this paper was supported by the National Science Foundation under Grant CMS–0219422, by the Finite Elements for Salinas contract with Sandia National Laboratories, and by the Air Force Office of Scientific Research under grant F49620-99-1-0007.

Appendix A. The mathematics of finite rotations

This Appendix collects formulas and results for the mathematical treatment of finite rotations in 3D space. Emphasis is placed on representations useful in the CR description of FEM. Several of the results are either new or simplifications of published results. Some statements in the literature concerning the exponential and Cayley maps are shown to be erroneous.

One difficulty for investigators and students learning the CR description is that different normalizations have been used by different authors. This topic is reviewed in some detail, and summary help provided in the form of Table 5.

A.1. Spatial rotations

Plane rotations are easy. A rotation in, say, the $\{x_1, x_2\}$ plane, is defined by just a scalar: the rotation angle θ about x_3. Plane rotations commute: $\theta_1 + \theta_2 = \theta_2 + \theta_1$, because the θs are numbers.

The study of spatial (3D) rotations is more difficult. The subject is dominated by a fundamental theorem of Euler:

> The general displacement of a rigid body with one point fixed is a rotation about some axis which passes through that point. (54)

Thus spatial rotations have both magnitude: the angle of rotation, and direction: the axis of rotation. These are nominally the same two attributes that categorize vectors. Not coincidentally, rotations are sometimes pictured as vectors but with a double arrow in Mechanics books. Finite 3D rotations, however, do not obey the laws of vector calculus, although infinitesimal rotations do. Most striking is commutation failure: switching two successive rotations does not yield the same answer unless the rotation axis is kept fixed. Within the framework of matrix algebra, finite rotations can be represented in two ways:

(a) As 3×3 real orthogonal matrices $\mathbf{R}$ called *rotators*. (An abbreviation for *rotation tensor*.)
(b) As 3×3 real skew-symmetric matrices $\mathbf{\Omega}$ called *spinors*. (An abbreviation for *spin tensor*.)

The spinor representation is important in theory and modeling because the matrix entries are closely related to the ingredients of Euler's theorem (54).

The rotator representation is convenient for numerical work, as well as being naturally related to the polar factorization of a transformation matrix. The two representations are connected as illustrated in Fig. 11, which also includes the axial vector introduced below. Of the $\mathbf{\Omega}\to\mathbf{R}$ links, the Rodrigues–Cayley version is historically the first, as discussed in [20], although not the most important one.

Table 5
Rotator forms for several spinor normalizations

Parametrization	γ	α	β	Spinor	Rotator $\mathbf{R}$
None (unscaled)	1	$\dfrac{\sin\theta}{\omega}$	$\dfrac{2\sin^2\frac{1}{2}\theta}{\omega^2}$	$\mathbf{\Omega}$	$\mathbf{I}+\dfrac{\sin\theta}{\omega}\mathbf{\Omega}+\dfrac{2\sin^2\frac{1}{2}\theta}{\omega^2}\mathbf{\Omega}^2$
Unit axial-vector	$\dfrac{1}{\omega}$	$\sin\theta$	$2\sin^2\dfrac{1}{2}\theta$	$\mathbf{N}=\gamma\mathbf{\Omega}$	$\mathbf{I}+\sin\theta\mathbf{N}+2\sin^2\dfrac{1}{2}\theta\mathbf{N}^2,$
Rodrigues–Cayley	$\dfrac{\tan\frac{1}{2}\theta}{\omega}$	$2\cos^2\dfrac{1}{2}\theta$	$2\cos^2\dfrac{1}{2}\theta$	$\mathbf{\Sigma}=\gamma\mathbf{\Omega}$	$\mathbf{I}+2\cos^2\dfrac{1}{2}\theta(\mathbf{\Sigma}+\mathbf{\Sigma}^2)=(\mathbf{I}+\mathbf{\Sigma})(\mathbf{I}-\mathbf{\Sigma})^{-1}$
Fraeijs de Veubeke	$\dfrac{\sin\frac{1}{2}\theta}{\omega}$	$2\cos\dfrac{1}{2}\theta$	2	$\mathbf{\Omega}_p=\gamma\mathbf{\Omega}$	$\mathbf{I}+2\cos\dfrac{1}{2}\theta\mathbf{\Omega}_p+2\mathbf{\Omega}_p^2$
Exponential map	$\dfrac{\theta}{\omega}$	$\dfrac{\sin\theta}{\theta}$	$\dfrac{\sin^2\frac{1}{2}\theta}{\theta^2}$	$\mathbf{\Theta}=\gamma\mathbf{\Omega}$	$\mathbf{I}+\dfrac{\sin\theta}{\theta}\mathbf{\Theta}+\dfrac{2\sin^2\frac{1}{2}\theta}{\theta^2}\mathbf{\Theta}^2=\mathrm{e}^{\mathbf{\Theta}}=\mathrm{e}^{\theta\mathbf{N}}$

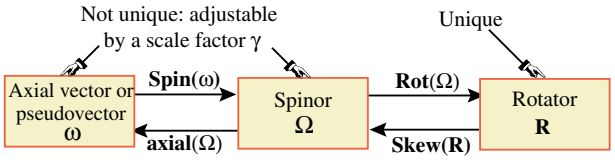

Fig. 11. Representations of finite spatial rotations. Note: Some authors write $e^{\mathbf{\Omega}}$ and $\mathrm{Log}_e(\mathbf{R})$ for **Rot(Ω)** and Skew(**R**), respectively. This is correct for a particular scale factor γ; cf. Table 5.

A 3×3 skew-symmetric matrix such as $\mathbf{\Omega}$ is defined by three scalar parameters. These three numbers can be arranged as components of an *axial vector* $\boldsymbol{\omega}$. Although $\boldsymbol{\omega}$ looks like a 3-vector, it violates certain properties of classical vectors such as the composition rule. Therefore the term *pseudovector* is sometimes used for $\boldsymbol{\omega}$.

In the EICR formulation presented here, axial vectors of rotations and spins function as incremental quantities directly connected to variations. Rotator matrices are used to record the global structure motions. See Table 2.

This Appendix intends to convey that finite 3D rotations can appear in alternative mathematical representations, as diagramed in Fig. 11. The following exposition expands on this topic, and studies the links shown there.

A.2. Spinors

Fig. 12(a) depicts a 3D rotation in space $\{x_1, x_2, x_3\}$ by an angle θ about an axis of rotation $\vec{\boldsymbol{\omega}}$. For convenience the origin of coordinates O is placed on $\vec{\boldsymbol{\omega}}$. The rotation axis is defined by three directors: ω_1, ω_2, ω_3, at least one of which must be nonzero. These components may be scaled by an nonzero factor γ through which the vector may be normalized in various ways discussed later. The rotation takes an arbitrary point $P(\mathbf{x})$, located by its position vector $\mathbf{x}$, into $Q(\mathbf{x}, \theta)$, located by its position vector $\mathbf{x}_\theta$. The center of rotation C is defined by projecting P on the rotation axis. The plane of rotation CPQ is normal to that axis at C.

The radius of rotation is vector $\mathbf{r}$ of magnitude r from C to P. As illustrated in Fig. 12(b) the distance between P and Q is $2r \sin \frac{1}{2}\theta$.

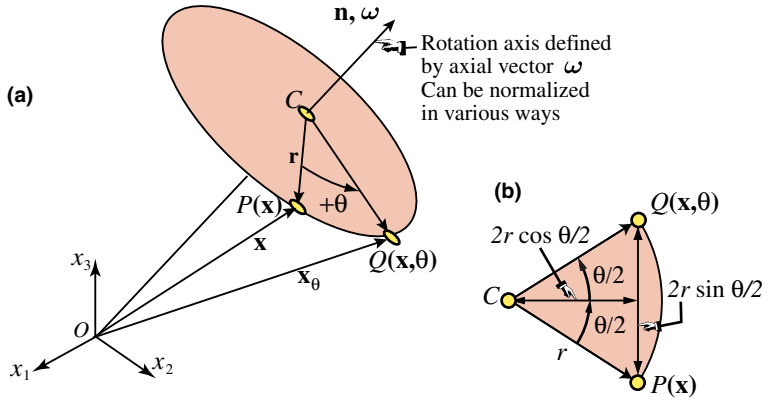

Fig. 12. The rotation angle θ is positive as shown, obeying the right-hand screw rule about the rotation axis.

The positive sense of θ obeys the RHS screw rule: positive counterclockwise if observed from the tip of the rotation axis. The angle shown in Fig. 12 is positive.

A.3. Spin tensor and axial vector

Given the three directors ω_1, ω_2, and ω_3 of the axis $\boldsymbol{\omega}$, we can associate with it a 3×3 skew-symmetric matrix $\boldsymbol{\Omega}$, called a *spin tensor*, *spin matrix* or briefly *spinor*, by the rule

$$\boldsymbol{\Omega} = \mathrm{Spin}(\boldsymbol{\omega}) = \begin{bmatrix} 0 & -\omega_3 & \omega_2 \\ \omega_3 & 0 & -\omega_1 \\ -\omega_2 & \omega_3 & 0 \end{bmatrix} = -\boldsymbol{\Omega}^{\mathrm{T}}. \tag{55}$$

The space of all $\boldsymbol{\Omega}$'s form the Lie algebra SO(3). Premultiplication of an arbitrary 3-vector $\mathbf{v}$ by $\boldsymbol{\Omega}$ is equivalent to the cross product of $\boldsymbol{\omega}$ and $\mathbf{v}$:

$$\boldsymbol{\omega}\times\mathbf{v} = \boldsymbol{\Omega}\mathbf{v} = \mathrm{Spin}(\boldsymbol{\omega})\mathbf{v} = -\mathrm{Spin}(\mathbf{v})\boldsymbol{\omega} = -\mathbf{v}\times\boldsymbol{\omega}. \tag{56}$$

In particular $\boldsymbol{\Omega}\boldsymbol{\omega} = \mathbf{0}$, and $\mathbf{v}^{\mathrm{T}}\boldsymbol{\Omega}\mathbf{v} = 0$, as may be directly verified. The operation converse to (55) extracts the 3-vector $\boldsymbol{\omega}$, called *axial vector* or *pseudovector*, from a given spin tensor:

$$\boldsymbol{\omega} = \mathrm{axial}(\boldsymbol{\Omega}) = \begin{bmatrix} \omega_1 \\ \omega_2 \\ \omega_3 \end{bmatrix}. \tag{57}$$

The length of this vector is denoted by ω

$$\omega = |\,\boldsymbol{\omega}\,| = +\sqrt{\omega_1^2+\omega_2^2+\omega_3^2}. \tag{58}$$

As general notational rule, we will use corresponding upper and lower case symbols for the spinor and its axial vector, respectively, if possible. For example, $\mathbf{N}$ and $\mathbf{n}$, $\boldsymbol{\Theta}$ and $\boldsymbol{\theta}$, $\mathbf{V}$ and $\mathbf{v}$. Exceptions are made in case of notational conflicts; for example the spinor built from the quaternion vector p_i is not denoted as $\mathbf{P}$ because that symbol is reserved for projectors.

A.4. Spinor normalizations

As noted, $\boldsymbol{\omega}$ and $\boldsymbol{\Omega}$ can be multiplied by a nonzero scalar factor γ to obtain various *normalizations*. In general γ has the form $g(\theta)/\omega$, where $g(\cdot)$ is a function of the rotation angle θ. The goal of normalization is to simplify the connections $Rot(\cdot)$ and $Skew(\cdot)$ to the rotator, to avoid singularities for special angles, and to connect the components ω_1, ω_2 and ω_3 closely to the rotation amplitude. This section overviews some normalizations that have practical or historical importance.

Choosing $\gamma = 1/\omega$ we obtain the unit axial-vector and unit spinor, which are denoted by $\mathbf{n}$ and $\mathbf{N}$, respectively:

$$\mathbf{n} = \begin{bmatrix} n_1 \\ n_2 \\ n_3 \end{bmatrix} = \begin{bmatrix} \omega_1/\omega \\ \omega_2/\omega \\ \omega_3/\omega \end{bmatrix} = \frac{\boldsymbol{\omega}}{\omega}, \quad \mathbf{N} = \mathrm{Spin}(\mathbf{n}) = \frac{\boldsymbol{\Omega}}{\omega} = \begin{bmatrix} 0 & -n_3 & n_2 \\ n_3 & 0 & -n_1 \\ -n_2 & n_3 & 0 \end{bmatrix}. \tag{59}$$

Taking $\gamma = \tan\frac{1}{2}\theta/\omega$ is equivalent to multiplying the n_i by $\tan\frac{1}{2}\theta$. We thus obtain the parameters $b_i = n_i \tan\frac{1}{2}\theta$, $i = 1,2,3$ attributed to Rodrigues [69] by Cheng and Gupta [20]. These are collected in the Rodrigues axial-vector $\mathbf{b}$ with associated spinor $\boldsymbol{\Sigma}$:

$$\mathbf{b} = \tan\tfrac{1}{2}\theta\mathbf{n} = \big(\tan\tfrac{1}{2}\theta/\omega\big)\boldsymbol{\omega}, \quad \boldsymbol{\Sigma} = \mathrm{Spin}(\mathbf{b}) = \tan\tfrac{1}{2}\theta\mathbf{N} = \big(\tan\tfrac{1}{2}\theta/\omega\big)\boldsymbol{\Omega}. \tag{60}$$

This representation permits an elegant formulation of the rotator via the Cayley transform studied later. However, it collapses as θ nears $\pm 180^\circ$ since $\tan\frac{1}{2}\theta \to \pm\infty$. One way to circumvent the singularity is through the use of the four Euler–Rodrigues parameters, also called *quaternion coefficients*:

$$p_0 = \cos\tfrac{1}{2}\theta, \quad p_i = n_i \sin\tfrac{1}{2}\theta = \omega_i/\omega \sin\tfrac{1}{2}\theta, \quad i = 1, 2, 3. \tag{61}$$

under the constraint $p_0^2 + p_1^2 + p_2^2 + p_3^2 = 1$. This set is often used in multibody dynamics, robotics and control. It comes at the cost of carrying along an extra parameter and an additional constraint.

A related singularity-free normalization introduced by Fraeijs de Veubeke [25] takes $\gamma = \sin\frac{1}{2}\theta/\omega$ and is equivalent to using only the last three parameters of (61):

$$\mathbf{p} = \sin\tfrac{1}{2}\theta\mathbf{n} = (\sin\tfrac{1}{2}\theta/\omega)\ \boldsymbol{\omega}, \quad \boldsymbol{\Omega}_p = \mathrm{Spin}(\mathbf{p}) = \sin\tfrac{1}{2}\theta\mathbf{N} = (\sin\tfrac{1}{2}\theta/\omega)\boldsymbol{\Omega}. \tag{62}$$

Fraeijs de Veubeke calls this representation "Rodrigues-Hamilton" without explanatory references.

Finally, an important normalization that preserves three parameters while avoiding singularities is that associated with the exponential map. Introduce a *rotation vector* $\boldsymbol{\theta}$ defined as

$$\boldsymbol{\theta} = \theta\mathbf{n} = (\theta/\omega)\boldsymbol{\omega}, \quad \boldsymbol{\Theta} = \mathrm{Spin}(\boldsymbol{\theta}) = \theta\mathbf{N} = (\theta/\omega)\boldsymbol{\Omega}. \tag{63}$$

For this normalization the angle is the length of the rotation vector: $\theta = |\ \boldsymbol{\theta}\ | = \sqrt{\theta_1^2 + \theta_2^2 + \theta_3^2}$. The selection of the sign of θ is a matter of convention.

A.5. Spectral properties

The study of the spinor eigensystem $\boldsymbol{\Omega}\mathbf{z}_i = \lambda_i\mathbf{z}_i$ is of interest for various developments. Begin by forming the characteristic equation

$$\det(\boldsymbol{\Omega} - \lambda\mathbf{I}) = -\boldsymbol{\lambda}^3 - \omega^2\lambda = 0, \tag{64}$$

where $\mathbf{I}$ denotes the identity matrix of order 3. It follows that the eigenvalues of $\boldsymbol{\Omega}$ are $\lambda_1 = 0$, $\lambda_{2,3} = \pm\omega\mathrm{i}$. Consequently $\boldsymbol{\Omega}$ is singular with rank 2 if $\omega \neq 0$, whereas if $\omega = 0$, $\boldsymbol{\Omega}$ is null.

The eigenvalues are collected in the diagonal matrix $\boldsymbol{\Lambda} = \mathrm{diag}(0, \omega\mathrm{i}, -\omega\mathrm{i})$ and the corresponding right eigenvectors $\mathbf{z}_i$ in columns of $\mathbf{Z} = [\mathbf{z}_1\ \mathbf{z}_2\ \mathbf{z}_3]$, so that $\boldsymbol{\Omega}\mathbf{Z} = \mathbf{Z}\boldsymbol{\Lambda}$. A cyclic-symmetric expression of $\mathbf{Z}$, obtained through *Mathematica*, is

$$\mathbf{Z} = \begin{bmatrix} \omega_1 & \omega_1 s - \omega^2 + \mathrm{i}(\omega_2 - \omega_3)\omega & \omega_1 s - \omega^2 - \mathrm{i}(\omega_2 - \omega_3)\omega \\ \omega_2 & \omega_2 s - \omega^2 + \mathrm{i}(\omega_3 - \omega_1)\omega & \omega_2 s - \omega^2 - \mathrm{i}(\omega_3 - \omega_1)\omega \\ \omega_3 & \omega_3 s - \omega^2 + \mathrm{i}(\omega_1 - \omega_2)\omega & \omega_3 s - \omega^2 - \mathrm{i}(\omega_1 - \omega_2)\omega \end{bmatrix}, \tag{65}$$

where $s = \omega_1 + \omega_2 + \omega_3$. Its inverse is

$$\mathbf{Z}^{-1} = \frac{1}{\omega^2}\begin{bmatrix} \omega_1 & -\frac{1}{2}\dfrac{\omega_2^2 + \omega_3^2}{\omega_1 s - \omega^2 - \mathrm{i}(\omega_2 - \omega_3)\omega} & -\frac{1}{2}\dfrac{\omega_2^2 + \omega_3^2}{\omega_1 s - \omega^2 + \mathrm{i}(\omega_2 - \omega_3)\omega} \\ \omega_2 & -\frac{1}{2}\dfrac{\omega_3^2 + \omega_1^2}{\omega_2 s - \omega^2 - \mathrm{i}(\omega_3 - \omega_1)\omega} & -\frac{1}{2}\dfrac{\omega_3^2 + \omega_1^2}{\omega_2 s - \omega^2 + \mathrm{i}(\omega_3 - \omega_1)\omega} \\ \omega_3 & -\frac{1}{2}\dfrac{\omega_1^2 + \omega_2^2}{\omega_3 s - \omega^2 - \mathrm{i}(\omega_1 - \omega_2)\omega} & -\frac{1}{2}\dfrac{\omega_1^2 + \omega_2^2}{\omega_3 s - \omega^2 + \mathrm{i}(\omega_1 - \omega_2)\omega} \end{bmatrix} \tag{66}$$

The real and imaginary part of the eigenvectors $\mathbf{z}_2$ and $\mathbf{z}_3$ are orthogonal. This is a general property of skew-symmetric matrices; cf. Bellman [6, p. 64]. Because the eigenvalues of $\mathbf{\Omega}$ are distinct if $\omega \neq 0$, an arbitrary matrix function $\mathbf{F}(\mathbf{\Omega})$ can be explicitly obtained as

$$\mathbf{F}(\mathbf{\Omega}) = \mathbf{Z}\begin{bmatrix} f(0) & 0 & 0 \\ 0 & f(\omega \mathrm{i}) & 0 \\ 0 & 0 & f(-\omega \mathrm{i}) \end{bmatrix}\mathbf{Z}^{-1}, \tag{67}$$

where $f(\cdot)$ denotes the scalar version of $\mathbf{F}(\cdot)$. One important application of (67) is the matrix exponential, for which $f(\cdot) \to e^{(\cdot)}$.

The square of $\mathbf{\Omega}$, computed through direct multiplication, is

$$\mathbf{\Omega}^2 = -\begin{bmatrix} \omega_2^2+\omega_3^2 & -\omega_1\omega_2 & -\omega_1\omega_3 \\ -\omega_1\omega_2 & \omega_3^2+\omega_1^2 & -\omega_2\omega_3 \\ -\omega_1\omega_3 & -\omega_2\omega_3 & \omega_1^2+\omega_2^2 \end{bmatrix} = \boldsymbol{\omega}\boldsymbol{\omega}^{\mathrm{T}} - \omega^2\mathbf{I} = \omega^2(\mathbf{n}\mathbf{n}^{\mathrm{T}} - \mathbf{I}). \tag{68}$$

This is a symmetric matrix of trace $-2\omega^2$ whose eigenvalues are $0, -\omega^2$ and $-\omega^2$. By the Cayley–Hamilton theorem, $\mathbf{\Omega}$ satisfies its own characteristic equation (64)

$$\mathbf{\Omega}^3 = -\omega^2\mathbf{\Omega}, \quad \mathbf{\Omega}^4 = -\omega^2\mathbf{\Omega}^2, \cdots \quad \text{and generally } \mathbf{\Omega}^n = -\omega^2\mathbf{\Omega}^{n-2},\ n \geqslant 3. \tag{69}$$

Hence if $n = 3, 5, \ldots$ the odd powers $\mathbf{\Omega}^n$ are skew-symmetric with distinct purely imaginary eigenvalues, whereas if $n = 4, 6, \ldots$, the even powers $\mathbf{\Omega}^n$ are symmetric with repeated real eigenvalues.

The eigenvalues of $\mathbf{I} + \gamma\mathbf{\Omega}$ and $\mathbf{I} - \gamma\mathbf{\Omega}$, are $(1, 1 \pm \gamma\,\omega\,\mathrm{i})$ and $(-1, 1 \pm \gamma\,\omega\,\mathrm{i})$, respectively. Hence those two matrices are guaranteed to be nonsingular. This has implications in the Cayley transform (82).

Example. Consider the pseudo-vector $\boldsymbol{\omega} = [6\ 2\ 3]^{\mathrm{T}}$, for which $\omega = \sqrt{6^2+2^2+3^2} = 7$. The associated spin matrix and its square are

$$\mathbf{\Omega} = \begin{bmatrix} 0 & -3 & 2 \\ 3 & 0 & -6 \\ -2 & 6 & 0 \end{bmatrix}, \quad \mathbf{\Omega}^2 = -\begin{bmatrix} 13 & -12 & -18 \\ -12 & 45 & -6 \\ -18 & -6 & 40 \end{bmatrix}, \quad \mathbf{\Omega}^3 = -49\mathbf{\Omega}, \ldots \tag{70}$$

The eigenvalues of $\mathbf{\Omega}$ are $(0, 7i, -7i)$ while those of $\mathbf{\Omega}^2$ are $(0, -7, -7)$.

A.6. From spinors to rotators

Referring to Fig. 12, a rotator is a linear operator that maps a generic point $P(\mathbf{x})$ to $Q(\mathbf{x}_\theta)$ given the rotation axis $\vec{\boldsymbol{\omega}}$ and the angle θ. We consider only rotator representations in the form of 3×3 *rotation matrices* $\mathbf{R}$, defined by

$$\mathbf{x}_\theta = \mathbf{R}\mathbf{x}, \quad \mathbf{x} = \mathbf{R}^{\mathrm{T}}\mathbf{x}_\theta. \tag{71}$$

The rotation matrix is *proper orthogonal*, that is, $\mathbf{R}^{\mathrm{T}}\mathbf{R} = \mathbf{I}$ and $\det(\mathbf{R}) = +1$. It must reduce to $\mathbf{I}$ if the rotation vanishes. The space of all $\mathbf{R}$s form the rotation group SO(3).

Remark 5. The definition (71) is taken to agree with the convention for positive rotation angle θ illustrated in Fig. 12 and the definition of $\mathrm{Spin}(\boldsymbol{\omega})$ given in (55). Several books, e.g. Goldstein [35], define as spin matrix $\mathbf{\Omega}$ the transpose of ours. The definition used here agrees with that of the historical review paper by Cheng and Gupta [20]. Readers consulting the literature or implementing finite rotation analysis are advised to check sign conventions carefully. A recommended verification is to work out the 2D case by hand, since the specialization to plane rotation should produce well known coordinate transformations.

A.7. Rotator parametrizations

A key attribute of $\mathbf{R}$ is the *trace property*

$$\mathbf{trace}(\mathbf{R}) = 1 + 2\cos\theta, \tag{72}$$

proofs of which may be found for example in Goldstein [35, p. 123] or Hammermesh [36, p. 326]. (It follows from the fact that the eigenvalues of $\mathbf{R}$ are 1, $e^{\theta i}$ and $e^{-\theta i}$ and their sum is (72).) The problem considered here is the construction of $\mathbf{R}$ from rotation data. The inverse problem: given $\mathbf{R}$, extract spin and/or rotation angles, is treated later. Now if $\mathbf{R}$ is assumed to be analytic in $\mathbf{\Omega}$ it must have the Taylor expansion $\mathbf{R} = \mathbf{I} + c_1\mathbf{\Omega} + c_2\mathbf{\Omega}^2 + c_3\mathbf{\Omega}^3 + \cdots$, where all c_i must vanish if $\theta = 0$. But because of the Cayley–Hamilton theorem (69), all powers of order 3 or higher may be eliminated. Thus $\mathbf{R}$ must be a linear function of $\mathbf{I}$, $\mathbf{\Omega}$ and $\mathbf{\Omega}^2$. For convenience this will be written

$$\mathbf{R} = \mathbf{I} + \alpha(\gamma\mathbf{\Omega}) + \beta(\gamma\mathbf{\Omega})^2. \tag{73}$$

Here γ is the spinor normalization factor whereas α and β are scalar functions of θ and of invariants of $\mathbf{\Omega}$ or $\boldsymbol{\omega}$. Since the only invariant of the latter is ω we may anticipate that $\alpha = \alpha(\theta,\omega)$ and $\beta = \beta(\theta,\omega)$, both vanishing if $\theta = 0$. Two techniques to determine those coefficients for $\gamma = 1$ are discussed in the next subsections. Table 5 collects several representations of a rotator in terms of the scaled $\mathbf{\Omega}$, used by different authors.

A.7.1. Rotator from algebra

It is possible to find α and β for $\gamma = 1$ (the unscaled spinor) directly from algebraic conditions. Taking the trace of (73) for $\gamma = 1$ and applying the property (72) requires

$$3 - 2\beta\omega^2 = 1 + 2\cos\theta \quad \text{whence } \beta = \frac{1-\cos\theta}{\omega^2} = \frac{2\sin^2\frac{1}{2}\theta}{\omega^2}. \tag{74}$$

The orthogonality condition $\mathbf{I} = \mathbf{R}^{\mathrm{T}}\mathbf{R} = (\mathbf{I} - \alpha\mathbf{\Omega} + \beta\mathbf{\Omega}^2)(\mathbf{I} + \alpha\mathbf{\Omega} + \beta\mathbf{\Omega}^2) = \mathbf{I} + (2\beta - \alpha^2)\mathbf{\Omega}^2 + \beta^2\mathbf{\Omega}^4 = \mathbf{I} + (2\beta - \alpha^2 - \beta^2\omega^2)\mathbf{\Omega}^2$ leads to

$$2\beta - \alpha^2 - \beta^2\omega^2 = 0 \quad \text{whence } \alpha = \frac{\sin\theta}{\omega}. \tag{75}$$

Therefore

$$\mathbf{R} = \mathbf{I} + \frac{\sin\theta}{\omega}\mathbf{\Omega} + \frac{1-\cos\theta}{\omega^2}\mathbf{\Omega}^2 = \mathbf{I} + \frac{\sin\theta}{\omega}\mathbf{\Omega} + \frac{2\sin^2\frac{1}{2}\theta}{\omega^2}\mathbf{\Omega}^2. \tag{76}$$

From a numerical standpoint the sine-squared form should be preferred to avoid the cancellation in computing $1 - \cos\theta$ for small θ. Replacing the components of $\mathbf{\Omega}$ and $\mathbf{\Omega}^2$ gives the explicit rotator form

$$\mathbf{R} = \frac{1}{\omega^2}\begin{bmatrix} \omega_1^2 + (\omega_2^2+\omega_3^2)\cos\theta & 2\omega_1\omega_2\sin^2\frac{1}{2}\theta - \omega_3\omega\sin\theta & 2\omega_1\omega_3\sin^2\frac{1}{2}\theta + \omega_2\omega\sin\theta \\ 2\omega_1\omega_2\sin^2\frac{1}{2}\theta + \omega_3\omega\sin\theta & \omega_2^2 + (\omega_3^2+\omega_1^2)\cos\theta & 2\omega_2\omega_3\sin^2\frac{1}{2}\theta - \omega_1\omega\sin\theta \\ 2\omega_1\omega_3\sin^2\frac{1}{2}\theta - \omega_2\omega\sin\theta & 2\omega_2\omega_3\sin^2\frac{1}{2}\theta + \omega_1\omega\sin\theta & \omega_3^2 + (\omega_1^2+\omega_2^2)\cos\theta \end{bmatrix}. \tag{77}$$

If $\gamma \neq 1$ but nonzero, the answers are $\alpha = \sin\theta/(\gamma\omega)$ and $\beta = (1-\cos\theta)/(\gamma^2\omega^2)$. It follows that (76) and (77) are independent of γ, as was to be expected.

A.7.2. Rotator from geometry

The vector representation of the rigid motion depicted in Fig. 12 is

$$\vec{\mathbf{x}}_\theta = \vec{\mathbf{x}}\cos\theta + (\vec{\mathbf{n}}\times\vec{\mathbf{x}})\sin\theta + \vec{\mathbf{n}}(\vec{\mathbf{n}}\cdot\vec{\mathbf{x}})(1-\cos\theta) = \vec{\mathbf{x}} + (\vec{\mathbf{n}}\times\vec{\mathbf{x}})\sin\theta + [\vec{\mathbf{n}}\times(\vec{\mathbf{n}}\times\vec{\mathbf{x}})](1-\cos\theta), \tag{78}$$

where $\vec{\mathbf{n}}$ is $\vec{\boldsymbol{\omega}}$ normalized to unit length as per (63). This can be recast in matrix form by substituting $\vec{\mathbf{n}} \times \vec{\mathbf{x}} \to \mathbf{N}\mathbf{x} = \boldsymbol{\Omega}\mathbf{x}/\omega$ and $\mathbf{x}_\theta = \mathbf{R}\mathbf{x}$. On cancelling $\mathbf{x}$ we get back (76).

A.8. Rotators for all seasons

If $\boldsymbol{\omega}$ is unit-length-normalized to $\mathbf{n}$ as per (59), $\gamma = 1/\omega$ and $\mathbf{R} = \mathbf{I} + \sin\theta\mathbf{N} + (1 - \cos\theta)\mathbf{N}^2$. This is the matrix form of (78). Because $\mathbf{N}^2 = \mathbf{n}\mathbf{n}^{\mathrm{T}} - \mathbf{I}$, an occassionally useful variant is

$$\mathbf{R} = \mathbf{R}^* + (1 - \cos\theta)\mathbf{n}\mathbf{n}^{\mathrm{T}}, \quad \mathbf{R}^* = \cos\theta\mathbf{I} + \sin\theta\mathbf{N}. \tag{79}$$

In terms of the three Rodrigues–Cayley parameters b_i introduced in (60), $\alpha = \beta = 2\cos^2\frac{1}{2}\theta$ and $\mathbf{R} = \mathbf{I} + 2\cos^2\frac{1}{2}\theta(\boldsymbol{\Sigma} + \boldsymbol{\Sigma}^2)$. This can be explicitly worked out to be

$$\mathbf{R} = \frac{1}{1 + b_1^2 + b_2^2 + b_3^2}\begin{bmatrix} 1 + b_1^2 - b_2^2 - b_3^2 & 2(b_1b_2 - b_3) & 2(b_1b_3 + b_2) \\ 2(b_1b_2 + b_3) & 1 - b_1^2 + b_2^2 - b_3^2 & 2(b_2b_3 - b_1) \\ 2(b_1b_3 - b_2) & 2(b_2b_3 + b_1) & 1 - b_1^2 - b_2^2 + b_3^2 \end{bmatrix}. \tag{80}$$

This form was first derived by Rodrigues [69] and used by Cayley [19, p. 332–336] to study rigid body motions. It has the advantage of being obtainable through an algebraic matrix expression: the Cayley transform, presented below. It becomes indeterminate, however, as $\theta \to 180^\circ$, since all terms approach 0/0. This indeterminacy is avoided by using the four Euler–Rodrigues parameters, which are also the quaternion coefficients, defined in (61). In terms of these we get

$$\mathbf{R} = 2\begin{bmatrix} p_0^2 + p_1^2 - \frac{1}{2} & p_1p_2 - p_0p_3 & p_1p_3 + p_0p_2 \\ p_1p_2 + p_0p_3 & p_0^2 + p_2^2 - \frac{1}{2} & p_2p_3 - p_0p_1 \\ p_1p_3 - p_0p_2 & p_2p_3 + p_0p_1 & p_0^2 + p_3^2 - \frac{1}{2} \end{bmatrix}. \tag{81}$$

This expression cannot become singular. This is paid, however, at the cost of carrying along an extra parameter in addition to the constraint $p_0^2 + p_1^2 + p_2^2 + p_3^2 = 1$.

The normalization of Fraeijs de Veubeke [25] introduced in (62): $p_i = (\omega_i/\omega)\sin\frac{1}{2}\theta$, leads to $\alpha = 2\cos\frac{1}{2}\theta$ and $\beta = 2$. Hence $\mathbf{R} = \mathbf{I} + 2\cos\frac{1}{2}\theta\boldsymbol{\Omega}_p + 2\boldsymbol{\Omega}_p^2$, with $\boldsymbol{\Omega}_p = (\sin\frac{1}{2}\theta/\omega)\boldsymbol{\Omega}$.

A.9. The Cayley transform

Given any skew-symmetric real matrix $\boldsymbol{\Sigma} = -\boldsymbol{\Sigma}^{\mathrm{T}}$, we can apply the transformation

$$\mathbf{Q} = (\mathbf{I} + \boldsymbol{\Sigma})(\mathbf{I} - \boldsymbol{\Sigma})^{-1}. \tag{82}$$

[Note: this mapping can be written in many different ways; some authors use $(\mathbf{I} - \boldsymbol{\Sigma})(\mathbf{I} + \boldsymbol{\Sigma})^{-1}$, some switch I and $\boldsymbol{\Sigma}$, while others prefer the involutory form $(\mathbf{I} + \boldsymbol{\Sigma})^{-1}(\mathbf{I} - \boldsymbol{\Sigma})$.] $\mathbf{Q}$ is a proper orthogonal matrix, that is $\mathbf{Q}^{\mathrm{T}}\mathbf{Q} = \mathbf{I}$ and $\det\mathbf{Q} = +1$. This is stated in several texts, e.g., Gantmacher [33, p. 288] and Turnbull [84, p. 156] but none gives a proof for general order. Here is the orthogonality proof: $\mathbf{Q}^{\mathrm{T}}\mathbf{Q} = (\mathbf{I} + \boldsymbol{\Sigma})^{-1}(\mathbf{I} - \boldsymbol{\Sigma})(\mathbf{I} + \boldsymbol{\Sigma})(\mathbf{I} - \boldsymbol{\Sigma})^{-1} = (\mathbf{I} + \boldsymbol{\Sigma})^{-1}\ (\mathbf{I} + \boldsymbol{\Sigma})(\mathbf{I} - \boldsymbol{\Sigma})(\mathbf{I} - \boldsymbol{\Sigma})^{-1} = \mathbf{I}^2 = \mathbf{I}$ because $\mathbf{I} + \boldsymbol{\Sigma}$ and $\mathbf{I} - \boldsymbol{\Sigma}$ commute. The property $\det\mathbf{Q} = +1$ can be shown to hold from the spectral properties of skew-symmetric matrices. The inverse transformation

$$\boldsymbol{\Sigma} = (\mathbf{Q} + \mathbf{I})^{-1}(\mathbf{Q} - \mathbf{I}), \tag{83}$$

produces skew-symmetric matrices from a source proper-orthogonal matrix $\mathbf{Q}$. Eqs. (82) and (83) are called the *Cayley transforms* after Cayley [20]. These formulas are sometimes useful in the construction of approximations for moderate rotations.

An interesting question is: given $\mathbf{\Omega}$ and θ, can (82) be used to produce the exact $\mathbf{R}$? The answer is: yes, if $\mathbf{\Omega}$ is scaled by a specific $\gamma = \gamma(\theta,\omega)$. We thus investigate whether $\mathbf{R} = (\mathbf{I} + \gamma\mathbf{\Omega})(\mathbf{I} - \gamma\mathbf{\Omega})^{-1}$ exactly for some γ. Premultiplying both sides by $\mathbf{I} - \gamma\mathbf{\Omega}$ and representing $\mathbf{R}$ by (73) we require

$$(\mathbf{I} - \gamma\mathbf{\Omega})(\mathbf{I} + \alpha\gamma\mathbf{\Omega} + \beta\gamma^2\mathbf{\Omega}^2) = \mathbf{I} + \gamma(\alpha - \gamma + \gamma\beta\omega^2)\mathbf{\Omega} + \gamma^2(\beta - \alpha)\mathbf{\Omega}^2 = \mathbf{I} + \gamma\mathbf{\Omega} \tag{84}$$

Identifying coefficients and assuming $\gamma \neq 0$ we get the conditions $\beta = \alpha$ and $\alpha - 1 + \beta\omega^2\gamma^2 = 1$, from which $\alpha = \beta = 2/(1 + \gamma^2\omega^2)$. Equating to $\beta = 2\sin^2\frac{1}{2}\theta/(\gamma^2\omega^2)$ and solving for $\gamma\omega$ gives as only solutions $\gamma = \pm\tan\frac{1}{2}\theta/\omega$. Adopting the + sign, this becomes the normalization (60). Consequently

$$\mathbf{R} = (\mathbf{I} + \mathbf{\Sigma})(\mathbf{I} - \mathbf{\Sigma})^{-1}, \quad \mathbf{\Sigma} = \frac{\tan\frac{1}{2}\theta}{\omega}\mathbf{\Omega}. \tag{85}$$

The explicit calculation of $\mathbf{R}$ in terms of the b_i leads to (80).

A.10. Exponential map

This is a final representation of $\mathbf{R}$ that has theoretical and practical importance. Given a skew-symmetric real matrix $\mathbf{W}$, the matrix exponential

$$\mathbf{Q} = \mathrm{e}^{\mathbf{W}} = \mathrm{Exp}(\mathbf{W}) \tag{86}$$

is proper orthogonal. Here is the simple proof of Gantmacher [33, p 287]. First, $\mathbf{Q}^{\mathrm{T}} = \mathrm{Exp}(\mathbf{W}^{\mathrm{T}}) = \mathrm{Exp}(-\mathbf{W}^{\mathrm{T}}) = \mathbf{Q}^{-1}$. Next, if the eigenvalues of $\mathbf{W}$ are λ_i, $\sum_i\lambda_i = \mathrm{trace}(\mathbf{W}) = 0$. The eigenvalues of $\mathbf{Q}$ are $\mu_i = \exp(\lambda_i)$; thus $\det(\mathbf{Q}) = \Pi_i\mu_i = \exp(\sum_i\lambda_i) = \exp(0) = +1$. The transformation (86) is called an *exponential map*. The converse is of course $\mathbf{W} = \mathrm{Log}_e(\mathbf{Q})$ with the principal value taken.

As in the case of the Cayley transform, one may pose the question of whether we can get the rotator $\mathbf{R} = \mathrm{Exp}(\gamma\mathbf{\Omega})$ exactly for some factor $\gamma = \gamma(\theta,\omega)$. To study this question we need an explicit form of the exponential. This can be obtained from the spectral form (67) in which the spin function is Exp so that the diagonal matrix entries are 1 and $\exp(\pm\gamma\omega i) = \cos\gamma\omega \pm i\sin\gamma\omega$. The following approach is more instructive and leads directly to the final result. Start from the definition of the matrix exponential

$$\mathrm{Exp}(\gamma\mathbf{\Omega}) = \mathbf{I} + \gamma\mathbf{\Omega} + \frac{\gamma^2}{2!}\mathbf{\Omega}^2 + \frac{\gamma^3}{3!}\mathbf{\Omega}^3 + \cdots \tag{87}$$

and use the Cayley–Hamilton theorem (69) to eliminate all powers of order 3 or higher in $\mathbf{\Omega}$. Identify the coefficient series of $\mathbf{\Omega}$ and $\mathbf{\Omega}^2$ with those of the sine and cosine, to obtain

$$\mathrm{Exp}(\gamma\mathbf{\Omega}) = \mathbf{I} + \frac{\sin(\gamma\omega)}{\gamma\omega}\mathbf{\Omega} + \frac{1 - \cos(\gamma\omega)}{\gamma^2\omega^2}\mathbf{\Omega}^2. \tag{88}$$

Comparing this to (76) requires $\gamma\omega = \theta$, or $\gamma = \theta/\omega$. Introducing $\theta_i = \theta\omega_i/\omega$ and $\mathbf{\Theta} = \mathrm{Spin}(\boldsymbol{\theta}) = \theta\mathbf{N} = (\theta/\omega)\mathbf{\Omega}$ as in (63), we find

$$\mathbf{R} = \mathrm{Exp}(\mathbf{\Theta}) = \mathbf{I} + \frac{\sin\theta}{\theta}\mathbf{\Theta} + \frac{1 - \cos\theta}{\theta^2}\mathbf{\Theta}^2 = \mathbf{I} + \frac{\sin\theta}{\theta}\mathbf{\Theta} + \frac{2\sin^2\frac{1}{2}\theta}{\theta^2}\mathbf{\Theta}^2. \tag{89}$$

On substituting $\mathbf{\Theta} = \theta\mathbf{N}$ this recovers $\mathbf{R} = \mathbf{I} + \sin\theta\mathbf{N} + (1 - \cos\theta)\mathbf{N}^2$, as it should.

This representation has several advantages: it is singularity free, the parameters θ_i are exactly proportional to the angle, and the differentiation of $\mathbf{R}$ is simplified. Because of these favorable attributes the exponential map has become a favorite of implementations where very large rotations may occur, as in orbiting structures and robotics.

Remark 6. Some authors state that the exponential map is exact whereas the Cayley transform is a (1, 1) Padé approximation to it. The foregoing treatment shows that the statement is incorrect. Both are exact for specific but different spinor normalizations, and inexact otherwise.

A.11. Skew-symmetric matrix relations

The following relations involving spinors are useful in some derivations. If **v** and **w** are two 3-vectors, and **V** = Spin(**v**) and **W** = Spin(**w**) the associated spinors, **VW** − **WV** is skew-symmetric and

$$\text{axial}(\mathbf{VW}-\mathbf{WV}) = \mathbf{Vw} = -\mathbf{Wv}. \tag{90}$$

Let **Q** be an arbitrary nonsingular 3×3 matrix whereas **W** = Spin(**w**) is skew-symmetric. It can be easily verified that $\mathbf{Q}^{\mathrm{T}}\mathbf{WQ}$ is skew-symmetric. Then

$$\det(\mathbf{Q})\mathbf{Q}^{-1}\mathbf{w} = \text{axial}(\mathbf{Q}^{\mathrm{T}}\mathbf{WQ}), \quad \det(\mathbf{Q})\mathbf{Q}^{-T}\mathbf{w} = \text{axial}(\mathbf{QWQ}^{\mathrm{T}}). \tag{91}$$

If **Q** is proper orthogonal, $\mathbf{Q}^{-1} = \mathbf{Q}^{\mathrm{T}}$ and det(**Q**) = 1, in which case

$$\mathbf{Q}^{\mathrm{T}}\mathbf{w} = \text{axial}(\mathbf{Q}^{\mathrm{T}}\mathbf{WQ}), \quad \mathbf{Qw} = \text{axial}(\mathbf{QWQ}^{\mathrm{T}}). \tag{92}$$

The inverse of $\mathbf{Q} = \mathbf{I} + \alpha\mathbf{W} + \beta\mathbf{W}^2$, in which **W** = Spin(**w**) is skew-symmetric, is

$$\mathbf{Q}^{-1} = \mathbf{I} + \frac{\alpha}{\alpha^2 w^2 + (\beta w^2 - 1)^2}\mathbf{W} + \frac{\alpha^2 + \beta(\beta w^2 - 1)}{\alpha^2 w^2 + (\beta w^2 - 1)^2}\mathbf{W}^2, \quad \text{with} \quad w^2 = \|\mathbf{w}\|^2 = w_1^2 + w_2^2 + w_3^2. \tag{93}$$

A.12. From rotators to spinors

If $\mathbf{R}(\mathbf{n}, \theta)$ is given, the extraction of the rotation angle θ and the unit pseudo-vector $\mathbf{n} = \boldsymbol{\omega}/\omega$ is often required. The former is easy using the trace property (72)

$$\cos\theta = \tfrac{1}{2}(\text{trace}(\mathbf{R}) - 1) \tag{94}$$

Recovery of **n** is straightforward from the unit-axial–vector form $\mathbf{R} = \mathbf{I} + \sin\theta\mathbf{N} + (1 - \cos\theta)\mathbf{N}^2$ since $\mathbf{R} - \mathbf{R}^{\mathrm{T}} = 2\sin\theta\mathbf{N}$, whence

$$\mathbf{N} = \frac{\mathbf{R} - \mathbf{R}^{\mathrm{T}}}{2\sin\theta}, \quad \mathbf{n} = \begin{bmatrix} n_1 \\ n_2 \\ n_3 \end{bmatrix} = \text{axial}(\mathbf{N}). \tag{95}$$

One issue is the sign of θ since (94) is satisfied by $\pm\theta$. If the sign is reversed, so is **n**. Thus it is possible to select $\theta \geqslant 0$ if no constraints are placed on the direction of the rotation axis.

The foregoing formulas are prone to numerical instability for angles near 0°, ±180°, etc., because $\sin\theta$ vanishes. A robust algorithm is that given by Spurrier [76] in the language of quaternions. Choose the algebraically largest of trace(**R**) and R_{ii}, $i = 1, 2, 3$. If trace(**R**) is the largest, compute

$$p_0 = \cos\frac{1}{2}\theta = \frac{1}{2}\sqrt{1 + \text{trace}(\mathbf{R})}, \quad p_i = n_i \sin\frac{1}{2}\theta = \frac{1}{4}(R_{kj} - R_{jk})/p_0, \quad i = 1, 2, 3, \tag{96}$$

where j and k are the cyclic permutations of i. Otherwise let R_{ii} be the algebraically largest diagonal entry, and again denote by i, j, k its cyclic permutation. Then use

$$p_i = n_i \sin\frac{1}{2}\theta = \sqrt{\frac{1}{2}R_{ii} + \frac{1}{4}(1 - \mathrm{trace}(\mathbf{R}))}, \quad p_0 = \cos\frac{1}{2}\theta = \frac{1}{4}(R_{kj} - R_{jk})/p_i,$$
$$p_m = \frac{1}{4}(R_{m,i} + R_{i,m})/p_i, \quad m = j,k. \tag{97}$$

From p_0, p_1, p_2, p_3 it is easy to pass to θ, n_1, n_2, n_3 once the sign of θ is chosen as discussed above.

The theoretical formula for the logarithm of a 3×3 orthogonal matrix is

$$\boldsymbol{\Theta} = \mathrm{Log}_e(\mathbf{R}) = \frac{\arcsin\tau}{2\tau}(\mathbf{R} - \mathbf{R}^{\mathrm{T}}), \quad \boldsymbol{\Omega} = \frac{\omega}{\theta}\boldsymbol{\Theta}, \quad \mathbf{N} = \frac{\boldsymbol{\Theta}}{\theta}, \tag{98}$$

where $\tau = \frac{1}{2}\|\mathrm{axial}(\mathbf{R} - \mathbf{R}^{\mathrm{T}})\|_2$. The formula fails, however, outside the range $[-\pi/2 \leqslant \theta \leqslant \pi/2]$ and is numerically unstable near $\theta = 0$.

A.13. Spinor and rotator transformations

Suppose $\boldsymbol{\Omega}$ is a spinor and $\mathbf{R} = \mathrm{Rot}(\boldsymbol{\Omega})$ the associated rotator, referred to a Cartesian frame $\mathbf{x} = \{x_i\}$. It is required to transform $\mathbf{R}$ to another Cartesian frame $\bar{\mathbf{x}} = \{\bar{x}_i\}$ related by $T_{ij} = \partial\bar{x}_i/\partial x_j$, where T_{ij} are entries of a 3×3 orthogonal matrix $\mathbf{T} = \partial\bar{\mathbf{x}}/\partial\mathbf{x}$. Application of (71) yields

$$\overline{\mathbf{K}\mathbf{R}} = \mathbf{T}\mathbf{R}\mathbf{T}^{\mathrm{T}}, \quad \overline{\mathbf{R}}^{\mathrm{T}} = \mathbf{T}\mathbf{R}^{\mathrm{T}}\mathbf{T}^{\mathrm{T}}, \quad \mathbf{R} = \mathbf{T}^{\mathrm{T}}\overline{\mathbf{R}}\mathbf{T}, \quad \mathbf{R} = \mathbf{T}^{\mathrm{T}}\overline{\mathbf{R}}^{\mathrm{T}}\mathbf{T}. \tag{99}$$

More details may be found in Chapter 4 of [35]. Pre and post-multiplying (95) by $\mathbf{T}$ and $\mathbf{T}^{\mathrm{T}}$, respectively, yields the transformed spinor $\overline{\mathbf{N}} = \mathbf{T}\mathbf{N}\mathbf{T}^{\mathrm{T}}$, which is also skew-symmetric because $\overline{\mathbf{N}}^{\mathrm{T}} = \mathbf{T}\mathbf{N}^{\mathrm{T}}\mathbf{T}^{\mathrm{T}} = -\overline{\mathbf{N}}$. Likewise for the other spinors listed in Table 5. Relations (92) with $\mathbf{Q} \to \mathbf{T}$ show how axial vectors transform.

A.14. Axial vector Jacobian

The Jacobian matrix $\mathbf{H}(\boldsymbol{\theta}) = \partial\boldsymbol{\theta}/\partial\boldsymbol{\omega}$ of the rotational axial vector $\boldsymbol{\theta}$ with respect to the spin axial vector $\boldsymbol{\omega}$, and its inverse $\mathbf{H}(\boldsymbol{\theta})^{-1} = \partial\boldsymbol{\omega}/\partial\boldsymbol{\theta}$, appear in the EICR. The latter was first derived by Simo [71] and Szwabowicz [77], and rederived by Nour-Omid and Rankin [54, p. 377]:

$$\mathbf{H}(\boldsymbol{\theta})^{-1} = \frac{\partial\boldsymbol{\omega}}{\partial\boldsymbol{\theta}} = \frac{\sin\theta}{\theta}\mathbf{I} + \frac{1-\cos\theta}{\theta^2}\boldsymbol{\Theta} + \frac{\theta - \sin\theta}{\theta^3}\boldsymbol{\theta}\boldsymbol{\theta}^{\mathrm{T}} = \mathbf{I} + \frac{1-\cos\theta}{\theta^2}\boldsymbol{\Theta} + \frac{\theta-\sin\theta}{\theta^3}\boldsymbol{\Theta}^2. \tag{100}$$

The last expression in (100), not given by the cited authors, is obtained on replacing $\boldsymbol{\theta}\boldsymbol{\theta}^{\mathrm{T}} = \theta^2\mathbf{I} + \boldsymbol{\Theta}^2$. Use of the inversion formula (93) gives

$$\mathbf{H}(\boldsymbol{\theta}) = \frac{\partial\boldsymbol{\theta}}{\partial\boldsymbol{\omega}} = \mathbf{I} - \frac{1}{2}\boldsymbol{\Theta} + \eta\boldsymbol{\Theta}^2 \quad \text{with } \eta = \frac{1 - \frac{1}{2}\theta\cot\left(\frac{1}{2}\theta\right)}{\theta^2}$$
$$= \frac{1}{12} + \frac{1}{720}\theta^2 + \frac{1}{30240}\theta^4 + \frac{1}{1209600}\theta^6 + \cdots \tag{101}$$

The η given in (101) results by simplifying the value $\eta = [\sin\theta - \theta(1+\cos\theta)]/[\theta^2\sin\theta]$ given by previous investigators. Care must be taken on evaluating η for small angle θ because it approaches 0/0; if $|\theta| < 1/20$, say, the series given above may be used, with error $<10^{-16}$ when 4 terms are retained. If θ is a multiple of 2π, η blows up since $\cot(\frac{1}{2}\theta) \to \infty$, and a modulo-$2\pi$ reduction is required.

In the formulation of the tangent stiffness matrix the spin derivative of $\mathbf{H}(\boldsymbol{\theta})^{\mathrm{T}}$ contracted with a nodal moment vector $\mathbf{m}$ is required:

$$\mathbf{L}(\boldsymbol{\theta},\mathbf{m}) = \frac{\partial \mathbf{H}(\boldsymbol{\theta})^{\mathrm{T}}}{\partial \boldsymbol{\omega}} : \mathbf{m} = \frac{\partial}{\partial \boldsymbol{\theta}}[\mathbf{H}(\boldsymbol{\theta})^{\mathrm{T}}\mathbf{m}]\mathbf{H}(\boldsymbol{\theta})$$
$$= \left\{\eta[(\boldsymbol{\theta}^{\mathrm{T}}\mathbf{m})\mathbf{I} + \boldsymbol{\theta}\mathbf{m}^{\mathrm{T}} - 2\mathbf{m}\boldsymbol{\theta}^{\mathrm{T}}] + \mu\boldsymbol{\Theta}^2\mathbf{m}\boldsymbol{\theta}^{\mathrm{T}} - \frac{1}{2}\mathrm{Spin}(\mathbf{m})\right\}\mathbf{H}(\boldsymbol{\theta}). \tag{102}$$

in which

$$\mu = \frac{\mathrm{d}\eta/\mathrm{d}\theta}{\theta} = \frac{\theta^2 + 4\cos\theta + \theta\sin\theta - 4}{4\theta^4\sin^2\left(\frac{1}{2}\theta\right)} = \frac{1}{360} + \frac{1}{7560}\theta^2 + \frac{1}{201600}\theta^4 + \frac{1}{5987520}\theta^6 + \cdots \tag{103}$$

This expression of μ was obtained by simplifying results given in [54, p. 378].

A.15. Spinor and rotator differentiation

Derivatives, differentials and variations of axial vectors, spinors and rotators with respect to various choices of independent variables appear in applications of finite rotations to mechanics. In this section we present only expressions that are useful in the CR description. They are initially derived for dynamics and then specialized to variations. Several of the formulas are new.

A.15.1. Angular velocities

We assume that the rotation angle $\boldsymbol{\theta}(t) = \theta(t)\mathbf{n}(t)$ is a given function of time t, which is taken as the independent variable. The time derivative of $\boldsymbol{\Theta}(t)$ is $\dot{\boldsymbol{\Theta}} = \mathrm{axial}(\dot{\boldsymbol{\theta}})$. To express rotator differentials in a symmetric manner we introduce an axial vector $\dot{\boldsymbol{\phi}}$ and a spinor $\dot{\boldsymbol{\Phi}} = \mathrm{Spin}(\dot{\boldsymbol{\phi}})$, related to $\dot{\boldsymbol{\Theta}}$ congruentially through the rotator:

$$\dot{\boldsymbol{\Theta}} = \mathrm{Spin}(\dot{\boldsymbol{\theta}}) = \begin{bmatrix} 0 & -\dot{\theta}_3 & \dot{\theta}_2 \\ \dot{\theta}_3 & 0 & -\dot{\theta}_1 \\ -\dot{\theta}_2 & \dot{\theta}_1 & 0 \end{bmatrix} = \mathbf{R}\dot{\boldsymbol{\Phi}}\mathbf{R}^{\mathrm{T}}, \quad \dot{\boldsymbol{\Phi}} = \mathrm{Spin}(\dot{\boldsymbol{\phi}}) = \begin{bmatrix} 0 & -\dot{\phi}_3 & \dot{\phi}_2 \\ \dot{\phi}_3 & 0 & -\dot{\phi}_1 \\ -\dot{\phi}_2 & \dot{\phi}_1 & 0 \end{bmatrix} = \mathbf{R}^{\mathrm{T}}\dot{\boldsymbol{\Theta}}\mathbf{R}. \tag{104}$$

From (92) it follows that the axial vectors are linked by

$$\dot{\boldsymbol{\phi}} = \mathbf{R}^{\mathrm{T}}\dot{\boldsymbol{\theta}}, \qquad \dot{\boldsymbol{\theta}} = \mathbf{R}\dot{\boldsymbol{\phi}}. \tag{105}$$

Corresponding relation between variations or differentials, such as $\delta\boldsymbol{\Theta} = \mathbf{R}\delta\boldsymbol{\Phi}\mathbf{R}^{\mathrm{T}}$ or $d\boldsymbol{\Theta} = \mathbf{R}d\boldsymbol{\Phi}\mathbf{R}^{\mathrm{T}}$ are incorrect as shown in below. In CR dynamics, $\dot{\boldsymbol{\theta}}$ is the vector of *inertial angular velocities* whereas $\dot{\boldsymbol{\phi}}$ is the vector of *dynamic angular velocities*.

Repeated temporal differentiation of $\mathbf{R} = \mathrm{Exp}(\boldsymbol{\Theta})$ gives the rotator time derivatives

$$\dot{\mathbf{R}} = \dot{\boldsymbol{\Theta}}\mathbf{R}, \quad \ddot{\mathbf{R}} = (\ddot{\boldsymbol{\Theta}} + \dot{\boldsymbol{\Theta}}^2)\mathbf{R}, \quad \dddot{\mathbf{R}} = (\dddot{\boldsymbol{\Theta}} + 2\ddot{\boldsymbol{\Theta}}\dot{\boldsymbol{\Theta}} + \dot{\boldsymbol{\Theta}}\ddot{\boldsymbol{\Theta}} + \dot{\boldsymbol{\Theta}}^3)\mathbf{R}, \ldots \tag{106}$$

$$\dot{\mathbf{R}} = \mathbf{R}\dot{\boldsymbol{\Phi}}, \quad \ddot{\mathbf{R}} = \mathbf{R}(\ddot{\boldsymbol{\Phi}} + \dot{\boldsymbol{\Phi}}^2), \quad \dddot{\mathbf{R}} = \mathbf{R}(\dddot{\boldsymbol{\Phi}} + 2\ddot{\boldsymbol{\Phi}}\dot{\boldsymbol{\Phi}} + \dot{\boldsymbol{\Phi}}\ddot{\boldsymbol{\Phi}} + \dot{\boldsymbol{\Phi}}^3), \ldots \tag{107}$$

The following four groupings appear often: $\mathbf{R}\dot{\mathbf{R}}^{\mathrm{T}}$, $\dot{\mathbf{R}}\mathbf{R}^{\mathrm{T}}$, $\mathbf{R}^{\mathrm{T}}\dot{\mathbf{R}}$ and $\dot{\mathbf{R}}^{\mathrm{T}}\mathbf{R}$. From the identities $\mathbf{R}\mathbf{R}^{\mathrm{T}} = \mathbf{I}$ and $\mathbf{R}^{\mathrm{T}}\mathbf{R} = \mathbf{I}$ it can be shown that they are skew-symmetric, and may be associated to axial vectors with physical meaning. For example, taking time derivatives of $\mathbf{R}\mathbf{R}^{\mathrm{T}} = \mathbf{I}$ yields $\mathbf{R}\dot{\mathbf{R}}^{\mathrm{T}} + \dot{\mathbf{R}}\mathbf{R}^{\mathrm{T}} = \mathbf{0}$, whence $\mathbf{R}\dot{\mathbf{R}}^{\mathrm{T}} = -\dot{\mathbf{R}}\mathbf{R}^{\mathrm{T}} = -(\mathbf{R}\dot{\mathbf{R}})^{\mathrm{T}}$. Pre- and post-multiplication of $\dot{\mathbf{R}}$ in (106) and (107) by $\mathbf{R}$ and $\mathbf{R}^{\mathrm{T}}$ furnishes

$$\dot{\mathbf{R}}\mathbf{R}^{\mathrm{T}} = -\mathbf{R}\dot{\mathbf{R}}^{\mathrm{T}} = \dot{\boldsymbol{\Theta}}, \qquad \mathbf{R}^{\mathrm{T}}\dot{\mathbf{R}} = -\dot{\mathbf{R}}^{\mathrm{T}}\mathbf{R} = \dot{\boldsymbol{\Phi}}. \tag{108}$$

Note that the general integral of $\dot{\mathbf{R}} = \dot{\mathbf{\Theta}}\mathbf{R}$ aside from a constant, is $\mathbf{R} = \mathrm{Exp}(\mathbf{\Theta})$, from which $\theta(t)$ can be extracted. On the other hand there is no integral relation defining $\phi(t)$; only the differential equation $\dot{\mathbf{R}} = \mathbf{R}\dot{\mathbf{\Phi}}$.

A.15.2. Angular accelerations

Postmultiplying the second of (106) by $\mathbf{R}^{\mathrm{T}}$ yields

$$\ddot{\mathbf{R}}\mathbf{R}^{\mathrm{T}} = \ddot{\mathbf{\Theta}} + \dot{\mathbf{\Theta}}^2 = \dot{\mathbf{\Theta}} + \dot{\boldsymbol{\theta}}\dot{\boldsymbol{\theta}}^{\mathrm{T}} - (\dot{\theta})^2\mathbf{I} = \begin{bmatrix} 0 & -\ddot{\theta}_3 & \ddot{\theta}_2 \\ \ddot{\theta}_3 & 0 & -\ddot{\theta}_1 \\ -\ddot{\theta}_2 & \ddot{\theta}_1 & 0 \end{bmatrix} + \begin{bmatrix} -\dot{\theta}_2^2 - \dot{\theta}_3^2 & \dot{\theta}_1\dot{\theta}_2 & \dot{\theta}_1\dot{\theta}_3 \\ \dot{\theta}_1\dot{\theta}_2 & -\dot{\theta}_3^2 - \dot{\theta}_1^2 & \dot{\theta}_2\dot{\theta}_3 \\ \dot{\theta}_1\dot{\theta}_3 & \dot{\theta}_2\dot{\theta}_3 & -\dot{\theta}_1^2 - \dot{\theta}_2^2 \end{bmatrix}, \tag{109}$$

in which $(\dot{\theta})^2 = \dot{\theta}_1^2 + \dot{\theta}_2^2 + \dot{\theta}_3^2$. When applied to a vector $\mathbf{r}$, $(\ddot{\mathbf{\Theta}} + \dot{\mathbf{\Theta}}\dot{\mathbf{\Theta}})\mathbf{r} = \ddot{\boldsymbol{\theta}} \times \mathbf{r} + \dot{\boldsymbol{\theta}}\dot{\boldsymbol{\theta}}^{\mathrm{T}}\mathbf{r} - (\dot{\theta})^2\mathbf{r}$. This operator appears in the expression of particle accelerations in a moving frame. The second and third term give rise to the Coriolis and centrifugal forces, respectively. Premultiplying the second derivative in (107) by $\mathbf{R}$ yields $\mathbf{R}\ddot{\mathbf{R}} = \ddot{\mathbf{\Phi}} + \dot{\mathbf{\Phi}}\dot{\mathbf{\Phi}}$, and so on.

A.15.3. Variations

Some of the foregoing expressions can be directly transformed to variational and differential forms while others cannot. For example, varying $\mathbf{R} = \mathrm{Exp}(\mathbf{\Theta})$ gives

$$\delta\mathbf{R} = \delta\mathbf{\Theta}\mathbf{R}, \qquad \delta\mathbf{R}^{\mathrm{T}} = -\mathbf{R}^{\mathrm{T}}\delta\mathbf{\Theta}. \tag{110}$$

This matches $\dot{\mathbf{R}} = \dot{\mathbf{\Theta}}\mathbf{R}$ and $\mathbf{R}^{\mathrm{T}} = -\mathbf{R}^{\mathrm{T}}\dot{\mathbf{\Theta}}$ from (106) on replacing $\dot{()}$ by δ. On the other hand, the counterparts of (107): $\dot{\mathbf{R}} = \mathbf{R}\dot{\mathbf{\Phi}}$ and $\dot{\mathbf{R}}^{\mathrm{T}} = -\dot{\mathbf{\Phi}}\mathbf{R}$ are *not* $\delta\mathbf{R} = \mathbf{R}\delta\dot{\Phi}$ and $\delta\mathbf{R}^{\mathrm{T}} = -\delta\dot{\mathbf{\Phi}}\mathbf{R}^{\mathrm{T}}$, a point that has tripped authors unfamiliar with moving frame dynamics. Correct handling requires the introduction of a third axial vector $\boldsymbol{\psi}$:

$$\delta\mathbf{R} = \mathbf{R}\delta\mathbf{\Psi}, \quad \delta\mathbf{R}^{\mathrm{T}} = -\delta\mathbf{\Psi}\mathbf{R}, \quad \text{in which } \delta\mathbf{\Psi} = \mathrm{Spin}(\delta\boldsymbol{\psi}) = \begin{bmatrix} 0 & -\delta\psi_3 & \delta\psi_2 \\ \delta\psi_3 & 0 & -\delta\psi_1 \\ -\delta\psi_2 & \delta\psi_1 & 0 \end{bmatrix} \tag{111}$$

Axial vectors $\boldsymbol{\psi}$ and $\boldsymbol{\phi}$ can be linked as follows. Start from $\delta\mathbf{R} = \mathbf{R}\delta\mathbf{\Psi}$and $\dot{\mathbf{R}} = \mathbf{R}\dot{\mathbf{\Phi}}$. Time differentiate the former: $\delta\dot{\mathbf{R}} = \mathbf{R}\delta\dot{\mathbf{\Psi}} + \dot{\mathbf{R}}\delta\mathbf{\Psi}$, and vary the latter: $\delta\dot{\mathbf{R}} = \delta\mathbf{R}\dot{\mathbf{\Phi}} + \mathbf{R}\delta\dot{\mathbf{\Phi}}$, equate the two right-hand sides, premultiply by $\mathbf{R}^{\mathrm{T}}$, replace $\mathbf{R}^{\mathrm{T}}\dot{\mathbf{R}}$ and $\mathbf{R}^{\mathrm{T}}\delta\mathbf{R}$ by $\dot{\mathbf{\Phi}}$ and $\delta\mathbf{\Psi}$, respectively, and rearrange to obtain

$$\delta\dot{\mathbf{\Phi}} = \delta\dot{\mathbf{\Psi}} + \dot{\mathbf{\Phi}}\delta\mathbf{\Psi} - \delta\mathbf{\Psi}\dot{\mathbf{\Phi}}, \quad \text{or } \delta\dot{\boldsymbol{\phi}} = \delta\dot{\boldsymbol{\psi}} + \dot{\mathbf{\Phi}}\delta\boldsymbol{\psi} = \delta\dot{\boldsymbol{\psi}} - \delta\mathbf{\Psi}\dot{\boldsymbol{\phi}}. \tag{112}$$

The last transformation is obtained by taking the axial vectors of both sides, and using (90). It is seen that $\delta\dot{\mathbf{\Psi}}$ and $\delta\dot{\mathbf{\Phi}}$ match if and only if $\dot{\mathbf{\Phi}}$ and $\delta\mathbf{\Psi}$ commute.

Higher variations and differentials can be obtained through similar techniques. The general rule is: if there is a rotator integral such as $\mathbf{R} = \mathrm{Exp}(\mathbf{\Theta})$, time derivatives can be directly converted to variations. If no integral exists, utmost care must be exerted. Physically quantities such as $\boldsymbol{\phi}$ and $\boldsymbol{\psi}$ are related to a moving frame, which makes differential relations rheonomic.

Appendix B. CR Matrices for triangular shell element

The element types tested in Part II [38] are shown in Fig. 13. Each element has 6 degrees of freedom (DOF) per node: three translations and three rotations. Shells include the drilling DOF. The linear internal

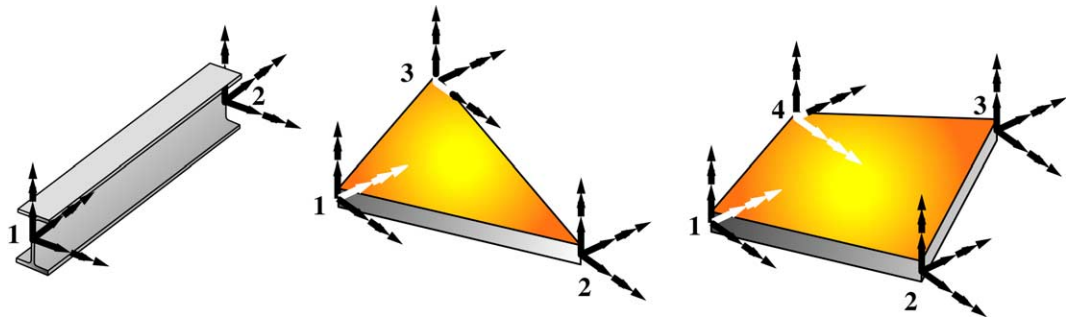

Fig. 13. Elements tested in Part II.

force and stiffness matrix of the shell elements are constructed with the assumed natural deviatoric strain (ANDES) formulation [27–32,53] in terms of the deformational displacements and rotations. ANDES is a direct descendent of the assumed natural strain (ANS) formulation of Park and Stanley [59] and the Free Formulation of Bergan and coworkers [11–14]. The derivation of the linear models is outlined in Part II [38].

The matrices required to implement the EICR are **T**, **P**, **S**, **G**, **H** and **L**. None of these depend on how the internal element force $\bar{\mathbf{p}}^e$ and stiffness matrix $\overline{\mathbf{K}}^e$ of the small-strain linear element are formed. In terms of implementation the EICR matrices can be classified into two groups:

(i) **T**, **H** and **L**, as well as the T-projector component $\mathbf{P}_u$ of **P**, are block diagonal matrices built up with 3×3 node blocks. These blocks can be formed by standard modules which are *independent of the element type*, as long as the element has the standard 6 DOFs per node. The only difference is the number of nodes.
(ii) The R-projector component of **P**, which is $\mathbf{P}_\omega = \mathbf{SG}$, does depend on element type, geometry and choice of CR frame through matrix **G**. These must be recoded for every change in those attributes.

In this Appendix we give the **G** and **S** matrices that appear in the "front end" of the EICR for the triangular shell element, as that illustrates the effect of CR frame selection. Matrices for the beam and quadrilateral element are given in Part II.

In the following sections, element axes labels are changed from $\{\bar{x}_1, \bar{x}_2, \bar{x}_3\}$ to $\{\bar{x}, \bar{y}, \bar{z}\}$ to unclutter nodal subscripting. Likewise the displacement components $\{\bar{u}_1, \bar{u}_2, \bar{u}_3\}$ are relabeled $\{\bar{u}_x, \bar{u}_y, \bar{u}_z\}$.

B.1. Matrix $\overline{\boldsymbol{S}}$

This 18×3 lever matrix is given by (written in transposed form to save space)

$$\overline{\mathbf{S}} = \begin{bmatrix} -\text{Spin}(\bar{\mathbf{x}}_1) & \mathbf{I} & -\text{Spin}(\bar{\mathbf{x}}_2) & \mathbf{I} & -\text{Spin}(\bar{\mathbf{x}}_3) & \mathbf{I}^{\mathrm{T}} \end{bmatrix}, \tag{113}$$

where **I** is the 3×3 identity matrix, and $\bar{\mathbf{x}}_a = [\bar{x}_a, \bar{y}_a, \bar{z}_a]^{\mathrm{T}}$, the position vector of node a in the deformed (current) configuration, measured in the element CR frame.

B.2. Matrix $\overline{\boldsymbol{G}}$

This 3×18 matrix connects the variation in rigid element spin to the incremental translations and spins at the nodes, both with respect to the CR frame. **G** decomposes into three 3×6 submatrices, one for each node:

$$\delta\boldsymbol{\omega}_{\mathrm{r}} = \overline{\mathbf{G}}\delta\bar{\mathbf{v}}, \quad \mathbf{G} = [\,\mathbf{G}_1 \quad \mathbf{G}_2 \quad \mathbf{G}_3\,], \quad \delta\bar{\mathbf{v}} = \begin{bmatrix} \delta\bar{\mathbf{v}}_1 \\ \delta\bar{\mathbf{v}}_2 \\ \delta\bar{\mathbf{v}}_3 \end{bmatrix}, \quad \delta\bar{\mathbf{v}}_a = \begin{bmatrix} \delta\bar{\mathbf{u}}_a \\ \delta\bar{\boldsymbol{\omega}}_a \end{bmatrix}, \quad a = 1,2,3. \tag{114}$$

Submatrices $\mathbf{G}_a$ depend on how the element CR frame is chosen. The origin of the frame is always placed at the element centroid. But various methods have been used to direct the axes $\{\bar{x}_i\}$. Three methods used in the present research are described.

B.2.1. $\overline{\boldsymbol{G}}$ by side alignment

This procedure is similar to that used by Rankin and coworkers [54,63–66]. They select side 1–3 for $\bar{x}_2$ and node 1 as frame origin. The approach used here aligns $\bar{x}_1$ with side 1–2 and picks the centroid as origin. Then

$$\overline{\mathbf{G}}_1 = \frac{1}{2A}\begin{bmatrix} 0 & 0 & \bar{x}_{32} & 0 & 0 & 0 \\ 0 & 0 & \bar{y}_{32} & 0 & 0 & 0 \\ 0 & -h_3 & 0 & 0 & 0 & 0 \end{bmatrix}, \quad \overline{\mathbf{G}}_2 = \frac{1}{2A}\begin{bmatrix} 0 & 0 & \bar{x}_{13} & 0 & 0 & 0 \\ 0 & 0 & \bar{y}_{13} & 0 & 0 & 0 \\ 0 & h_3 & 0 & 0 & 0 & 0 \end{bmatrix},$$
$$\overline{\mathbf{G}}_3 = \frac{1}{2A}\begin{bmatrix} 0 & 0 & \bar{x}_{32} & 0 & 0 & 0 \\ 0 & 0 & \bar{y}_{32} & 0 & 0 & 0 \\ 0 & 0 & 0 & 0 & 0 & 0 \end{bmatrix}, \tag{115}$$

where $h_3 = 2A/L_3$ is the distance of corner 3 to the opposite side, A the triangle area, and L_3 the length of side 12. This choice satisfies the decomposition property (37) that guards against unbalanced force effects while iterating for equilibrium. On the other hand it violates invariance: the choice of CR frame depends on node numbering, and different results may be obtained if the mesh is renumbered.

B.2.2. $\overline{\boldsymbol{G}}$ by least square angular fit

Nygård [57] and Bjærum [18] place $\mathscr{C}^R$ in the plane of the deformed element with origin at node 1. The inplane orientation of the CR element is determined by a least square fit of the side angular errors. Referring to Fig. 14. the squared error is $d^2 = \phi_1^2 + \phi_2^2 + \phi^2$. Rotating by an additional angle χ this becomes $d^2(\chi) = (\phi_1 + \chi)^2 + (\phi_2 + \chi)^2 + (\phi + \chi)^2$. Miniminization respect to χ: $\partial d^2/\partial\chi = 0$ yields $\chi = -(\phi_1 + \phi_2 + \phi_3)/3$. Consequently the optimal in-plane position according to this criterion is given by the mean of the side angular errors.

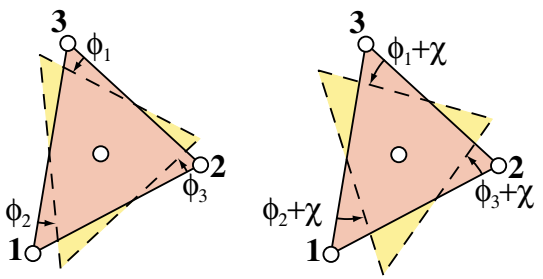

Fig. 14. Side angular error measure for triangular shell element.

This condition yields for the nodal submatrices

$$\overline{\mathbf{G}}_i = \frac{1}{2A}\begin{bmatrix} 0 & 0 & \bar{x}_{kj} & 0 & 0 & 0 \\ 0 & 0 & \bar{y}_{kj} & 0 & 0 & 0 \\ \frac{2A}{3}\left(-\frac{s_{jy}}{l_j}+\frac{s_{ky}}{L_k}\right) & \frac{2A}{3}\left(\frac{s_{jx}}{l_j}-\frac{s_{kx}}{L_k}\right) & 0 & 0 & 0 & 0 \end{bmatrix}, \tag{116}$$

where L_i is the side length opposite corner i and $\{s_{kx}, s_{ky}\}$ the projections of that side on the $\{x, y\}$ axes. An advantage of this fitting method is that it satisfies invariance with respect to node numbering. On the other hand, the rotator gradient matrix cannot be decomposed as in (37) leading to an approximate projector away from equilibrium. This disadvantage is not serious for a flat triangular element, however, since the CR and deformed configurations remain close on the assumption of small membrane strains.

A more serious shortcoming is that the procedure reintroduces the problem of spurious normal-to-the-plane rotations when an element with drilling freedoms is subjected to pure stretch. The difficulty is illustrated in Fig. 15, where a two triangle patch is subject to uniform stretch in the $\bar{y}$ direction. Under this state all rotations should vanish. The elements do rotate, however, because of the in-plane skewing of the diagonal. A deformational rotation is picked up since a predictor step gives no drilling rotations at the nodes, whereas the deformational drilling rotation is the total minus the rigid body rotation: $\theta_{\rm d} = \theta - \theta_{\rm r}$.

The problem is analogous to that discussed by Irons and Ahmad [45, p. 289] when defining node drilling freedoms as the mean of rotations of element sides meeting at that node; such elements grossly violate the patch test. This difficulty was overcome by Bergan and Felippa [14] by defining the node drilling freedom as the continuum mechanics rotation $\theta_z = \frac{1}{2}(\partial\bar{u}_y/\partial\bar{x} - \partial\bar{u}_x/\partial\bar{y})$ at the node. It is seen that the problem of spurious drilling rotations has been reintroduced for the nonlinear case by the choice of CR frame positioning. In fact this problem becomes even more serious with the side alignment procedure described in the foregoing subsection.

B.2.3. Fit according to CST rotation

The infinitesimal drilling rotation of a plane stress CST element (Turner triangle, linear triangle), is given by [27,32]

$$\bar{\theta}^{\rm lin}_{\rm CST} = \frac{1}{2}\left(\frac{\partial\bar{u}_y}{\partial\bar{x}} - \frac{\partial\bar{u}_x}{\partial\bar{y}}\right) = \frac{1}{4A}\left(\bar{x}_{23}\bar{u}_{x1} + \bar{x}_{31}\bar{u}_{x2} + \bar{x}_{12}\bar{u}_{x3} + \bar{y}_{23}u_{y1} + \bar{y}_{31}\bar{u}_{y_2} + \bar{y}_{12}\bar{u}_{y3}\right) \tag{117}$$

in which $\bar{x}_{ij} = \bar{x}_i - \bar{x}_j$, $\bar{y}_{ij} = \bar{x}_i - \bar{y}_j$, etc. The extension of this result to finite rotations can be achieved through a mean finite strain rotation introduced by Novozhilov [55, p. 31]; cf. also [81, Section 36]

$$\tan\bar{\theta}_{\rm CST} = \frac{\bar{\theta}^{\rm lin}_{\rm CST}}{\sqrt{(1+\bar{\epsilon}_{xx})(1+\bar{\epsilon}_{yy}) - \frac{1}{4}\bar{\gamma}^2_{xy}}} \tag{118}$$

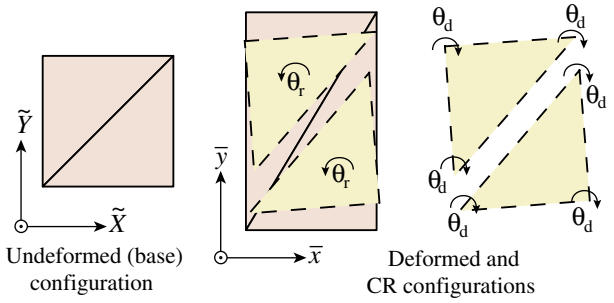

Fig. 15. Finite stretch patch test for two triangle elements equipped with corner drilling freedoms.

in which $\epsilon_{xx} = \partial\bar{u}_x/\partial\bar{x}$, $\bar{\epsilon}_{yy} = \partial\bar{u}_y/\partial\bar{y}$ and $\bar{\gamma}_{xy} = \partial\bar{u}_y/\partial\bar{x} + \partial\bar{u}_x/\partial\bar{y}$ are the infinitesimal strains (constant over the triangle) computed from the CST displacements. Novozhilov proves that this rotation measure is invariant with respect to the choice of CR axes $\{\bar{x}, \bar{y}\}$ since it is obtained as a rotational mean taken over a 2π sweep about $\bar{z}$. If this result is applied to the finite stretch path test of Fig. 15 it is found that the CR frames of both elements do not rotate, and the test is passed. The rotation gradient submatrices are

$$\widetilde{\mathbf{G}}_i = \frac{1}{2A}\begin{bmatrix} 0 & 0 & \bar{x}_{kj} & 0 & 0 & 0 \\ 0 & 0 & \bar{y}_{kj} & 0 & 0 & 0 \\ -\frac{1}{2}\bar{x}_{kj} & -\frac{1}{2}\bar{y}_{kj} & 0 & 0 & 0 & 0 \end{bmatrix}, \tag{119}$$

where j, k denote cyclic permutations of $i = 1, 2, 3$. The resulting $\mathbf{G}$ matrix satisfies the geometric separabilty condition.

B.2.4. Best fit by minimum LS deformation

The best fit solution by least-squares minimization of relative displacements given in Appendix C as equation (127) was obtained in 2000 [29]. Unlike the previous ones it has not been tested as part of a CR shell program. The measure is invariant, but it is not presently known whether it passes the stretch patch test, or if the associated $\mathbf{G}$ satisfies the geometric separability condition (37).

Appendix C. Best fit CR frame

To define the CR frame of an individual element e we must find $\mathbf{c}$ and $\mathbf{R}_0$ from the following information. (In what follows the element index e is suppressed for brevity.)

(i) The geometry of the base element. This is defined through $\mathbf{x}$, which is kept fixed.
(ii) The motion, as defined by the total displacement field $\mathbf{v}(\mathbf{x})$ recorded in the global frame as stated in Table 2.

In dynamic analysis there is a third source of data:

(iii) *Mass distribution*. Associated with each $\mathbf{x}$ in $\mathscr{C}^0$ there is a volume element $\mathrm{d}V$ and a mass density ρ giving a mass element $\mathrm{d}m = \rho\mathrm{d}V$. This mass may include nonstructural components. The case of time-varying mass because of fuel consumption or store drop is not excluded.

Finding $\mathbf{c}$ and $\mathbf{R}_0$ as functions of $\mathbf{x}$ and $\mathbf{v}$, plus the mass distribution in case of dynamics, is the *shadowing problem* introduced previously. What criterion should be used to determine $\mathbf{c}$ and $\mathbf{R}_0$? Clearly some nonnegative functional of the motion (but not the motion history) should be minimized. Desirable properties of the functional are:

Versatility. It must work for statics, dynamics, rigid bodies and nonstructural bodies (e.g., a fuel tank). These requirements immediately rule out any criterion that involves the strain energy, because it cannot be used for a nonstructural or rigid body.

Invariance. Should be insensitive to element node numbering. It would be disconcerting for a user to get different answers depending on how mesh nodes are numbered.

Rigid bodies. For a rigid body, it should give the same results as a body-attached frame. This simplifies the coupling of FEM-CR and multibody dynamics codes.

Finite stretch patch test satisfaction. If a group of elements is subjected to a uniform stretch, no spurious deformational rotations should appear. This test is particularly useful when considering shell elements with drilling freedoms, as discussed in Section B.2 for the triangle.

Fraeijs de Veubeke [25] proposed two criteria applicable to flexible and rigid bodies: minimum kinetic energy of relative motion, and minimum Euclidean norm of the deformational displacement field. As both lead to similar results for dynamics and the first one is not applicable to statics, the second criterion is used here.

An open research question is whether a universal best fit criterion based on the polar decomposition of the element motion could be developed.

C.1. Minimization conditions

In statics the density ρ may be set to unity and mass integrals become volume integrals. These are taken over the base configuration, whence $\int,\ldots,\mathrm{d}V$ means $\int_{\mathscr{C}^0},\ldots,\mathrm{d}V$. Furthermore the element global frame is made to coincide with the base frame to simplify notation. $\mathbf{x}\equiv\tilde{\mathbf{x}}$, $\mathbf{u}\equiv\tilde{\mathbf{u}}$ and $\mathbf{a}=\mathbf{0}$. Coordinates $\mathbf{x}^0$ and $\mathbf{x}^R$ of the base are relabeled $\mathbf{X}$ and $\mathbf{x}=\mathbf{X}+\mathbf{u}$, respectively, to avoid superscripts clashing with transpose signs. Because C^0 is by definition at the base element centroid

$$\int \mathbf{X}\mathrm{d}V=0, \tag{120}$$

The centroid C of $\mathscr{C}^D$ is located by the condition $\int\mathbf{x}\,\mathrm{d}V=\int(\mathbf{X}+\mathbf{u})\mathrm{d}V=\int\mathbf{u}\,\mathrm{d}V=\mathbf{c}\,\mathrm{V}$, where $V=\int\mathrm{d}V$ is the element volume. From (22) with $\mathbf{a}=\mathbf{0}$ and $\mathbf{x}^0\to\mathbf{X}$, the best-fit functional is

$$J[\mathbf{c},\mathbf{R}_0]=\frac{1}{2}\int\mathbf{u}_\mathrm{d}^\mathrm{T}\mathbf{u}_\mathrm{d}\mathrm{d}V=\frac{1}{2}\int[\mathbf{u}-\mathbf{c}+(\mathbf{I}-\mathbf{R}_0)\,\mathbf{X}]^\mathrm{T}[\mathbf{u}-\mathbf{c}+(\mathbf{I}-\mathbf{R}_0)\mathbf{X}]\mathrm{d}V \tag{121}$$

Minimizing $\bar{\mathbf{u}}_\mathrm{d}^\mathrm{T}\bar{\mathbf{u}}_\mathrm{d}$ leads to the same result, since $\mathbf{u}_\mathrm{d}$ and $\bar{\mathbf{u}}_\mathrm{d}$ only differ by a rotator.

C.2. Best origin

Denote by $\Delta\mathbf{c}$ the distance between C_R and C. Taking the variation of J with respect to $\mathbf{c}$ yields

$$\begin{aligned}\frac{\partial J}{\partial\mathbf{c}}\delta\mathbf{c}&=-\int(\delta\mathbf{c})^\mathrm{T}\mathbf{u}_\mathrm{d}\mathrm{d}V=-\delta\mathbf{c}^\mathrm{T}\int[\mathbf{u}-\mathbf{c}+(\mathbf{I}-\mathbf{R}_0)\mathbf{X}]\mathrm{d}V=-\delta\mathbf{c}^\mathrm{T}\int(\mathbf{u}-\mathbf{c})\mathrm{d}V=0,\\ \Rightarrow\quad\mathbf{c}\int\mathrm{d}V&=\mathbf{c}V=\int\mathbf{u}\,\mathrm{d}V=(\mathbf{c}+\Delta\mathbf{c})V,\end{aligned} \tag{122}$$

where (120) has been used. Consequently $\Delta\mathbf{c}=\mathbf{0}$. That is, the centroids of $\mathscr{C}^R$ and $\mathscr{C}$ must coincide: $C_R\equiv C$.

C.3. Best rotator

The variation with respect to $\mathbf{R}_0$ gives the condition

$$\frac{\partial J}{\partial\mathbf{R}_0}\delta\mathbf{R}_0=\int\mathbf{X}^\mathrm{T}\delta\mathbf{R}_0[\mathbf{u}-\mathbf{c}+(\mathbf{I}-\mathbf{R}_0)\mathbf{X}]\mathrm{d}V=0. \tag{123}$$

Replacing $\delta\mathbf{R}_0=\delta\boldsymbol{\Theta}\mathbf{R}_0$ and noting that $\mathbf{X}^\mathrm{T}\delta\boldsymbol{\Theta}\mathbf{X}=0$ and $\int\mathbf{X}^\mathrm{T}\delta\boldsymbol{\Theta}\mathbf{R}_0\mathbf{c}\,\mathrm{d}V=0$ yields

$$\int\mathbf{X}^\mathrm{T}\delta\boldsymbol{\Theta}\mathbf{R}_0(\mathbf{X}+\mathbf{u})\mathrm{d}V=\int\mathbf{X}^\mathrm{T}(\delta\boldsymbol{\theta}\times\mathbf{R}(\mathbf{X}+\mathbf{u}))\mathrm{d}V=0. \tag{124}$$

Applying (124) to each angular variation: $\delta\theta_1$, $\delta\theta_2$ and $\delta\theta_3$ of $\delta\boldsymbol{\Theta}$ in turn, provides three nonlinear scalar equations to determine the three parameters that define $\mathbf{R}_0$. For the two-dimensional case, in which only $\delta\theta_3$ is varied and $\mathbf{R}_0$ depends only on $\theta=\theta_3$, the following equation is obtained:

$$\int [(X_1 + u_1)(x_2 \cos\theta_3 - X_1 \sin\theta_3) - (X_2 + u_2)(x_1 \cos\theta_3 + X_2 \sin\theta_3)]\mathrm{d}V = 0, \tag{125}$$

whence

$$\tan\theta_3 = \frac{\int (X_2 u_1 - X_1 u_2)\mathrm{d}V}{\int [X_1(X_1 + u_1) + X_2(X_2 + u_2)]dV} = \frac{\int (X_2 u_1 - X_1 u_2)\mathrm{d}V}{\int (X_1 x_1 + Y_2 x_2)\mathrm{d}V}. \tag{126}$$

For the three-dimensional case a closed form solution is not available. This is an open research topic. Fraeijs de Veubeke [25] reduces (124) to an eigenvalue problem in the axial vector of $\mathbf{R}_0$, with a subsidiary condition handled by a Lagrange multiplier. Rankin [67] derives a system equivalent to (124) for an individual finite element by lumping the mass equally at the nodes whereupon the integral over the body is reduced to a sum over nodes. The nonlinear system is solved by Newton–Raphson iteration.

C.4. Linear triangle best fit

Consider a constant thickness three-node linear plane stress triangle (also known as Turner triangle and CST), displacing in two dimensions as illustrated in Fig. 16. To facilitate node subscripting, rename $X_1 \to X$, $X_2 \to Y$, $x_1 \to x$, $x_2 \to y$, $u_1 \to u_x$, $u_2 \to u_y$. Using triangular coordinates $\{\zeta_1,\zeta_2,\zeta_3\}$, the position coordinates and displacements are interpolated linearly: $X = X_1\zeta_1 + X_2\zeta_2 + X_3\zeta_3$, $Y = Y_1\zeta_1 + Y_2\zeta_2 + Y_3\zeta_3$, $x = x_1\zeta_1 + x_2\zeta_2 + x_3\zeta_3$, $y = y_1\zeta_1 + y_2\zeta_2 + y_3\zeta_3$, $u_x = u_{y_1}\zeta_1 + u_{x_2}\zeta_2 + u_{x_3}\zeta_3$ and $u_y = u_{y_1}\zeta_1 + u_{y_2}\zeta_2 + u_{y_3}\zeta_3$, in which numerical subscripts now denote node numbers. Insert into (126) and introduce side conditions $X_1 + X_2 + X_3 = 0$, $Y_1 + Y_2 + Y_3 = 0$, $u_{x_1} + u_{x_2} + u_{x_3} = x_1 + x_2 + x_3$ and $u_{y_1} + u_{y_2} + u_{y_3} = y_1 + y_2 + y_3$ for centroid positioning. *Mathematica* found for the best fit angle

$$\tan\theta_3 = \frac{x_1 Y_1 + x_2 Y_2 + x_3 Y_3 - y_1 X_1 - y_2 X_2 - y_3 X_3}{x_1 X_1 + x_2 X_2 + x_3 X_3 + y_1 Y_1 + y_2 Y_2 + y_3 Y_3}, \tag{127}$$

where $x_a = X_a + u_{xa}$, $y_a = y_a + u_{ya}$, $a = 1,2,3$. The same result can be obtained with any three-point integration rule where the Gauss points are placed on the medians. In particular, Rankin's idea of using the three corners as integration points [67] gives the same answer.

This solution is interesting in that it can be used as an approximation for any three-node triangle undergoing three dimensional motion (for example, a thin shell facet element) as long as axis $\bar{x}_3$ is preset normal to the plane passing through the three deformed corners. The assumption is that the best fit is done only for the in-plane displacements.

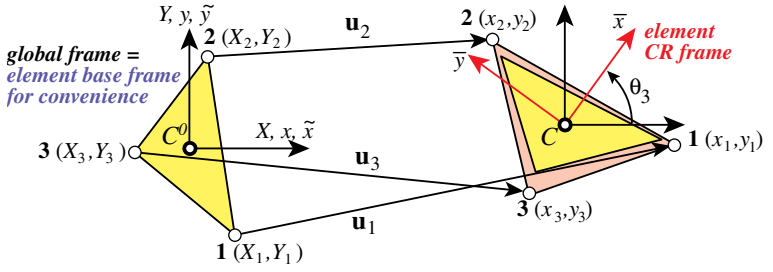

Fig. 16. Best CR frame fit to 3-node linear triangle in 2D. Axes relabeled as explained in the text.

C.5. Rigid body motion verification

Suppose the element motion $\mathbf{u} = \mathbf{u}_r$ is rigid ($\mathbf{u}_d = 0$) with rotator $\mathbf{R}_r$. If so $\mathbf{u}_r = \mathbf{c} - (\mathbf{I} - \mathbf{R}_r)\mathbf{X}$. Inserting into (121) yields

$$J = \frac{1}{2}\int \mathbf{X}^{\mathrm{T}}(\mathbf{R}_r - \mathbf{R}_0)^{\mathrm{T}}(\mathbf{R}_r - \mathbf{R}_0)\mathbf{X}\,\mathrm{d}V. \tag{128}$$

in which $\mathbf{X} = \mathbf{x}^G - \mathbf{a}$. This is clearly minimized by $\mathbf{R}_0 = \mathbf{R}_r$, so the body attached frame is a best fit CR frame. (There may be additional solutions if $(\mathbf{R}_r - \mathbf{R}_0)\mathbf{X} \equiv \mathbf{0}$ for some $\mathbf{R}_0 \neq \mathbf{R}_r$, for example by relabeling axes.) This check verifies that the functional (121) also works as expected for rigid body components of a structural or non-structural model.

Appendix D. Nomenclature

The notation used by different investigators working in CR formulations has not coalesced, since the topic is in flux. This Appendix identifies the symbols used here. The general scheme of notation is

Non-bold letters: scalars. Uppercase bold letters (roman and greek): matrices and tensors. Lowercase bold letters (roman and greek): column vectors, but there are occasional exceptions such as **X** and **Y**.

a	As subscript: generic nodal index
b	As subscript: generic nodal index
b_i	Components of Rodrigues–Cayley axial vector
c_i	Generic coefficients. Components of vector **c**
d	As subscript: deformational
e	Base of natural logarithms. As superscript: element index
e_{ij}	Strains
f_i	Components of force vector **f**
h_i	Triangle heights
i	As subscript: generic index. Imaginary unit in complex numbers
j	As subscript: generic index
k	As superscript: iteration count
l	As subscript: generic index
m	As subscript: generic index
n	As subscript: incremental step number
n_i	Components of vector **n**
p_i	Quaternion components
r	As subscript: rigid
s_{kx}, s_{ky}	Projections of triangle side L_k on $\{x, y\}$ axes
t	Time
u	Displacement magnitude
u_i, $\tilde{u}_i$, $\bar{u}_i$	Displacement components in x_i, $\tilde{x}_i$, $\bar{x}_i$ axes, respectively
u_{di}, $\tilde{u}_{di}$, $\bar{u}_{di}$	Deformational displacement components in x_i, $\tilde{x}_i$, $\bar{x}_i$ axes, respectively
u_{ri}, $\tilde{u}_{ri}$, $\bar{u}_{ri}$	Rigid displacement components in x_i, $\tilde{x}_i$, $\bar{x}_i$ axes, respectively
x	x_1-axis when using $\{x, y, z\}$ notation
x_i	Components of global-frame position vector **x**
$\tilde{x}_i$	Components of element base-frame position vector $\tilde{\mathbf{x}}$
$\bar{x}_i$	Components of element CR-frame position vector $\bar{\mathbf{x}}$

y	x_2 axis when using $\{x,y,z\}$ notation
z	x_3 axis when using $\{x,y,z\}$ notation
A	Area
C	Generic centroid of body or element in statics. Center of mass in dynamics
C^0, C^R, C	Body or element centroid in base, CR and deformed configurations, respectively
L	Length of 2-node element. Generic length
L_k	Length of triangle side opposite node k
N	Number of structure nodes
N^e	Number of nodes of element e
O	Origin of global frame
T	Kinetic energy
U	Internal energy, strain energy
W	External work
X	x_1 axis when using $\{X,Y,Z\}$ notation
X_i	Material global Cartesian axes
Y	x_2 axis when using $\{X,Y,Z\}$ notation
Z	x_3 axis when using $\{X,Y,Z\}$ notation
$\mathbf{a}$	Position vector of C^0 from origin of global frame. Generic vector
$\mathbf{b}$	Position vector of $C^R \equiv C$ from origin of global frame. Generic vector
$\mathbf{c}$	Displacement of base element centroid C^0 to $C^R \equiv C$
$\mathbf{d}$	Deformational displacement. Array of nodal DOF, collecting translations and rotations
$\bar{\mathbf{d}}$	Array of nodal deformational DOF, collecting translations and rotations
$\mathbf{e}$	Strains arranged as vector
$\mathbf{f}$	Generic force vector. External force vector
$\bar{\mathbf{f}}$	External force vector in element CR frame
$\mathbf{f}_b$	Balance (self-equilibrated) force vector
$\mathbf{f}_u$	Unbalanced (out of equilibrium) force vector
$\mathbf{i}$	Base unit vector
$\mathbf{m}$	Generic nodal moment vector
$\mathbf{m}_a$	Nodal moment components at node a
$\mathbf{n}$	Unit normal. Direction of rotation vector in 3D
$\mathbf{n}_a$	Translational force components at node a
$\mathbf{0}$	Null matrix or vector
$\mathbf{p}$	Internal force vector of structure
$\mathbf{p}^e$	Element internal force vector in global frame
$\bar{\mathbf{p}}^e$	Element internal force vector in CR frame
$\mathbf{r}$	Force residual vector
$\mathbf{u}$	Displacement vector. Also generic vector: meaning from context
$\mathbf{v}$	Denotes vector collecting nodal displacements and rotations, displacements and spins, or displacements and rotators. See Table 2 Also generic vector: meaning from context
$\mathbf{w}$	Generic vector: meaning from context
$\hat{\mathbf{v}}$	Global DOF vector for complete structure
$\mathbf{x}$	Global-frame spatial position vector
$\tilde{\mathbf{x}}$	Element base-frame position vector
$\bar{\mathbf{x}}$	Element CR-frame position vector
$\vec{\mathbf{x}}$	Frame independent position vector
$\mathbf{y}$	Alternative notation for position vector. Generic vector

$\vec{\mathbf{y}}$	Frame independent position vector
$\mathbf{z}_i$	Spinor eigenvector
$\mathbf{A}$	Generic matrix
$\mathbf{B}_{\mathrm{d}}$	Matrix relating strains to deformational displacements. Generic matrix
$\mathbf{C}$	Strain–stress (compliance) matrix
$\mathbf{D}$	Diagonal matrix of zeros and ones. Generic diagonal matrix, size from context
$\mathbf{E}$	Stress–strain (elasticity) matrix
$\mathbf{F}$	Generic matrix function
$\mathbf{F}_n$, $\mathbf{F}_{nm}$	Auxiliary matrices in tangent stiffness derivations
$\mathbf{G}$	Element spin-fitter matrix linking $\delta\boldsymbol{\omega}^e_{\mathrm{r}}$ to $\delta\mathbf{v}^e$
$\mathbf{G}_a$	Component of $\mathbf{G}$ associated with node a
$\mathbf{H}$	Block diagonal matrix built with $\mathbf{H}_a$ and $\mathbf{I}$ blocks
$\mathbf{H}_a$	Evaluation of $\mathbf{H}(\boldsymbol{\theta})$ at node a
$\mathbf{H}(\boldsymbol{\theta})$	Jacobian of $\boldsymbol{\theta}$ with respect to $\boldsymbol{\omega}$
$\mathbf{I}$	Identity matrix, size from context
$\mathbf{J}$	Jacobian matrix in general
$\mathbf{J}_{ab}$	Jacobian matrix relating quantities at nodes a and b
$\mathbf{K}$	Tangent stiffness matrix of structure
$\mathbf{K}^e$	Element tangent stiffness matrix in global frame
$\overline{\mathbf{K}}^e$	Linear element stiffness matrix in local CR frame
$\overline{\mathbf{K}}^e_R$	Element tangent stiffness matrix in local CR frame
$\mathbf{K}_{\mathrm{GM}}$	Moment correction geometric stiffness matrix
$\mathbf{K}_{\mathrm{GP}}$	Equilibrium projection geometric stiffness matrix
$\mathbf{K}_{\mathrm{GR}}$	Rotational geometric stiffness matrix
$\mathbf{K}_M$	Material stiffness matrix
$\mathbf{L}$	Block diagonal built with $\mathbf{L}_a$ and $\mathbf{0}$ blocks
$\mathbf{L}_a$	Evaluation of $\mathbf{L}(\boldsymbol{\theta},\mathbf{m})$ at node a
$\mathbf{L}(\theta,\mathbf{m})$	Contraction of $\partial\mathbf{H}(\boldsymbol{\theta})^{\mathrm{T}}/\partial\boldsymbol{\omega}$with vector $\mathbf{m}$
$\mathbf{M}$	Mass matrix
$\mathbf{N}$	Spinor for vector $\mathbf{n}$
$\mathbf{P}$	Projector matrix
$\mathbf{P}_u$	Translational projector matrix, a.k.a. T-projector
$\mathbf{P}_\omega$	Rotational projector matrix, a.k.a. R-projector
$\mathbf{Q}$	Generic orthogonal matrix
$\mathbf{R}$	Orthogonal rotation matrix: the matrix representation of a rotator
$\mathbf{R}_0$	Transformation rotator between element base frame and CR frame
$\widetilde{\mathbf{R}}_0$, $\overline{\mathbf{R}}_0$	Rotator $\mathbf{R}_0$ referred to element base and CR frames, respectively
$\mathbf{S}$	Spin-lever (a.k.a. moment-arm) matrix built up of $\mathbf{S}_a$ blocks. Generic skew-symmetric matrix
$\mathbf{S}_a$	Spin-lever matrix for node a
$\mathbf{T}$	Element CR-to-global transformation matrix built from $\mathbf{T}_R$ blocks
$\mathbf{T}_0$	Transformation rotator from element base frame to global frame
$\mathbf{T}_R$	Transformation rotator from element CR frame to global frame
$\mathbf{U}_{ab}$	Building block of translational projector $\mathbf{P}_u$
$\mathbf{V}$	Generic skew-symmetric matrix
$\mathbf{W}$	Generic skew-symmetric matrix
$\mathbf{X}$	Global position vector with X_i as components
$\vec{\mathbf{X}}$	Coordinate free material position vector
$\widetilde{\mathbf{X}}$	Element base position vector with $\tilde{x}_i$ as components

$\overline{\mathbf{X}}$ Element CR position vector with $\bar{x}_i$ as components
$\mathbf{Y}$ Position vector collecting y_i as components
$\mathbf{Z}$ Matrix of right eigenvectors of spinor
α Coefficient in parametrized rotator representation
β Coefficient in parametrized rotator representation
γ Spinor normalization factor
δ Variation symbol
δ_{ab} Kronecker delta
ϵ Small scalar
ζ_i Triangular coordinates
η Coefficient in $\mathbf{H}(\boldsymbol{\theta})$
θ Rotation angle in general. Magnitude of rotation vector $\boldsymbol{\theta}$
κ Curvature
λ Lagrange multiplier
μ Coefficient in $\mathbf{L}(\boldsymbol{\theta},\mathbf{m})$
ν Poisson's ratio
ρ Mass density
σ_{ij} Stresses
τ Coefficient in $\mathrm{Log}_e(\mathbf{R})$ formula
$\chi, \phi, \varphi, \psi$ Generic angle symbols
ψ Generic angle
ω Magnitude of spin vector $\boldsymbol{\omega}$
$\sum$ Summation symbol
$\sum_a, \sum_b$ Abbreviations for $\sum_{a=1}^{N^e}$ and $\sum_{b=1}^{N^e}$
$\boldsymbol{\theta}$ Rotation axial vector (a.k.a. rotation pseudovector)
$\boldsymbol{\phi}$ Axial vector built from ϕ_i angles
$\boldsymbol{\psi}$ Axial vector built from ψ_i angles
$\boldsymbol{\sigma}$ Stresses arranged as vector
$\boldsymbol{\sigma}_0$ Initial stresses (in the base configuration) arranged as vector
$\boldsymbol{\omega}$ Spin axial vector (a.k.a. spin pseudovector)
$\boldsymbol{\Gamma}$ Auxiliary matrix used in the decomposition of $\mathbf{G}$
$\boldsymbol{\Theta}$ Spinor built from rotation axial vector
$\boldsymbol{\Lambda}$ Diagonal matrix of eigenvalues of $\boldsymbol{\Omega}$
$\boldsymbol{\Xi}$ Auxiliary matrix used in the decomposition of $\mathbf{G}$
$\boldsymbol{\phi}$ Spinor built from axial vector $\boldsymbol{\phi}$
$\boldsymbol{\psi}$ Spinor built from axial vector $\boldsymbol{\psi}$
$\boldsymbol{\Sigma}$ Spinor built from the Rodrigues–Cayley parameters b_i
$\boldsymbol{\Omega}$ Spinor built from spin axial vector $\boldsymbol{\omega}$
$\boldsymbol{\Omega}_p$ Spinor build from quaternion parameters p_i.
$\mathscr{C}$ Configuration: see Table 1 for further identification by superscripts
CR Abbreviation for corotational (a.k.a. corotated) kinematic description
DOF Abbreviation for degree of freedom
EICR Abbreviation for element independent corotational formulation
Rotator Abbreviation for rotation tensor (or 3×3 rotation matrix)
Spinor Abbreviation for spin tensor (or 3×3 spin matrix)
TL Abbreviation for total Lagrangian kinematic description
UL Abbreviation for updated Lagrangian kinematic description
$\dot{(\cdot)}$ Abbreviation for $d(\cdot)/\mathrm{d}t$

$(\cdot)^0$ or $(\cdot)_0$ $(\cdot)$ pertains to base (initial) configuration $\mathscr{C}^0$
$(\cdot)^D$ or $(\cdot)_D$ $(\cdot)$ pertains to deformed configuration $\mathscr{C}^D$
$(\cdot)^G$ or $(\cdot)_G$ $(\cdot)$ pertains to globally aligned configuration $\mathscr{C}^G$
$(\cdot)^R$ or $(\cdot)_R$ $(\cdot)$ pertains to corotated configuration $\mathscr{C}^R$
$(\cdot)_{\mathrm{d}}$ $(\cdot)$ is deformational
$(\cdot)^e$ $(\cdot)$ pertains to element e
$(\cdot)_{\mathrm{r}}$ $(\cdot)$ is rigid
$()^{\mathrm{T}}$ Matrix or vector transposition
$()^{-1}$ Matrix inverse
axial$(\cdot)$ Extraction of axial vector from skew-symmetric matrix argument
$\mathrm{e}^{(\cdot)}$ Matrix exponential if $(\cdot)$ is a square matrix
Exp$(\cdot)$ Alternative form for matrix exponential
$\mathrm{Log}_e(\cdot)$ Matrix natural logarithm
Rot$(\cdot)$ Construction of rotator from spinor argument
Skew$(\cdot)$ Extraction of spinor from rotator argument
Spin$(\cdot)$ Construction of spinor from axial vector argument
trace$(\cdot)$ Sum of diagonal entries of matrix argument

References

[1] J.H. Argyris, An excursion into large rotations, Comput. Methods Appl. Mech. Engrg. 32 (1982) 85–155.
[2] J.-M. Battini, C. Pacoste, Co-rotational beam elements with warping effects in instability problems, Comput. Methods Appl. Mech. Engrg. 191 (2002) 1755–1789.
[3] J.-M. Battini, C. Pacoste, Plastic instability of beam structures using co-rotational elements, Comput. Methods Appl. Mech. Engrg. 191 (2002) 5811–5831.
[4] K.-J. Bathe, Finite Element Procedures in Engineering Analysis, Prentice-Hall, 1982.
[5] K.-J. Bathe, E. Ramm, E.L. Wilson, Finite element formulations for large deformation dynamic analysis, Int. J. Numer. Methods Engrg. 7 (1973) 255–271.
[6] R. Bellman, Introduction to Matrix Analysis, McGraw-Hill, New York, 1960.
[7] T. Belytschko, B.J. Hsieh, Nonlinear transient finite element analysis with convected coordinates, Int. J. Numer. Methods Engrg. 7 (1973) 255–271.
[8] T. Belytschko, B.J. Hsieh, Application of higher order corotational stretch theories to nonlinear finite element analysis, Comput. Struct. 11 (1979) 175–182.
[9] T. Belytschko, An overview of semidiscretization and time integration operators, in: T. Belytschko, T.J.R. Hughes (Eds.), Computational Methods for Transient Analysis, North-Holland, Amsterdam, 1983, pp. 1–66 (Chapter 1).
[10] P.G. Bergan, G. Horrigmoe, Incremental variational principles and finite element models for nonlinear problems, Comput. Methods Appl. Mech. Engrg. 7 (1976) 201–217.
[11] P.G. Bergan, L. Hanssen, A new approach for deriving 'good' finite elements, in: J.R. Whiteman (Ed.), MAFELAP II Conference, Brunel University, 1975, The Mathematics of Finite Elements and Applications, vol. II, Academic Press, London, 1976, pp. 483–497.
[12] P.G. Bergan, Finite elements based on energy orthogonal functions, Int. J. Numer. Methods Engrg. 15 (1980) 1141–1555.
[13] P.G. Bergan, M.K. Nygård, Finite elements with increased freedom in choosing shape functions, Int. J. Numer. Methods Engrg. 20 (1984) 643–664.
[14] P.G. Bergan, C.A. Felippa, A triangular membrane element with rotational degrees of freedom, Comput. Methods Appl. Mech. Engrg. 50 (1985) 25–69.
[15] P.G. Bergan, M.K. Nygård, Nonlinear Shell Analysis Using Free Formulation Finite Elements, in Finite Element Methods for Nonlinear Problems, Springer Verlag, Berlin, 1989, 317–338.
[16] M.A. Biot, The Mechanics of Incremental Deformations, McGraw-Hill, New York, 1965.
[17] R.B. Bird, R.C. Amstrong, O. Hassager, Dynamics of Polymeric Liquids, Vol. 1, Fluid Dynamics, Wiley, New York, 1977.
[18] R.O. Bjærum, Finite element formulations and solution algorithms for buckling and collapse analysis of thin shells. Dr. Ing. Thesis, Division of Structural Mechanics, Norwegian Institute of Technology, Trondheim, Norway, 1992.

[19] A. Cayley, Collected Works, Cambridge Univ. Press, 1898.
[20] H. Cheng, K.C. Gupta, An historical note on finite rotations, J. Appl. Mech. 56 (1989) 139–145.
[21] M. Chiesa, B. Skallerud, D. Gross, Closed form line spring yield surfaces for deep and shallow cracks: formulation and numerical performance, Comput. Struct. 80 (2002) 533–545.
[22] M.A. Crisfield, A consistent corotational formulation for nonlinear three-dimensional beam element, Comput. Methods Appl. Mech. Engrg. 81 (1990) 131–150.
[23] M.A. Crisfield, G.F. Moita, A unified co-rotational for solids, shells and beams, Int. J. Solids Struc. 33 (1996) 2969–2992.
[24] M.A. Crisfield, Nonlinear Finite Element Analysis of Solids and Structures, Vol. 2, Advanced Topics, Wiley, Chichester, 1997.
[25] B.M. Fraeijs de Veubeke, The dynamics of flexible bodies, Int. J. Engrg. Sci. 14 (1976) 895–913.
[26] C. Farhat, P. Geuzaine, G. Brown, Application of a three-field nonlinear fluid-structure formulation to the prediction of the aeroelastic parameters of an F-16 fighter, Computers and Fluids 32 (2003) 3–29.
[27] C.A. Felippa, C. Militello, Membrane triangles with corner drilling freedoms: II. The ANDES element, Finite Elements Anal. Des. 12 (1992) 189–201.
[28] C.A. Felippa, S. Alexander, Membrane triangles with corner drilling freedoms: III. Implementation and performance evaluation, Finite Elements Anal. Des. 12 (1992) 203–239.
[29] C.A. Felippa, A systematic approach to the element-independent corotational dynamics of finite elements, Report CU-CAS-00-03, Center for Aerospace Structures, College of Engineering and Applied Sciences, University of Colorado at Boulder, January 2000.
[30] C.A. Felippa, K.C. Park, The construction of free-free flexibility matrices for multilevel structural analysis, Comput. Methods Appl. Mech. Engrg. 191 (2002) 2111–2140.
[31] C.A. Felippa, Recent advances in finite element templates, in: B.H.V. Topping (Ed.), Computational Mechanics for the Twenty-First Century, Saxe-Coburn Publications, Edinburgh, 2000, pp. 71–98 (Chapter 4).
[32] C.A. Felippa, A study of optimal membrane triangles with drilling freedoms, Comput. Methods Appl. Mech. Engrg. 192 (2003) 2125–2168.
[33] F.R. Gantmacher, The Theory of Matrices, Vol. I, Chelsea, New York, 1960.
[34] M. Geradin, Finite element approach to kinematic and dynamic analysis of mechanisms using Euler parameters, in: C. Taylor, E. Hinton, D.R.J. Owen (Eds.), Numerical Methods for Nonlinear Problems II, Pineridge Press, Swansea, 1984.
[35] H. Goldstein, Classical Mechanics, Addison-Wesley, Reading, Massachussets, 1950.
[36] M. Hammermesh, Group Theory and Its Application to Physical Problems, Dover, New York, 1989.
[37] B. Haugen, Buckling and stability problems for thin shell structures using high-performance finite elements, Ph.D. Dissertation, Department of Aerospace Engineering Sciences, University of Colorado, Boulder, CO, 1994.
[38] B. Haugen, C.A. Felippa, A unified formulation of small-strain corotational finite elements: II. Applications to shells and mechanisms (in preparation).
[39] G. Horrigmoe, Finite element instability analysis of free-form shells, Dr. Ing. Thesis, Division of Structural Mechanics, Norwegian Institute of Technology, Trondheim, Norway, 1977.
[40] G. Horrigmoe, P.G. Bergan, Instability analysis of free-form shells by flat finite elements, Comput. Methods Appl. Mech. Engrg. 16 (1978) 11–35.
[41] A.S. Householder, The Theory of Matrices in Numerical Analysis, Blaisdell, New York, 1964.
[42] T.J.R. Hughes, W.-K. Liu, Nonlinear finite element analysis of shells: Part I. Three-dimensional shells, Comput. Methods Appl. Mech. Engrg. 26 (1981) 331–362.
[43] T.J.R. Hughes, W.-K. Liu, Nonlinear finite element analysis of shells: Part II. Two-dimensional shells, Comput. Methods Appl. Mech. Engrg. 27 (1981) 167–182.
[44] T.J.R. Hughes, J. Winget, Finite rotation effects in numerical integration of rate constitutive equations arising in large deformation analysis, Int. J. Numer. Methods Engrg. 15 (1980) 1862–1867.
[45] B.M. Irons, S. Ahmad, Techniques of Finite Elements, Ellis Horwood Ltd., 1980.
[46] B. Kråkeland, Large displacement analysis of shells considering elastoplastic and elastoviscoplastic materials, Dr. Ing. Thesis, Division of Structural Mechanics, Norwegian Institute of Technology, Trondheim, Norway, 1977.
[47] E. Levold, Solid mechanics and material models including large deformations, Dr. Ing. Thesis, Div. of Structural Mechanics, Norwegian Institute of Technology, Trondheim, Norway, 1990.
[48] K.M. Mathisen, Large displacement analysis of flexible and rigid systems considering displacement-dependent loads and nonlinear constraints. Dr. Ing. Thesis, Division of Structural Mechanics, Norwegian Institute of Technology, Trondheim, Norway, 1990.
[49] K.M. Mathisen, T. Kvamsdal, K.M. Okstad, Adaptive strategies for nonlinear finite element analysis of shell structures, in: C. Hirsch et al. (Eds.), Numerical Methods in Engineering '92, Elsevier Science Publishers B.V., Amsterdam, 1992.
[50] K. Mattiasson, On the corotational finite element formulation for large deformation problems, Dr. Ing. Thesis, Department of Structural Mechanics, Chalmers University of Technology, Göteborg, 1983.

[51] K. Mattiasson, A. Samuelsson, Total and updated Lagrangian forms of the co-rotational finite element formulation in geometrically and materially nonlinear analysis, in: C. Taylor, E. Hinton, D.R.J. Owen (Eds.), Numerical Methods for Nonlinear Problems II, Pineridge Press, Swansea, 1984, pp. 134–151.
[52] K. Mattiasson, A. Bengston, A. Samuelsson, On the accuracy and efficiency of numerical algorithms for geometrically nonlinear structural analysis, in: P.G. Bergan, K.J. Bathe, W. Wunderlich (Eds.), Finite Element Methods for Nonlinear Problems, Springer-Verlag, Berlin, 1986, pp. 3–23.
[53] C. Militello, C.A. Felippa, The first ANDES elements: 9-DOF plate bending triangles, Comput. Methods Appl. Mech. Engrg. 93 (1991) 217–246.
[54] B. Nour-Omid, C.C. Rankin, Finite rotation analysis and consistent linearization using projectors, Comput. Methods Appl. Mech. Engrg. 93 (1991) 353–384.
[55] V.V. Novozhilov, Foundations of the Nonlinear Theory of Elasticity, Graylock Press, Rochester, 1953.
[56] M.K. Nygård, P.G. Bergan, Advances in treating large rotations for nonlinear problems, in: A.K. Noor, J.T. Oden (Eds.), State-of the Art Surveys on Computational Mechanics, ASME, New York, 1989, pp. 305–332 (Chapter 10).
[57] M.K. Nygård, Large displacement analysis of flexible and rigid systems considering displacement-dependent loads and nonlinear constraints. Dr. Ing. Thesis, Division of Structural Mechanics, Norwegian Institute of Technology, Trondheim, Norway, 1990.
[58] C. Pacoste, Co-rotational flat facet triangular elements for shell instability analysis, Comput. Methods Appl. Mech. Engrg. 156 (1998) 75–110.
[59] K.C. Park, G.M. Stanley, A curved C^0 shell element based on assumed natural-coordinate strains, J. Appl. Mech. 53 (1986) 278–290.
[60] W. Pietraszkiewicz, Finite rotations in shells, in: Theory of Shells, Proceedings of the 3rd IUTAM Symp on Shell Theory, Tsibili, 1978, North Holland, Amsterdam, 1980, pp. 445–471.
[61] W. Pietraszkiewicz (Ed.), Finite Rotations in Structural Mechanics, Lecture Notes in Engineering, 19, Springer-Verlag, Berlin, 1985.
[62] E. Ramm, A plate/shell element for large deflections and rotations, in: Proceedings of the US–Germany Symposium on Formulations and Algorithms in Finite Element Analysis, MIT-Cambridge, MA, 264–293, 1976.
[63] C.C. Rankin, F.A. Brogan, An element-independent corotational procedure for the treatment of large rotations, ASME J. Pressure Vessel Technology 108 (1986) 165–174.
[64] C.C. Rankin, Consistent linearization of the element-independent corotational formulation for the structural analysis of general shells, NASA Contractor Report 278428, Lockheed Palo Alto Res. Lab., CA, 1988.
[65] C.C. Rankin, B. Nour-Omid, The use of projectors to improve finite element performance, Comput. Struct. 30 (1988) 257–267.
[66] C.C. Rankin, Consistent linearization of the element-independent corotational formulation for the structural analysis of general shells, NASA Contractor Report 278428, Lockheed Palo Alto Research Laboratory, Palo Alto, CA, 1988.
[67] C.C. Rankin, On choice of best possible corotational element frame, in: S.N. Atluri, P.E. O'Donoghue (Eds.), Modeling and Simulation Based Engineering, Tech Science Press, Palmdale, CA, 1998.
[68] C.C. Rankin, F.A. Brogan, W.A. Loden, H. Cabiness, STAGS User Manual, LMMS P032594, Version 3.0, January 1998.
[69] O. Rodrigues, Des lois géometriques qui regissent les déplacements d'un systéme solide dans l'espace, et de la variation des coordonnées provenant de ces déplacement considerées indépendent des causes qui peuvent les produire, J. de Mathématiques Pures et Appliquées 5 (1840) 380–400.
[70] J.G. Simmonds, D.A. Danielson, Nonlinear shell theory with finite rotation and stress function vectors, J. Appl. Mech. 39 (1972) 1085–1090.
[71] J.C. Simo, A finite strain beam formulation. Part I: The three-dimensional dynamic problem, Comput. Methods Appl. Mech. Engrg. 49 (1985) 55–70.
[72] J.C. Simo, L. Vu-Quoc, A finite strain beam formulation. Part II: Computational aspects, Comput. Methods Appl. Mech. Engrg. 58 (1986) 79–116.
[73] O.I. Sivertsen, Virtual Testing of Mechanical Systems: Theories and Techniques, Swets & Zeitlinger Publishers, Heereweg, Netherlands, 2001.
[74] B. Skallerud, B. Haugen, Collapse of thin shell structures: Stress resultant plasticity modeling within a co-rotated ANDES finite element formulation, Int. J. Numer. Methods Engrg. 46 (1999) 1961–1986.
[75] B. Skallerud, K. Holthe, B. Haugen, Combining high-performance thin shell and surface crack finite elements for simulation of combined failure modes, in: Proceedings of the 7th US National Congress in Computational Mechanics, Albuquerque, NM, July 2003.
[76] R.A. Spurrier, A comment on singularity-free extraction of a quaternion from a direction cosine matrix, J. Spacecrafts Rockets 15 (1978) 255.
[77] M.L. Szwabowicz, Variational formulation in the geometrically nonlinear thin elastic shell theory, Int. J. Solids Struc. 22 (1986) 1161–1175.
[78] R. Tanner, Engineering Rheology, Oxford University Press, 1985.

[79] J.G. Teigen, Nonlinear analysis of concrete structures based on a 3D shear-beam element formulation, Ph.D Dissertation, Department of Mathematics, Mechanics Division, University of Oslo, Oslo, Norway, 1994.
[80] C. Truesdell, Continuum Mechanics I: The Mechanical Foundations of Elasticity and Fluid Dynamics, Gordon & Breach, New York, 1966 (corrected reprint of Continuum Mechanics I: The Mechanical Foundations of Elasticity and Fluid Dynamics, J. Rational Mech. Anal. 1 (1952) 125–300).
[81] C. Truesdell, R.A. Toupin, The classical field theories, in: S. Flügge (Ed.), Handbuch Der Physik, vol. III/1, Springer Verlag, Berlin, 1960, pp. 226–790.
[82] C. Truesdell, Hypoelasticity, J. Ration. Mech. 4 (1955), pp. 83–133, 1019–1020 (Reprinted in Foundations of Elasticity Theory, Gordon & Breach, New York, 1965).
[83] C. Truesdell, W. Noll, The nonlinear field theories of mechanics, in: S. Flügge (Ed.), Handbuch Der Physik, vol. III/3, Springer-Verlag, Berlin, 1965.
[84] H.W. Turnbull, The Theory of Determinants, Matrices and Invariants, Blackie and Son, London, 1929.
[85] K.C. Valanis, A theory of viscoplasticity without a yield surface, Part II: Application to mechanical behavior of metals, Arch. Mech. 23 (1971) 535–551.
[86] G.A. Wempner, Finite elements, finite rotations and small strains of flexible shells, Int. J. Solids Struc. 5 (1969) 117–153.